ACCESSIBILITY - **OPEN**

OSLO METROPOLITAN UNIVERSITY
STORBYUNIVERSITETET

Master's Degree in

Structural Engineering and Building Technology

Department of Civil Engineering and Energy Technology

MASTER THESIS

THESIS TITLE	DATE
The influence of straight steel fibers on the fresh and mechanical properties of Ultra-high-performance concrete (UHPC)	25.05.2022
	NUMBER OF PAGES 117/0
AUTHOR(S) Sirak Daniel Kibreab – S304950 Ahmed Mohamed Omar – S349450	SUPERVISOR(S) Mahdi Kioumarsi Katalin Vertes

CO. SUPERVISORS	CONTACT PERSON Maziar Kazemian Behrouz Shafei

SUMMARY

This study investigated the effect of steel fiber and UHPC constituents on the fresh and mechanical properties. With the help of a systematic review and experimental program, the study shows that an increase in fiber content leads to decrease in flowability. With the usage of particle packing theory and preliminary laboratory tests, a recipe was created, and based on this recipe, 7 mixtures were developed. In terms of mechanical properties, mixture 3 with a steel fiber concentration of 1% had the highest compressive strength among the five total mixtures. However, when it came to flexural strength, the same mixture 3 had the lowest value of all five mixes, whereas mixture 5 had the greatest.

3 KEYWORDS
Ultra-High Fiber Reinforced Concrete - UHPFRC
Compressive and Flexural Strength
Digital Image Correlation (DIC)

ACKNOWLEDGEMENTS

This thesis is a conclusion of our Master of Science degree (MSc.) and prepared for the Department of Civil Engineering and Energy Technology at Oslo Metropolitan University (OsloMet) and within the field of Structural Engineering. This work is conducted within a period of half a year, from January to May 2022, and counts for a total of 30 ECTS credits. In addition, this thesis is a collaborative work and study between authors/students of OsloMet, Sirak Daniel, and Ahmed Mohamed Omar.

The Department of Civil Engineering at OsloMet offers a variety of highly relevant and interesting in-depth studies through its specialization in structural engineering. These different studies are firmly connected to the AEC industry and its development. Within the field of structural engineering, a topic like concrete technology with the main focus on Ultra-high-performance fiber reinforced concrete has been a topic of relevance and interest for us. By being able to work with such a topic for our master thesis, we were able to take ourselves further into the knowledge and understanding of what lies behind the theory of the topic and additionally, gain practical experience. This topic is highly relevant for the future of material technology within the AEC industry and very interesting for us at an early stage of our careers.

We would like to express our gratitude to all those who provided support, help, and input for our thesis. Deepest gratitude to our supervisor Associate Professor Mahdi Kioumarsi within OsloMet, and Associate Professor Behrouz Shafei and Ph.D. Candidate Maziar Kazemian from Iowa State University. The knowledge and experience we have gained while working under their guidance are invaluable, and grateful for their patience, continuous support, and inspiration. We would also like to extend a special thank you to Associate Professor Katalin Vertes. We are very thankful to the Department of Civil Engineering at OsloMet for providing us with the resources and support needed for this thesis. We would like to extend our sincere thank you to the Concrete Lab supervisor Saja Al-Batat from the Civil Engineering Department.

We would also like to acknowledge Sondre Moe Pekeberg from Master Builders Solutions for providing superplasticizer, Ahmed Khalifa from Elkem, and Bremseth Sigrun Kjær from Norcem for providing us their technical support.

Finally, we would also like to extend our sincere thank you to Rune Orderløkken for his immense technical support with Digital Image Correlation (DIC) and Olav-Johan Øye for providing with filming equipment used to document the experimental program.

This work is a part of the TRANSFORM project. TRANSFORM has received funding from the Directorate for Higher Education and Competence (HK-dir) under grant agreement UTF-2020/10107.

Sirak Daniel

Ahmed Mohamed Omar

Oslo, 25.05.2022

ABSTRACT

Ultra-high-performance concrete (UHPC) is a new cement-based material with a character of exceptional mechanical properties and excellent durability. UHPC possesses a compressive strength higher than 150 MPa, which is approximately three times that of conventional concrete. Ultra-high-performance concrete (UHPC) is a new cement-based material with a character of exceptional mechanical properties and excellent durability. UHPC possesses a compressive strength higher than 150 MPa. This is approximately three times that of conventional concrete. The superior durability also leads to a long service life with a reduced need for maintenance. The usage of UHPC with high mechanical properties (compressive and flexural) has been significantly increasing in our modern-day construction. One of the main obstacles to the production of UHPC is the cost; however, using locally available materials can significantly reduce the cost gap.

This thesis/research study aims to develop ultra-high-performance fiber reinforced concrete (UHPFRC) using locally available materials in Norway, characterized by high compressive and flexural strength. As per requirement within ASTM 1856, this study focuses on developing UHPFRC with a compressive strength minimum of 120 MPa. This is achieved through an experimental program, and initially, this was supposed to be validated with the help of numerical simulation and Digital Image Correlation (DIC). However, due to certain complications and limitations, only an experimental program is achieved in this research study, and DIC is slightly utilized to provide information about crack propagation, displacement, stress, and strain development within the specimen.

A new modified recipe was developed for the experimental program. To achieve this result, mix optimization with the help of a modified Anderson and Anderson model and an extensive series of preliminary laboratory tests were adopted. The application of mixture optimization with a modified A&A model helped produce and evaluate different mixture proportions and helped us achieve the best outcome for this research study. Similarly, a large series of preliminary laboratory tests were carried out to evaluate the effects of material content and different mixture proportions on the workability and compressive strength of UHPC.

Through extensive literature study and an experimental program, the fresh and mechanical properties of UHPC, such as workability/flowability of the mixture and compressive and

flexural strength, were studied and investigated. In this research study, with the help of an experimental program, compressive strength of 135.56 MPa and a significantly high flexural strength value of 24.17 MPa was attained. This was achieved under standard curing conditions of water, submerging our specimen at a constant temperature of 20±2◦C. Furthermore, it was observed that the addition of fibers has a significant effect on compressive - and flexural strength. The compressive strength exhibits a rising pattern with an increase in fiber content up to 1%. Then, a decreasing pattern followed this up to 1.5 %, and lastly, the compressive strength continued to increase with a maximum steel fiber content of 2%. However, when the fiber content increased, the flexural strength increased, reaching a maximum of 2%. Although the workability of our mixture decreased as the fiber concentration increased, we were still able to produce a self-compacting UHPC.

When it comes to the investigation of materials, the optimum dosage of silica fume was 25% by weight of cement, using a higher content of fine sand and a water-to-binder ratio of 0.2 (w/c = 0.25) produced a better result for fresh and mechanical properties. Additionally, the superplasticizer of type MasterEase 2050 showed the best result compared to Dynamo SN-X. This was mainly owing to its high solid content. The dosage range was also experimented with, and 5.5% was sufficient to provide us with the lowest flow value of 22.5 cm (225mm). Since the target value was 20cm, this was well within our target range.

Finally, we see that the results obtained through this research study show that it was entirely possible to produce UHPC under standard conditions. However, one must consider choosing suitable materials and proportioning them appropriately.

Table of content

LIST OF FIGURES

LIST OF TABLES

EQUATIONS

1 INTRODUCTION

1.1 Background

Because of its extensive applicability, concrete is the most frequently utilized building material in the construction sector [1]–[4]. The global concrete manufacture is anticipated to be over 6 billion cubic meters per year, whereas China is responsible for roughly 40% of global concrete output [4], [5]. Concrete's remarkable properties, such as durability, strength, and flowability, along with the fact that it is less expensive than other building materials, make it one of the most effective and popular materials in the construction industry [1], [5]. However, even though many structures are built of concrete, there are certain restrictions to its usage, such as its low ductile behavior due to its brittleness and very poor tensile strength. Moreover, by utilizing fiber reinforcement in concrete, it is possible to reduce the restrictions prohibiting conventional concrete from being a high-performance material [1]–[3].

UHPC is a high-performance cement-based composite material with remarkable properties. UHPC outperforms conventional concrete in strength, durability, ductility, and flowability [6]. This is mainly due to its material ingredients and composition, distinguishing UHPC from conventional concrete. UHPC is typically composed of steel fibers, high content of cement, silica fume (SF), extremely low water-to-binder ratio (w/c), high dosage of superplasticizer (SP), and very fine quartz sand (QS). Fine quartz sand is preferred over regular aggregates for concrete mixtures, mainly because it provides greater mechanical properties [7], [8]. Furthermore, this has sparked some debate because some studies do not recognize UHPC as concrete. This is mainly because of the elimination of coarse aggregates in the mixture. Nevertheless, as UHPC may be used in structural elements, the term “concrete” has stayed in usage instead of “mortar” [5].

The important factor in producing UHPC is to ensure dens particle packing and mechanical homogeneity as this is help providing exceptional durability and strength. For the materials in the matrix to be combined in good proportion, the mixture designs are developed on optimal particle packing theory. Therefore, constituents are designated explicitly by considering particle size and distribution to obtain maximized packing density [9]. Once the particles are dispersed in such a way that the matrix cavities are eliminated, and a high packing density is attained. As a result, compressive strength of at least 120 MPa should be reached, as stated in ASTM C1856 [10].

Although UHPC provides far greater qualities than conventional concrete, it is not broadly applied in Norway and other countries. This is due to a number of causes, and the most important one been materials are fairly expensive because it does not employ coarse aggregates but only fine materials, and they are relatively pricey. Additionally, UHPC commonly contains high cement content to achieve high strength. However, cement manufacturing accounts for 7% of total CO2 emissions globally [11]. UHPCs, high CO2 emissions, energy consumption, lack of design guidelines, and material cost, are common drawbacks that hinder their widespread use [6], [12]. Hence, apart from attempts to enhance building materials, the topic of sustainability has been a main emphasis in the building industry in recent years [13].

1.2 Objective

Compared to conventional concrete, UHPC is a patented product that possesses superior mechanical properties, but as a result of extensive research globally over the past few decades production of UHPC is no longer a patented product. This has given rise to several research study possibilities, with the influence of fiber content on UHPC mixtures being one of the most prominent. Furthermore, another major issue with UHPC is that it is not cost-effective. As described in several scientific studies, the cost is almost 20 times that of regular concrete. This problem can be addressed by utilizing locally available materials.

Based on these reflections we were eventually able to develop our research objectives. The main goals of this thesis have undergone several modifications. The initial objective was to investigate the effect of fiber type, content, ratio, and combination on the fresh and mechanical characteristics of UHPC. These results were to be investigated with the means of an experimental program and validated with the help of numerical analysis and Digital Image Correlation (DIC). In addition, the effect of locally used materials on the fresh and mechanical properties were also to be investigated.

However, due to the limitations, we faced throughout this thesis, the object of this thesis was reduced to investigating the influence of straight steel fibers on different properties such as flowability, the compressive – and flexural strength of our UHPC mixture. To achieve this, we needed to develop a design mix for UHPC based on particle packaging theory and preliminary laboratory tests. Additionally, some of the materials used in this research were also investigated for their influence on the expressed properties of UHPC. Finally, within our knowledge capacity, DIC has been utilized to investigate to see if it can be used as a validation tool.

1.3 Scope

This master's thesis conducted a literature review on UHPC at the initial stage. Following that, separate chapters are covering the experimental program, the thesis outcome, and the conclusion. Table 1.1 presents the outline of the master's dissertation, which consists of 8 chapters.

Table 1.1 Outline of the master thesis

Outline of the master thesis	
Chapter 1 Introduction	Briefly description of both concrete and UHPC. UHPC's material background, the research aims, and the scope of this thesis.
Chapter 2 Literature review	Extensive research on material constituents, mechanical qualities, and rheological properties of UHPC.
Chapter 3 Research question	An explanation of the thesis's topic. The research questions for the thesis, as well as related sub-questions and the thesis' limitations, are provided.
Chapter 4 Case study	The optimized particle packing model and the material employed in this investigation are described. A detailed explanation of the experimental investigation and presentation of the final UHPC recipe.
Chapter 5 Methodology	An explanation of how the literature review, chosen methods, and laboratory experiments were used to address the thesis's questions.
Chapter 6 Results and discussions	Presentation of all the different results and discussion of the findings in relation to the theoretical foundation.
Chapter 7 Conclusion	In this chapter, the important findings from the experiments are discussed, and the researcher's questions and sub-questions are concretely answered.
Chapter 8 Future work	Recommendations for future study in the relevant field.
Reference	All sources used in the thesis are listed in a detailed reference list.
Appendix	The report's attachments are included here.

2 LITERATURE REVIEW

2.1 General Background

Applying reinforcement in the concrete is not something new, as this has been practiced for over a thousand years. Previously, straws and horsehair were utilized to enhance the mechanical properties of concrete that were subjected to brittleness[1], [6].

In the recent era, fiber reinforcement has been used in concrete in the building sector for over six decades. In the 1960s, a determined scientific attempt was undertaken to improve the compressive strength of concrete [5], [14].

Concrete's compressive strength in the 1960s varied between 15-20 MPa. However, it took a decade for the compressive strength to be improved up to 45-60 MPa. This is because the water reduction substance was not efficient enough and unable to minimize the water to binder ratio. Additionally, in the 1970s, research with tiny specimens attained a compressive strength of 510MPa. However, it was manufactured under unusual circumstances, including vacuum, pressure, and heat curing, which made it difficult to prepare and used a lot of energy.

Furthermore, in the 1980s, a study used a superplasticizer and a large quantity of silica fume to achieve a compressive strength of 345 MPa, utilizing pressure and heat curing. However, despite its impressive compressive strength, this type of concrete was afflicted by brittleness. As a result, steel fibers were therefore utilized to tackle brittleness difficulties. To make this a reality, different solutions were investigated for workability challenges in the development of UHPC [5], [15]–[17].

Richard & Cheyrezy [17] created "Reactive Powder Concrete" (RPC) in the 1990s using heat treatment and materials with improved reactivity and fineness. This was achieved by making the particle dispersion in RPC concrete as dense as possible, a breakthrough for UHPC. RPC is defined by its high binder content, low w/c, exceptionally high cement content, application of silica fume (SF), fine quartz powder, quartz sand, superplasticizers (SP), and fibers. Additionally, the concrete demonstrated high workability; however, the material employed in this type of concrete is somewhat costly [5], [17], [18].

In the past two decades, UHPC has evolved further due to additional studies and research that have improved the material's knowledge. In addition to its high strength, UHPC also offers remarkable ductility and durability in this era [5], [15].

UHPC does not entirely comply with current conventional concrete manufacture, structural standards, and regulations. As a result, considerable resources have been spent so that it can help provide solid standards and recommendations. In addition to contributing a great material knowledge to the building sector [5], [6]. The German Research Foundation [19] spent 12 million euros on a research initiative in 2005, intending to develop standards and expand expertise within UHPC. More than 20 research institutes participated in this research program, which focuses on 34 research topics [20].

Furthermore, researchers have begun to develop UHPC standards and guidelines in recent years. Several countries, notably Germany [21], Canada [22], Switzerland [23], Japan [24], Australia [25], and Spain [26], are among the countries that have developed national guidelines. Nevertheless, when it comes to UHPC design and material classification, the different countries have different demands and criteria for the emerging national standards and guidelines [5], [6].

2.2 Definition of UHPC

2.2.1 Material properties

There is no commonly agreed definition of UHPC at the moment [27]. However, according to numerous studies and standards [7], [15], [17], [20], [28]–[30], UHPC is defined as fiber-reinforced cement-based material having a compressive strength of 150MPa. Moreover, with increased durability owing to its discontinuous pore structure. However, although the compressive strength is defined as 150MPa, lower strength is occasionally permitted or required depending on the application [20], [31]. According to Meng et al. [31], [32], an ordinary curing regime results in compressive strengths of 125 MPa and higher, whereas heat curing results in over 150 MPa. As for ASTM C1856 [Source], compressive strength of 120 MPa is allowed. Depending on the organization and research the compressive strength and other material properties are varying. Therefore, Shahrokhinasab [33] provided an overview of the minimum UHPC definition from different organizations, research, and standards, as displayed in Table 2.1.

Table 2.1 Minimum UHPC definition [33]

Reference	Location	Document	Min. Compressive strength [MPa]	Min. Tensile strength [MPa]
[10]	USA	ASTM C1856-17	120	--
[34]	USA	Federal Highway Administration	150	5 (post crack)
[35]	USA	ACI PRC-239-18	150	--
[36]	USA	PCI	117	10 (first crack) 13 (post crack)
[30]	France	AFNOR NF P18-470	150	6 (first crack)
[37]	Canada	CSA A23.1	120	4 (first crack)
[38]	Switzerland	SIA 2052	120	7 (first crack)

Furthermore, the tensile strength is a feature that sets UHPC apart from other concretes. Therefore, the tensile strength demands are also included in the definitions of UHPC in terms of the material's pre-and post-cracking strength. The tensile strength before and after cracking must be larger than 5 MPa [20]. Nevertheless, minimum values of other documents are displayed in Table 2.1.

Figure 2.1 displays a comparison of the typical tensile stress-strain curve of UHPC and conventional concrete. Since UHPC is exceedingly brittle in the absence of steel fibers, the addition of steel fibers enhances the material properties such as strength and ductility. Therefore, when reinforced with steel fiber, UHPC can withstand considerably larger strain and stress than conventional concrete. This is mainly because UHPC will achieve strain hardening after the first cracking, as illustrated in the Figure below [39].

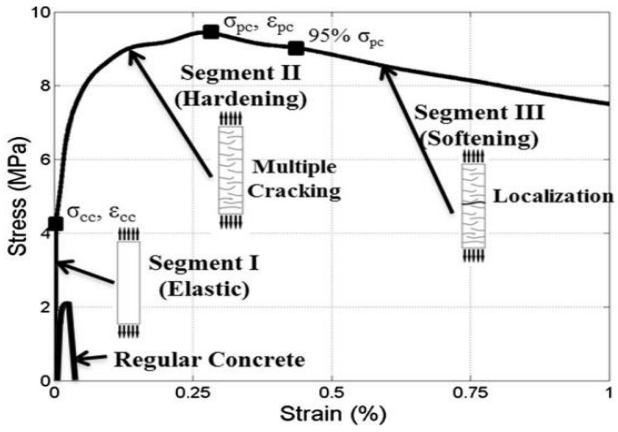

Figure 2.1 Difference between regular concrete and UHPC [39].

Graybeal B. [20] categorized UHPC's tensile stress-strain behavior into four primary phases when fiber reinforcement is incorporated, as shown in Figure 2.2. Phase I indicates that the tensile behavior of the material is elastic in the first part, and there is no crack beginning formatted in this phase. This linear-elastic response proceeds until the material exhibits an initial crack, referred to as phase II or first cracking. In this phase, multiple cracks begin to form in the UHPC matrix. Furthermore, in phase III, the material undergoes strain hardening until it reaches its maximum strength, and in the UHPC matrix, wider cracks begin to appear. Eventually, the material starts to show crack localization after the strain hardening region, phase IV. In this phase, the material decreases in strength as it has reached its peak tensile strength. In addition, the fibers that are bridging the cracks begin to detach from the matrix in this phase [20], [39].

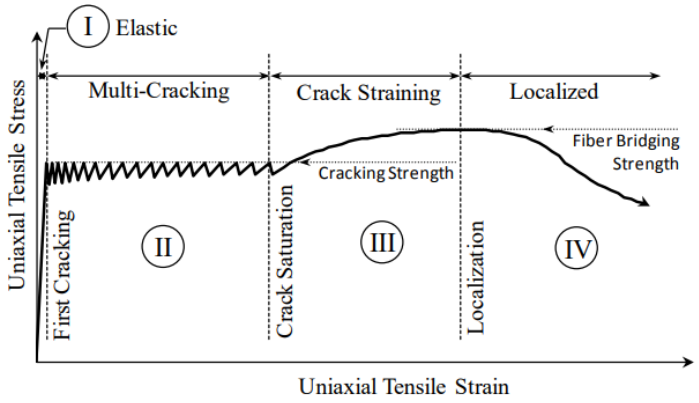

Figure 2.2 UHPC's tensile stress-strain behavior [20].

There is considerable information available regarding UHPC's mechanical characteristics, Therefore, Table 2.2 outlines typical ranges of the most common material properties for UHPC according to [20], [31], [34], [40]–[43].

Table 2.2 Typical mechanical properties of UHPC

Properties	Typical Range
7-Days Compressive Strength	100 to 135 MPa
28-Days Compressive Strength	> 120 MPa
28-Days Flexural Strength	Up to 40 MPa
Tensile cracking Strength	6 to 15 MPa
Modulus of elasticity	40 to 70 GPa
Poisson's ratio	0.2
Flowability	175 to 300 mm

2.2.2 UHPC Composition

The key factor in producing UHPC is to improve the micro and macro properties of its mixture ingredients. There are some main compositions of UHPC: Cement, low water to cement ratio (w/c ratio), high dosage of superplasticizer (SP), fine aggregates, steel fibers, and ultrafine cementitious materials [44]–[49].

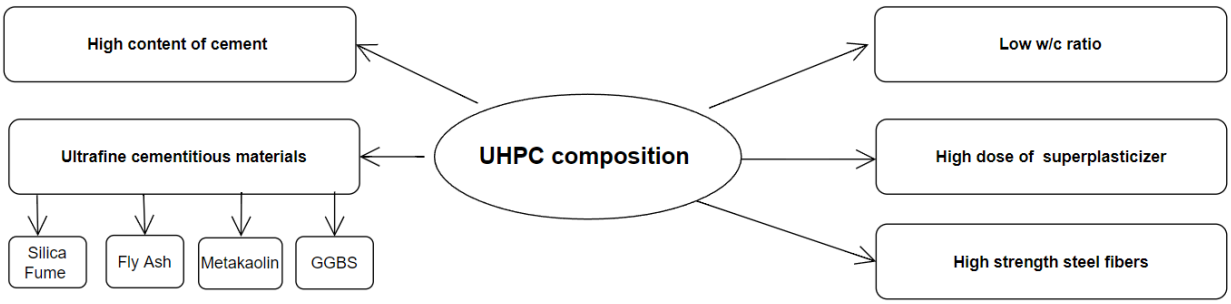

Figure 2.3 Typical composition in UHPC [50]

Thankfully, numerous studies have found a suitable range of constituents to produce UHPC successfully. Based on these various studies, a typical composition of UHPC and its range can be estimated and is presented in Table 2.3 [44]–[49].

Table 2.3 Composition and Range of different UHPC constituents [44]–[49].

UHPC Materials	Percentage (by weight)
Cement	28-44
Silica Fume	1-11
Sand	32-61
Superplasticizer	1-5
Water	6-12
Steel fiber	0-14

This shows that UHPC is not different from conventional concrete. The main difference lies in quantity, matrix volume, low w/c-ratio, fiber content, and the size of the aggregates. The use of superplasticizers to achieve acceptable workability is also an attribute of UHPC. This relationship can be observed in Figure 2.4 and shows almost the same composition, but the quantity ratio is very different even though they both contain much of the same ingredients.

Compared to conventional concrete, the matrix of UHPC is much denser. Therefore, when producing UHPC, it is essential to obtain the maximum possible packing density of all granulated constituents [51]. This will provide us with improved durability and mechanical

properties. To achieve this dense matrix, its necessary to optimize the packing density of all granular raw materials, such as cement, cementitious materials, fillers, and aggregates.

A more extensive explanation of the different constituents is provided in Chapter 2.5, based on a systematic literature study conducted for this thesis.

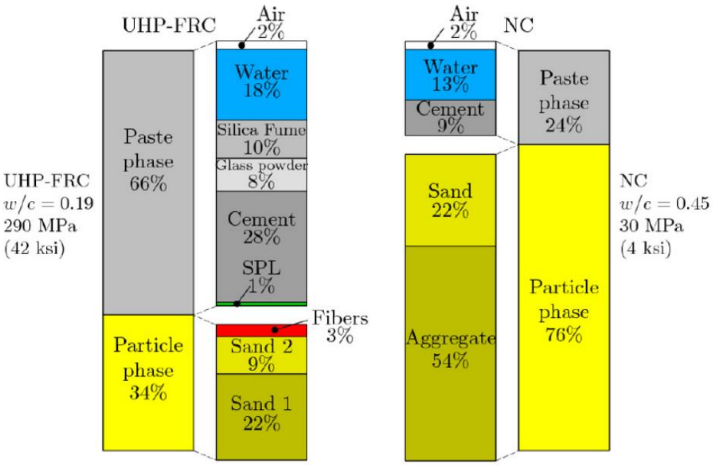

Figure 2.4 Mix proportion example by volume comparing Normal Concrete and Ultra-High-Performance Reinforced Concrete (UHPC) [15].

2.2.3 UHPC standards

For assessing the performance of UHPC, the conventional concrete tests method may be employed as-is or with minor changes. Typically, the fresh properties of UHPC are determined by flow or slump tests, while compressive - and tensile strength tests determine the mechanical properties. There are different approaches and standards for determining the procedure for the different experiments [20]. For UHPC fabrication and material testing, ASTM C1856 “Standard Practice for Fabricating and Testing Specimens of Ultra-High-Performance Concrete” [10] provides standardized guidelines. The standard outlines the various tests that must be carried out and the requirements that must be applied. Table 2.4 shows the ASTM C1856 requirements for UHPC in the fresh, hardened, mechanical, and durability states [10].

Table 2.4 Requirements for developing UHPC in accordance with ASTM C1856 [10].

State	Property	ASTM	Common test name	ASTM C1856 Requirement
Fresh	Workability (Flow)	C1437	Flow table	Yes
		C1611	Slump Flow	No
	Air content (%)	C173	Air	No
	Density	C138	Unit Weight	No
Hardened	Creep in compression	C512	Creep Test	Yes
	Length Change	C157	Length Change	Yes
	Setting Time	C191	Vicat	Yes
		C403	Penetrometer	No
Mechanical	Compressive strength (1,3,7 and 28 days)	C39	4X8 Cylinder	Yes
		C109	2X2 Cube	No
	Flexural strength (7 and 28 days)	C1609	Four-point flexural test	Yes
	Modulus of elasticity (7 and 28 days)	C469	Modulus of elasticity	Yes
Durability	Resistance to abrasion	C944	Rotating cutter	Yes
	Resistance to freezing and thawing	C666	Rapid Freeze-Thaw	Yes
	Penetration of chloride ions	C1202	Rapid Chloride Permeability test	Yes

However, by following the methods and approaches described in previous research [33], [34], [52]–[55], and ASTM C1856 [10], the generated mixtures in this thesis were evaluated for flow, compressive strength, and flexural strength, as shown in Table 2.5, as only these are possible to perform at the lab.

Table 2.5 Standards and objectives of the test methods in this study

Test and properties	Test Method	Specimen size	No. of samples/specimens	Main Measurements
Flowability	ASTM C1437 ASTM C1611	--	Multiple samples throughout the casting process.	Workability and flow
Casting	EN 12390-2 EN 14651	--	Multiple samples	Casting direction in the mold
Compressive Strength	NS-EN 12390-3	100 mm cubes	Multiple specimens, at each age of testing, three specimens were taken for each mixture.	7- and 28-days Compressive Strength
Flexural tensile Strength	NS-EN 12390-5	100 x100 x 500 mm prism	Multiple specimens, at each age of testing, three specimens were taken for each mixture.	28 days Flexural tensile strength

2.3 Advantages

The use of cutting-edge technologies like UHPC allows for infrastructure production with lower life cycle costs [52]. In addition, UHPC can provide a financial advantage in the construction industry as its exceptional mechanical properties. Reduced labor and construction expenses, as well as material savings, arise from the UHPC's capability to reduce the cross-section of a structural component. The idea behind the reduction of cross-section enables the fabrication of lighter structures, benefiting the precast concrete industry. Furthermore, since there are no layers of rebars, staff's safety and mobility are enhanced. UHPC can also be used in locations where there is a need for high ductility and regions where excessive reinforcing is necessary. Furthermore, structural components, rehabilitation and maintenance works of high rises, bridges, dams, turbine towers, military construction, architectural elements, and offshore constructions are examples of possible UHPC applications [7].

2.4 Application

The most predominant UHPC usages are highway bridges and pedestrian footbridges. The first UHPC pedestrian bridge was constructed in Canada in 1997. Subsequently, around 26 bridges have been constructed with UHPC, entirely or as a component. Globally it is estimated that above 200 bridges with UHPC elements exist today. Japan, Australia, Croatia, Italy, Netherland, Malaysia, Austria, Slovenia, Switzerland, and South Korea are among the nations processing UHPC bridges. UHPC has also been used in buildings to create visually and

architecturally pleasing constructions. In France, UHPC elements have been used in roof components, sunshades, and cladding. Table 2.6 lists some of the current global applications of UHPC [5], [7], [20], [56]–[60].

Table 2.6: Different application of UHPC adopted from [5], [7], [20], [56]–[60].

Construction type	**Location**	**Year**	**Contribution**
Pedestrian bridge	Sherbrooke, Canada	1997	• The very first UHPC construction • Used reactive powder concrete (RPC)
Pedestrian bridge	Sakata, Japan	2002	• Lighter structure as it weighs 20% of conventional reinforced concrete construction self-weight. A 10% cost reduction was achieved. • Exposed to an aggressive corrosion environment, but the bridge remains in good shape and retains its outstanding characteristics such as compressive strength and flexural strength after more than 10 years.
Pedestrian bridge	Seoul, South Korea	2004	• For the first time, a 120m span arch bridge was built with UHPC.
Roof structure	Shawnessy LRT Station, Calgary Canada	2004	• Developed for aesthetically appealing and lightweight structure with low maintenance
Road bridge	Bourg-les Valence, France	2005	• Due to the limited usage of steel bar reinforcing, the construction's self-weight is decreased. • After 28 days, the compressive strength was 180 MPa. Due to continued cement hydration, compressive strength rose by roughly 20% after 12 years.
Road bridge	Iowa, United States	2006	• The first UHPC bridge was built in the United States. • There was no shear reinforcement.
Haneda airport slab	Tokyo, Japan	2010	• Self-weight is minimized, and span is increased by fiber reinforcement. • Tensile strength of 11.3 MPa was achieved.
Façade, footbridge, roof & column	MUCEM, Marseille France	2013	• Novel layouts and creative architectural designs • Use of tree-like Y-shaped columns and façade.
Façade &Roof	Jean Bouin stadium, Paris France	2013	• The roof and façade are both waterproof. • Precast UHPC components.
Cladding & panels	Foundation Louis Vuitton, Paris France	2014	• Unique prefabricated panels were employed to produce a one-of-a-kind and innovative design.

Figures 2.5 and 2.6 depict some of the structural and architectural applications of UHPC presented in Table 2.6.

Figure 2.5 Structural application of UHPC: (a) Sherbrooke Footbridge, Canada [20], (b) Sakata- Mirai bridge, Japan [20], (c) Footbridge of peace, South Korea [20], (d) Roof structure of light rail station, Canada [61], (e) Haneda airport slab, Japan [56].

Figure 2.6 Architectural application of UHPC: (a) Jean Bouin stadium, France [62], (b) MUCEM, France [56], (c) Foundation Louis Vuitton, France [56].

2.5 UHPC Constituent Materials

2.5.1 Cement

When it comes to non-proprietary UHPC, the common ingredients are cement, filler, fine aggregate, and pozzolanic reactive materials, i.e., SCMs, SP, and fibers. The main binder in UHPC is cement, and SCMs help to improve the particle packaging. The result is a denser structure and enhanced strength due to the pozzolanic reactions. In addition to this, fillers are also used to improve particle packing

A relatively high proportion of cement is used in UHPC mixtures compared to that used in traditional concrete-like normal-strength (NS) and high-performance concrete (HPC) [63]. UHPC uses almost twice the amount of cement as traditional concrete (approx. 20% of the total volume of UHPC). The main chemical compounds of Portland cement (PC) are C_2S, C_3S, C_3A, and C_4AF. The hydration of C_2S and C_3S is essential here, mainly since they are the main contributors to strength in the concrete. The cement content in UHPC lies typically between 600 and 1000 kg/$m^{3,}$ and the fineness of the cement should be between 3000 and 4500 cm^3/kg.

Regarding the type of cement, Portland cement (PC) with a low C_3A content can is recommended because of its low water requirement. The hydration of C_3A occurs fast, mainly due to its high surface area, resulting in an increased demand for water, thus affecting the viscosity of the fresh concrete. In other words, a low quantity of C_3A will reduce; the required water amount, formation of ettringite, and hear of hydration. As a result, a cement with C_3A content lower than 8 % is preferred [64]. So, cement with a high amount of C_2S and C_3S, low C_3A, and moderate fineness will provide good performance for UHPC. Within most of the research, the commonly used type of cement is Type I/II Portland cement (PC), mainly due to its low content of C_3A. However, there are also cases where other types of cement, such as Type III, were used mainly because of their smaller particles than type I and II. Cement in UHPC is not usually fully hydrated, and the remaining particles can be regarded as filler, primarily when fine cement particles are used [7]. In conclusion, Table 2.7 summarizes the key features of cement used in UHPC.

Table 2.7 Main features of cement used in UHPC [50].

Features	Significance or negative impact	Limitations
Surface area	The finer the cement, the faster will the chemical reactions become	$\geq 400\ m^2/kg$
C_2S, C_3S	Higher content will increase strength gain	
C_3A	This will cause rapid hydration and increase water demand [65]	$\leq 8\ \%$
Content	A high content of cement will raise the strength	$1700 m^3$ [66]

Compared to conventional concrete, cement accounts for most of the amount in UHPC mixture alongside fine powders, as mentioned previously. Several studies [67]–[69] have found that increasing the cement content in the mixture increases the compressive strength of the UHPC. Furthermore, it has been discovered that the compressive strength is lowered when the ideal cement concentration exceeds 1700kg/m3. This might be due to the high cement content, which prevents aggregates from contributing to the mixture [7].

The impact of different kinds of cement on UHPC compressive and flexural strength has received little attention. Alkaysi et al. [70] investigated three distinct cement types: White Cement Type I, Portland Type V, and a GGBS / Portland Type I blend. The compressive -and flexural strengths of white cement Type I was determined to be 191 MPa and 9.3 MPa, respectively. Furthermore, the compressive and tensile strengths of the GGBS / Portland type I blend mixes were 180 MPa and 8.9 MPa, respectively. Lastly, the Portland Type V had the lowest compressive and flexural strengths, at 179 MPa and 8.4 MPa, respectively. However, it turns out that all types of cement evaluated, namely those by Alkaysi et al. satisfied the compressive strength threshold of 150MPa for UHPC. Furthermore, Yu et al. [12] studied substituting the cement in the UHPC mixture with GGBS, limestone powder, and fly ash. GGBS exhibited the highest flexural and compressive strength compared to the other two materials.

Enormous amounts of Portland cement ranging from 500- 1200 kg/m^3 are usually required for the production of UHPC. The formation of greenhouse gases during the production process appears to have major environmental repercussions. For every ton of Portland cement produced, at least one ton of CO2 is emitted. Additionally, the large quantity of cement might

cause shrinkage difficulties due to the heat of hydration [71]. Moreover, cement is also an expensive material. Some research on a low cement UHPC [72]–[74] has recently been published to reduce the burden of UHPC and make it more acceptable.

Azmee et al. [73] researched lowering cement content by substituting it with large quantities of fly ash and silica fume and comparing it to a reference mix of ordinary Portland cement. This resulted in compressive strength of 130MPa for 28 days and 160MPa for 90 days. The amounts of fly Ash and silica fume used to achieve this were 40% and 10%, respectively. Between 28 and 90 days, the compressive strength increases by about 20%. This might be related to the slow setting phase of fly ash, which was previously stated. Adding 10% silica fume will help increase the strength while also filling voids and achieving denser particle packing.

Xiao et al. [74] analyzed a UHPC composed of superfine cement that was partially replaced by Ordinary Portland cement and admixtures such as GGBS and fly ash. Replacing superfine cement with 30% GGBS and 10% fly ash resulted in the greatest compressive strength, of 160MPa, whereas replacing superfine cement with 40% GGBS alone resulted in 158MPa.

2.5.2 SCM

Ground Granulated Blast-Furnace Slag (GGBS)

GGBS (slag) is another SCM that is commonly used in UHPC. It is a by-product of the iron and steel industry and is made of molten iron slag from a blast furnace. Generally, the particles of slag have a rough and angular shape, and when mixed with cement and water, they will hydrate and set, similar to OPC [75]. Slag is composed of silica, lime, and alumina, with a small amount of iron oxide, alkali, and magnesia. The molten iron slag is first satiated with steam or water, which will result in a product with a glassy granular look. This product will then be dried and granulated into a fine powder. This can then be used with OPC and in combination with other pozzolanic materials. GGBs enhance the durability of concrete structures, by providing higher resistance to chloride penetration and attack by sulfate and other malicious compounds. In addition, it will also reduce the risk of damage caused by the alkali-silica reaction.[76],[77]

Studies by Malagavelli [77],[43] show GGBS can replace up to 50% of cement without negatively affecting the compressive strength.

In addition to those materials mentioned above, other materials, such as quartz powder, are utilized in mixtures because they are believed to provide a better particle packing of UHPC [78].

Fly ash

Fly ash (FA) for use in concrete is a by-product of the furnace with pulverized coal (often power plants) and is one of the most extensively used SCMs. FA can be either a calcium-silicate or aluminosilicate, depending on how silicon dioxide (SiO_2) is chemically combined. Due to the presence of silicon dioxide (SiO_2), which both contain, fly ash will have a pozzolanic property [79]. The reaction between SiO_2 and Ca $(OH)_2$ (pozzolanic reaction) will slowly continue to increase the strength at a later age. Previous research found that 90-day compressive strength was 30% greater than 28 days [66]. This means we can replace a portion of cement content to enhance the properties of the mixture.

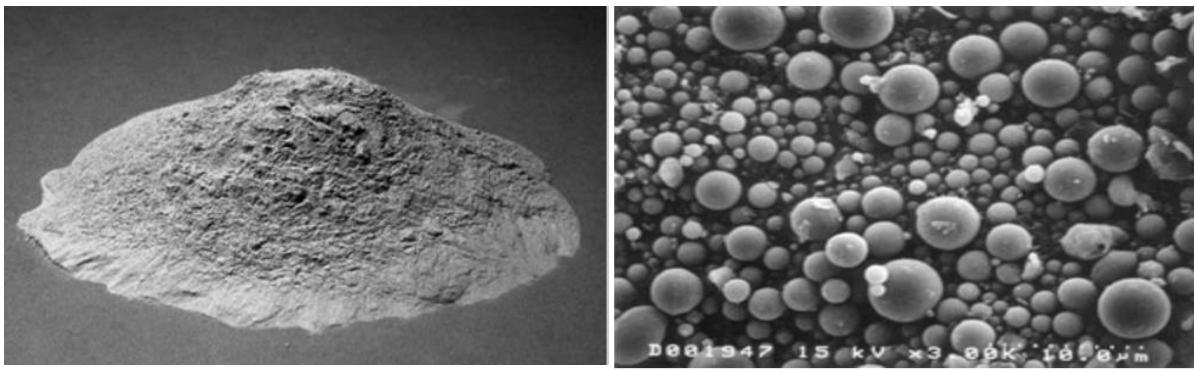

Figure 2.7 Left – Fly ash; Right - Fly ash particles at 2000x magnification with scanning Electron Microscope (SEM) [80],[81].

Table 2.8 Main features of FA use in UHPC [50].

Features	Significance or negative impact	Limitations
Round and ultra/fine particles	• Improve workability • Reduce long term permeability • It enhances resistance to sulfate attack caused by reaction with Ca(OH)2	0.1 – 45 µm
High surface and packing density	Stimulates the reaction between Ca(OH)2 and SiO2	300 – 500 m2/kg
High content of SiO2	High reactive with Ca(OH)2	

The following are some of the characteristics and overview of FA's effects on the properties of concrete[82]:

- The Concretes with FA have shown a decreased permeability, reduced sulfate attacks, and lower alkali-silica-reaction.
- The majority of FA particles have a solid spherical shape; due to its lubricating and "ball-bearing effect, FA can enhance the flowability of fresh concrete. This will result in FA acquiring a water-reducing effect.
- Therefore, replacing cement with FA will increase setting time and decrease the hardening rates in the early stages. From a long-term perspective and compared with traditional concrete with only OPC, the mechanical properties of concrete can be improved.

2.5.3 Silica Fume

Silica Fume (SF) is a common pozzolanic material used to fabric UHPC and a by-product of the smelting process used to produce silicon metal and ferrosilicon. It can help improve the packing density and prevent pore formation in the UHPC. The main characteristics of SF are the following: an amorphous structure, SiO_2 content between 85-98%, and spherical shape with mean particle size in the range of 0.1 to 0.2 um. Therefore, SF is an essential part of UHPC, and this is principal because, during the pozzolanic reaction, SF will react with Calcium Hydroxide ($Ca(OH)_2$) from the hydration of cement. This will then produce more CSH binder, which is the main hydration product responsible for the strength of concrete. So, when CH is replaced by CSH, which has much higher strength, the porosity of concrete decreases in the bulk and, in particular, in the interfacial transition zone (ITZ). This, in return, will result in a significant increase in strength.

SF consists of particles that are much smaller than those cement particles (about 1/100) and this makes them a very efficient filler, which will increase the packing density. Regarding workability and water demand, when we think about high-strength concrete, such as UHPC, it is beneficial to regard SF as a water replacement. In a pure cement paste binder scenario, a certain amount of water is necessary to fill the void space and make the flow possible. Additionally, by combining SF with water-reducing agents, we can lower the void space volume and disperse the cement flock, hence the water demand. Since SF can replace the water in void spaces and, at the same time, increase the workability when superplasticizers (SP) are used, there is even further possibility of water reduction. Some studies found that the perfect

amount of SF to be used as a percentage in UHPC mixture will range between (15-30)% of the cement content. This would of course, be dependent on other constituents [83],[84],[65],[41]. In the same manner for cement, we will also summarize the main features of SF we can use in UHPC.

Table 2.9. Main features of SF use in UHPC [50].

Features	Significance or negative impact	Limitations
Very fine and non-crystalline structure	Enhances the packing density	0.1 – 0.2 µm
Content, SF/cement ratio	High reactive with Ca(OH)2	25 % [85]
High content of SiO2	High reactive with Ca(OH)2	≥ 85 %
Heat treatment at 80 – 90 C	Accelerates reaction with CA(OH)2 à Produces more CSH, reduces porosity, and increases strength	

Several papers such as [70], [86]–[94] have studied the effect and contribution of silica fume and nano-silica on the mechanical properties of UHPC. Yail et al. [88] discovered that the quantity of SiO_2 in silica fume is a significant element influencing the strength of the UHPC. A SIO_2 level of 92 percent performed better in compressive strength than a SiO_2 content of 85 percent. SiO_2 generates a pozzolanic calcium silicate hydrate whenever it interacts with CA(OH), resulting in a stronger connection between cement particles. Rong and Sun et al. [90] also studied the influence of SiO_2 content on UHPC compressive and tensile strength. The researchers determined that using a binder with a SiO_2 level of up to 3% will result in the maximum compressive and tensile strength. Exceeding this amount of SIO_2 will result in Silica Fume clustering and diminish the compressive - and tensile strength.

Both Yu et al. [91] and Huang et al. [92] studied the ideal nano-silica content for attaining the highest compressive strength. Yu et al. found that a nano-silica concentration of 3.71 percent in the binder provided the best strength, whereas Huang et al. found that 3 percent nano-silica provided the best strength. Both studies also discovered that after 28 days, compressive strength changes minimally. This is due to nano-silica clustering, which impedes the hydration process.

Mosaberpanah et al. [87] investigated nano-silica concentrations of 0 to 5% of the weight of cement. The use of nano-silica compounds increased compressive strength after 28 days.

Different silica fume concentrations were also evaluated by different researchers, such as Akayis et al. [70], who analyzed silica fume content ranging from 25 to 35 % by cement weight. According to this study, silica fume had a minor influence on compressive strength at this level, with just a 1.5 % enhancement when the silica fume content was raised by 15 vol-%. Compressive strength of 183.4 MPa and 186.3 MPa were achieved for 25% and 35% silica fume contents, respectively. On the other hand, the tensile strength was somewhat diminished, resulting in a slight reduction in the steel fibers' capacity to carry tensile load. Wu et al. [86] investigated silica fume concentrations ranging from 0 to 25% of cement weight. If the amount of silica fume in the cement exceeds roughly 25% of the total weight, the compressive strength would be reduced. In this study, the optimal content was between 10-15%, which resulted in the maximum compressive and tensile strength. However, this level gave lower viscosity, but silica fume acts as a filler by reducing porosity, enhancing microstructure density, and strengthening the fiber bond matrix, as previously mentioned.

2.5.4 Aggregates

In UHPC, coarse aggregates (the most significant fractions) are generally not used. Instead, it is desirable to use only fine sand aggregates due to the influence of maximum paste thickness (MTP). This represents the mean distance between two aggregates when they are surrounded by cement paste. This cement past has a thickness proportional to the diameter of the aggregate. This observation was confirmed and reported by [95], who stated that even if the UHPC design contains coarse aggregates, they will be smaller and lower (> 6mm) compared to NC. Usually, aggregates with high strength, low water absorption, and high quality with optimized particle packing are recommended [96]. Some good examples of fine aggregates include quartz, basalt, and limestone. However, silica sand is one of the most commonly used fine aggregates in UHPC. Mainly due to its availability and cost. Another important aspect when using fine aggregates in UHPC is that they should be strong and chemically stable and financially and environmentally desirable. In Table 2.10, we have summarized different particle size aggregates and their frequency of usage within UHPC.

Table 2.10. The maximum particle size of aggregates and their frequency of usage in UHPC.

Maximum size of aggregates	Wille et at., 2011(b)	Naaman et al., 2021	Ambily et al., 2014	Yu et al., 2014 (a)	Yu et al., 2014 (b)	Yu et al., 2015	Alkasy et al., 2016	Meng et al., 2016	Wu et al., 2016	Meng et al., 2017	Hamiruddin et al., 2018
0.016 mm							X				
0.063 mm											X
0.150 mm		X	X								
0.300 mm											X
0.500 mm							X				
0.600 mm											X
0.800 mm		X									X
1.000 mm				X	X	X					X
2.000 mm	X							X		X	
2.360 mm			X	X					X		
4.750 mm								X		X	

As explained previously, eliminating coarse aggregates in the UHPC mixture is beneficial. This is mainly because conventional concrete failure is initiated by damage between the aggregates and cementitious matrix (ITZ). Moreover, this will reduce weaknesses induced by ITZ flaws (which influence the overall porosity in the matrix) and enhance the mechanical strength [97]. So, with the elimination of coarse aggregates, this is where fine aggregate like quartz sand (QS) plays an important role. Their main task is to reduce the MPT, which happens to be the key factor in the mixture design of UHPC. The next important factor is finding an optimum sand-to-cement ratio. This is not an easy task, and after much research, the general value was estimated to be 1.4 for a QS size of 0.8 mm [64].

However, having an optimum ratio is not always the answer to our problems, so more research was conducted on types, content, and gradation throughout the decade to understand the influence of aggregates on UHPC better. For example, Pu Zhang [99] showed the influence of the number of different particle sizes of Sintered Bauxite on the compressive strength when it comes to the content. As shown in Figure 2.8, in the experiment, different size of aggregates was tested by holding the ratio of the other parameters constant. The result shows that the compressive strength of UHPC increased with an increase in the ratio is 0-1 mm to 1-3 mm. This was achieved when the ratio of 0-1 mm to 1-3 mm was 1.255:0 and achieved a strength of 155.5 MPa. Additionally, when the ratio was 0.755 (1.15:1), the UHPC achieved the best fluidity.

Material (kg/m³)	B1	B2	B3	C1	C2	C3	D1	D2	D3	E1	E2
Cement	846	752	658	752	752	752	940	940	940	940	940
GGBFS	94	188	282	188	188	188	—	—	—	—	—
FA	—	—	—	—	—	—	28.2	56.4	84.6	—	—
SF	282	282	282	282	282	282	253.8	225.6	197.4	282	282
0-1 mm bauxite	240	240	240	240	240	240	240	240	240	710	1180
1~3 mm bauxite	940	940	940	940	940	940	940	940	940	470	0
Steel fiber	234	234	234	234	234	234	234	234	234	234	234
SP (L/m³)	70.5	70.5	70.5	70.5	70.5	70.5	70.5	70.5	70.5	70.5	70.5
Water	237	237	237	212	225	237	237	237	237	237	237
Water/binder	0.194	0.194	0.194	0.174	0.184	0.194	0.194	0.194	0.194	0.194	0.194
Compressive strength (MPa)											
7 days	106.2	105.3	89.6	106.5	108	105.3	119.2	106.5	115.2	115.7	121.2
28 days	141.4	140.1	121.5	132	131.7	140.1	144.6	137.6	148.6	152.4	155.5
Slump (cm)	9.2	10.1	12	2	3.5	10.1	9.6	7.2	14.1	12	7.3

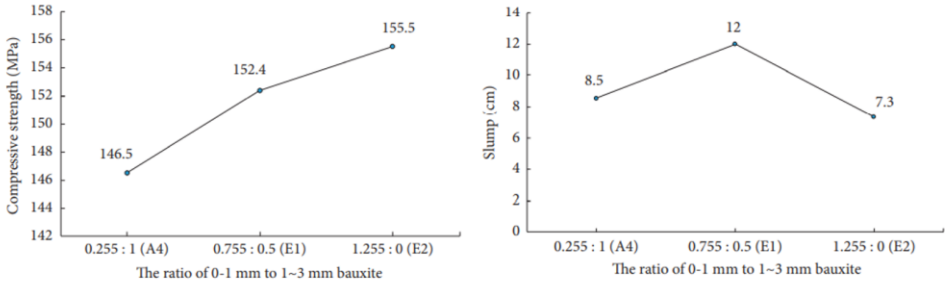

Figure 2.8. Composition of mixture with test result presented in a table form and graph [98].

Another study also investigated the effects of different gradations on compressive strength. From their experimental investigation, they managed to conclude that sand grading with 600 – 1800 um obtained the highest compressive strength of 100 MPa at 28 days. This is presented in Figure 2.9.

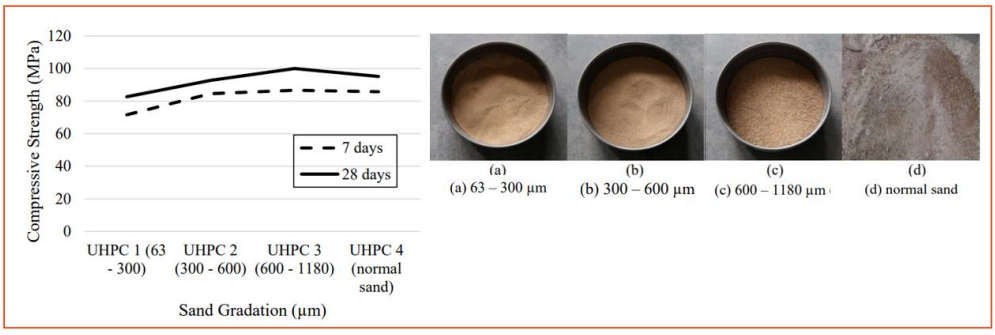

Figure 2.9. Different sand gradations and their influence on the strength of UHPC [99].

2.5.5 Water

When Portland cement-based composites are used, a sufficient potable water supply is necessary for the hydration process to occur. Therefore, the same water criteria and quality apply to conventional concrete and UHPC mixtures. Additionally, apart from the water's participation in the hydration process, the temperature of the water is a significant factor. The reason for it is that when it comes to adding water to the dry mixture, the temperature of the water has a significant impact on the fresh concrete's overall quality. Mainly, chilled water is used throughout the mixing to lower the temperature of the UHPC so that the UHPC mixture does not overheat under the hydration process. This is because UHPC requires more energy input than conventional concrete because of its composition, resulting in longer mixing times. As a result, by applying chilled water, the water absorption rate will be lowered, while flowability will improve [34]. Graybeal B. [34], [100] proposes using ice cubes to replace some or all of the mixed water to cool down the mixture.

2.5.6 Admixtures

When we talk about chemical admixtures, the most commonly used one in UHPC is a high-range, water-reducing (HRWR) admixture, also known as “Superplasticizer (SP).” The main task for SP is to reduce the amount of water required in the mix, and due to the low w/b ratio, SP is very crucial in achieving a UHPC with sufficient workability. In the market, there are different types of plasticizers used; however, the most commonly used and most effective superplasticizer for UHPC is Polycarboxylate ether-based HRWR. The development of UHPC could not have happened without SP admixtures, and to gain sufficient workability, a quantity of up to 5 mass-% of cement can be used, and with this, one can save a sufficient amount of water to make the concrete workable.[51].

The required dosage of SP mainly depends on the compatibility and the type of SP admixture used. This will mean that good mixture compatibility will lead to a low requirement of SP dosage. However, when it comes to the enhancing property SP will have on UHPC, this will depend on different factors such as; type, addition method (stepwise or delayed or maybe all at once), and of course, dosage amount. Li et al. [101] investigated the effect of SP on spread flow, slump life, and early-age strength development, among other things. The aim was to understand the influence of different PCE SP types and dosage, and in general, four different types (SP1, SP2, SP3, and SP4) of SPs were used. Moreover, when it came to the early-age strength of UHPC, two studies were conducted. Initially, all four SPs were fixed to a dosage of

2.2% (the dosages of SP were determined by the dry matter weight, based on the total mass of all powders).

Then, another UHPC mixture was prepared with SP3 dosages of 1.85, 2,6%, and 3.0%. The results are presented below and show that the different dosages of SPs for 1-day strength contribute to a large difference in early-age strength development. However, the difference becomes minimal after three days, and almost comparative strength is achieved after seven days.

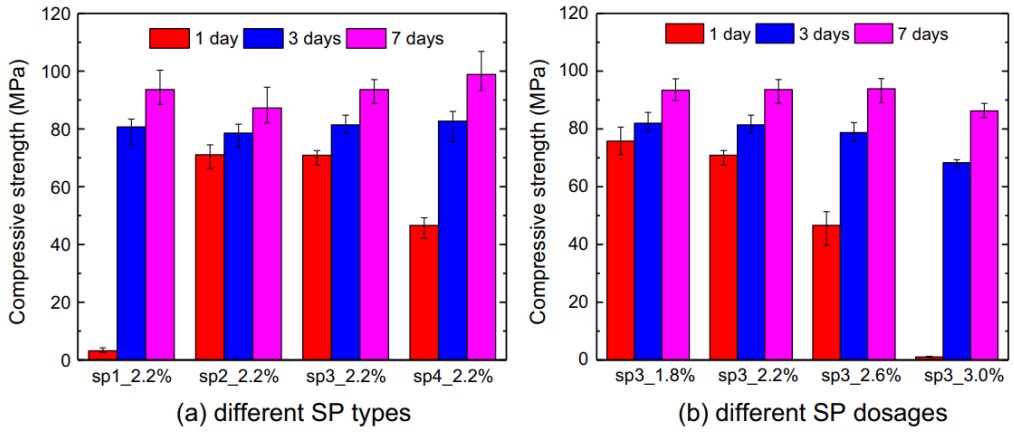

Figure 2.10 Compressive strength if UHPC with different types of SPs at a fixed dosage and the same SP at a different dosage [101].

Another study by Shi et al. [102] investigated eight different types of PC-based SPs. Figure 2.11 displays the effect of SP on the fresh and hardened properties of UHPC. The study showed a significant variation in the setting time and a good indication of the early-age strength development. In this case, a mixture incorporating P5 and P11 with a long side chain showed the highest early-age strength development. In terms of compressive and flexural strength, they correspond very well with each other.

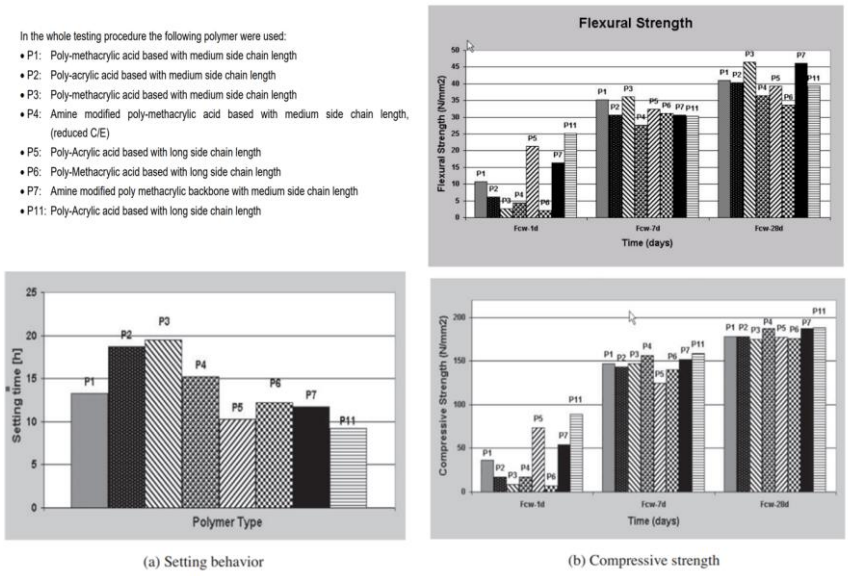

(a) Setting behavior (b) Compressive strength

Figure 2.11. Effects of different SPs on fresh, hardened, and mechanical properties of UHPC [103].

2.5.7 Steel fibers

General

UHPC is highly brittle, and the "Performance" part of its name relies on the addition of different types of fibers. This help to enhance the ductility of our material in both compression and tension. Steel fibers have a major role in increasing flexural strength, while the contribution to compressive strength will be relatively modest. In addition, it will also help in reducing the propagation of cracks. In light of cracking processes and the role of fibers, Rossi [104] divides the process between the material and structural properties. He describes this process as the following:

- Micro-crack: crack considered to be small compared to the size of the structure/specimen
- Macro-crack: crack which is not very small compared to the structure/specimen
- Active crack: crack having a displacement (normal or tangential)
- Critical active crack: crack that can end up leading to a concentration of stress and localized strains within the specimen.

This concluded that the cracking starts as a behavior of materials and then will develop into a behavior of the structure.

When workability is not essential, the long fibers can work on both the scale of material and structure (meaning on both micro-cracks and macro-cracks). A perfect example of this might be roller-compacted fiber-reinforced concrete (RCC). From research, there exists an "upper limit" for the maximum amount of long fibers we can mix into our concrete without significantly affecting the workability. However, when workability is of importance, fibers added to the concrete mixture are usually a large number of short fibers and a small number of long fibers. This is typical for pumped, sprayed, or poured fiber-reinforced concretes. [104]

When speaking of "long" or "short" fibers, the "effect of scale" needs to be taken into consideration, meaning the type and amount of fibers need to be considered. This is mainly to the geometry of our structure and the type of stress that will influence the cracks. So, depending on the size, type, and amount, the effectiveness of the fibers might not apply to all structures (small vs. large).

Type of fibers

When considering the amount of fiber that needs to be added to concrete, this is usually measured as a percentage of the total volume. This is usually referred to as "volume fraction (V_f). Another term also used for fiber is "slenderness or aspect ratio (I/d)." In addition to the distribution of fibers throughout the matrix, the shape of fibers is also one of the most important parameters affecting the properties of the composite. The shape of the fiber reinforcement is determined by their aspect ratio (I/d) and can be calculated by dividing fiber length (I) by its diameter (d). Another way to characterize and compare the properties of different fiber-reinforced concretes is actually by using this so-called "fiber factor."[105]

$$Fiber\ factor\ =\ Vf\ *\ aspect\ ratio\ =\ Vf\ *\ I/d \qquad 2.1$$

The different types of materials used in the production of fiber-reinforced concrete and their different properties will be presented in Figure 2.12.

Table 2.11 Physical and mechanical properties of different fiber types [106].

Type of fiber	Unit Weight [kg/dm^3]	Tensile strength [MPa]	Modulus of elasticity [GPA]	Strain at fracture [‰]	Alkali resistance [-]	Max temperature [°C]	Diameter [µm]
Steel	7.8	500-2600	200	5-35	high	1000	100-500
Alkali resistant glass	2.6	2000-4000	75	20-35	med./low	800	12-20
Carbon	1.75-1.91	2000-4000	200-450	4-15	high	3000	15
Polypropylene	0.98	450-700	7.5-12	60-90	high	150	50
Polyvinyl alcohol	1.3	800-900	26-30	50-75	high	240	13-300
polyesters	1.4	800-1100	10-19	8-20	med.	240	10-50
Aramide	1.42	700-3600	70-130	21-40	med.	600	12

Steel fiber is the most commonly used fiber compared to the different types. Table 2.11 show most of the frequently used ones. This is mainly due to the many favorable properties of the fiber types. The properties in reference here are high strength, high modulus of elasticity, high ductility, and excellent durability in the alkaline environment when it comes to concrete.

Steel fibers are protected in an alkaline environment when it comes to corrosion. Those closer to the surface where the concrete may be carbonated, the steel fiber might end up being corroded in the presence of moisture. However, this is not sufficient to build enough pressure that can cause spalling of the concrete. The main cause for this is the slenderness of fibers. From an esthetical point of view, this might be a problem due to the discoloration on the surface, but this will not cause any significant damage from a safety perspective.[106]

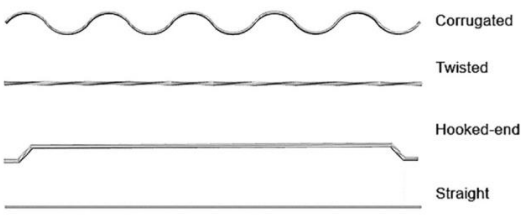

Figure 2.12. Some of the frequently used steel fibers [6]

When we compare the physical properties of fiber used in conventional and UHPC, the dimensions and content vary. In ordinary fiber-reinforced concrete, the length of steel fibers can vary between 12.7 mm to 63.5mm, and the aspect ratio will lie between 20 – 100. The diameter range is between 0.45 – 1 mm, and the amount of steel fiber will be between 0.25 % - 2 % [107]. However, the commercially available UHPC-mix, on the other hand, can have a diameter smaller than 12mm, and the total content varies between 2 and 6 vol-%[108]. It has been proven that approximately 2 – 2.5 vol-% of steel fiber at aspect ratio (I/d) between 40 to 60 is recommended for best results.

2.6 Water and binder ratio

In a UHPC mixture, a low water/binder ratio (w/b) is utilized. Previous studies [103],[110] suggest an optimum w/b ratio of 0.13-0.20 if one is to achieve a maximum relative density and spread flow. However, compressive strength of 150 MPa was achieved using a w/b ratio of 0.25 [64]. Recent studies have also shown similar results where the effect of the water to binder ratio on UHPC-performance was evaluated. An experimental study [109], with five different w/b ratios, showed how an increasing ratio influenced UHPC properties such as the fluidity and compressive strength. As expected, the result showed that the increase of w/b promotes fluidity in UHPC. In addition, we also observed the decrease in w/b ratio and showed the inverse increase of strength, as shown in Figure 2.13. The results also reflected the volume of density, and here when the ratio is 0.20, the volume of the hardened decreases by almost 1.35%, meaning the compactness decreases, resulting in UHPC. Finally, the compressive strength before and after w/b of 0.21 ratio will not increase.

No.	Water-binder Ratio	Mortar-binder Ratio	Slump Expansion mm	Volume Density kg/m^3	28-day Compressive Strength MPa
1	0.19	1.37	352	2390	117.2
2	0.20	1.37	468	2414	123.4
3	0.21	1.37	524	2391	134.1
4	0.22	1.37	569	2360	111.8
5	0.23	1.37	620	2345	96.1

Figure 2.13 Effects of w/b ratio of UHPC [109].

Similarly, another study [112] observed the effect of w/b ratio variation by holding other factors constant. The composition mixture is shown in Figure 2.14. This study aimed to see the influence of w/b on fluidity and compressive strength, as shown in Figure 2.14.

As shown in both studies, the compressive strength decreased with the increase of the w/b ratio. The range of w/b was held between 0.164 – 0.204, and the compressive strength reached its peak at 0.174. after that, we see a reduction in compressive strength, and the main reason for this is that when the w/b ratio is reduced, it will increase the viscosity of the fresh concrete. The consequence of this will be that the concrete will become challenging to vibrate and compact, leading to microcracks and large bubbles within the structure, which will reduce the compressive strength of the structure.

Material (kg/m^3)	A1	A2	A3	A4	A5
Cement	940	940	940	940	940
GGBFS	—	—	—	—	—
FA	—	—	—	—	—
SF	282	282	282	282	282
0-1 mm bauxite	240	240	240	240	240
1~3 mm bauxite	940	940	940	940	940
Steel fiber	234	234	234	234	234
SP (L/m^3)	70.5	70.5	70.5	70.5	70.5
Water	200	212	225	237	250
Water/binder	0.164	0.174	0.184	0.194	0.204
Compressive strength (MPa)					
7 days	128	130.5	115.5	110.6	120.5
28 days	149.7	150.5	145.7	146.5	141.3
Slump (cm)	0	3.9	5	8.5	10.1

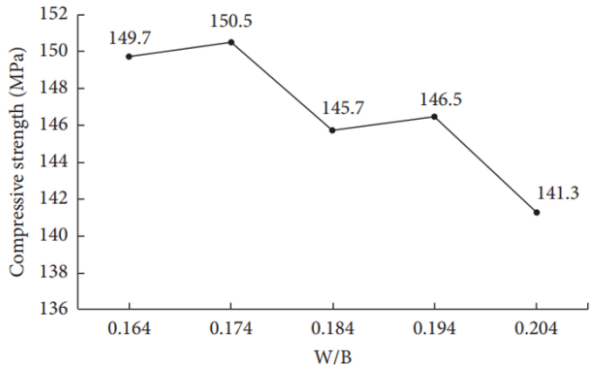

Figure 2.14 Composition mixture of UHPC and the influence of w/b on compressive strength [110].

2.7 Factors

2.7.1 Curing regimes

Since the concept of concrete maturity was introduced by Carino et al. [111], the curing temperature and curing age in the strength development of concrete have been an important topic. This has led to finding specific curing regime applications depending on resources and environmental conditions, such as why high-temperature steam curing is preferred in a precast concrete plant [112]. However, when it comes to UHPC, a more complex and close relationship exists between curing temperature and strength development than conventional concrete. This is heavily due to the presence of a large amount of silica fume and its various characteristics that influence strength development.

However, it is difficult to apply an ideal curing scheme in terms of moisture and temperature when, for example, the UHPC has been cast on-site. Furthermore, since the construction site has an inferior and unpredictable condition compared to the laboratory or a concrete plant, it is crucial to devise a realistic curing scheme based on the current condition.

When it comes to curing regimes, different applications have been implemented to observe its effect on the performance of UHPC and its influence on the mechanical properties. In earlier research, curing conditions such as standard room temperature curing, steam curing in a fog room, heat curing under atmospheric pressure, and a combination of those have been observed. In a study conducted by Koh et al. [113], he reported the result of different curing conditions, Figure 2.15. We see that 190 MPa was achieved with 90 ◦C steam curing when comparing the three different regimes. The next best out of those three was 20 ◦C water curing. When it comes to long-term strength development, we see that after almost 90 days, one can achieve almost relative values. However, what was interesting here was that when it comes to the early-age strength development between steam and water curing, almost 90% of strength development was achieved already within the first seven days. While with water curing, close to 60% of that same strength is achieved. When it comes to dry curing, only 80% of 190 MPa has been achieved within 91 days.

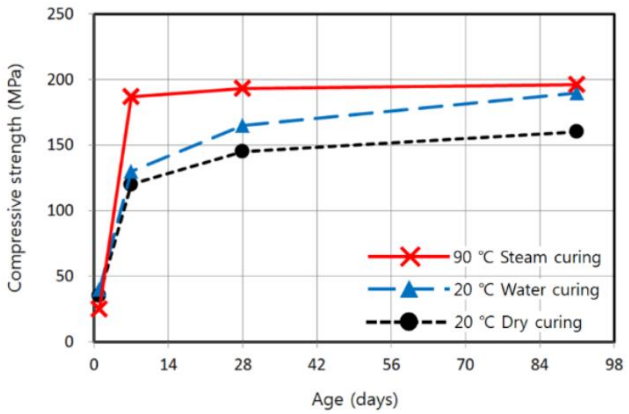

Figure 2.15. Compressive strength development with different curing conditions [113].

Room temperature, heat curing under atmospheric pressure, and auto clave curing are some of the often-used curing regimes for the production of UHPC. In another study [102], these three effects on the interfacial bonding strength between fiber and various matrices were studied to see the effects of curing on UHPC performance and mechanical properties. Results are presented in Figure 2.16.

Standard room temperature curing, one of the most common, economical, and environmentally friendly processes, achieved the lowest result among these three regimes. This is mainly because the C-S-H chain length was too short in this case, and the pozzolanic activities are weak when we have a room temperature of 20 ˚C. In contrast, a 15 – 30 MPa increase could be gained when those specimens were through steam curing. Concerning standard curing, steam curing at 90 ˚C for 12 days increased the compressive strength of these mixtures. The same effect was also shown when it came to flexural strength. Finally, compared to the two previous curing methods, autoclave curing was superior. After only 8 hours of autoclave curing, compressive strength of 200 MPa could be achieved with 3% or 4% of fiber [114]. In the same way [115], Yazici found that a UHPC mixture with a high volume of mineral admixtures that were high-pressure steam cured at 210 ˚C will have greater compressive strength than those cured at room temperature.

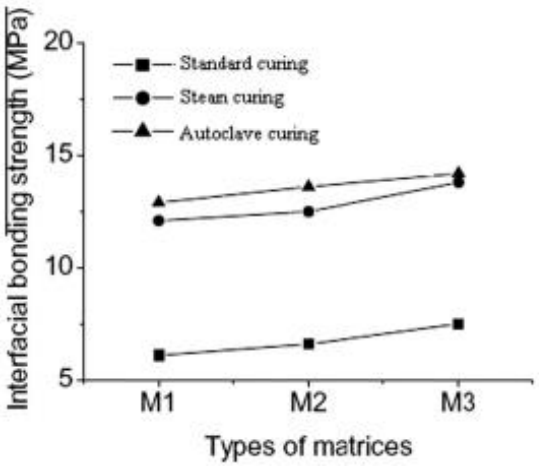

Figure 2.16. Effects of three different curing regimes on the interfacial bonding between fiber and various matrices [113].

2.7.2 Specimen size and shape

Based on previous research [116]–[118], it has become a well-known fact that the size and shape of our specimen have a significant influence on the mechanical properties of UHPC, such as compressive and flexural strength. When it comes to the size difference, Skazlic et al. 2008 (page 295) [119] observed the geometry effect of cylinders on UHPC and concluded that there is an influence when it comes to the size of specimens and that we will achieve more considerable compressive strength with smaller specimens, Figure 2.17. In addition, he also pressed on the importance and need for conversion factors that can help us enable correlation and comparison of results on specimens with different sizes.

Sample	**UHPC mixture**										**Mean increase**
size, mm	M1	M2	M3	M4	M5	M6	M7	M8	M9	M10	**(%)**
Ø70/140	13,51	5,05	7,14	4,68	21,32	-10,57	-7,10	8,29	9,16	-5,89	**4,56**
Ø150/300	21,26	-7,07	-20,00	-5,06	-6,47	-10,34	-12,57	-9,73	-12,36	-11,79	**-7,41**

Figure 2.17. The influence of specimen size on the compressive strength. These "values" are compared to a sample size Ø100/200 mm [119]. M1-M10 shows the mean value, MPa difference between those two samples against Ø100/200 mm.

In another study where both size and shape were considered for the mechanical properties of UHPC (compression and flexural). Kazemi et al. 2012 researched cubes, cylinders, and prisms with different dimensions. In the case of shapes, he compared cubes and cylinders and their influence on the compressive strength and found that cube samples consistently had higher strength than a cylinder. The results found were in agreement with previous research [117]. In the case of size effect on compressive strength, the result came to a similar conclusion as

Skazlic et al. 2008 [119] that it will decrease compressive or flexural strength as we increase the size of the specimen (Cubes, cylinders, and prisms). In conclusion, the size influence for compression and flexural strength is the same and will decrease with size increase. These are presented in Figures 2.18 and 2.19.

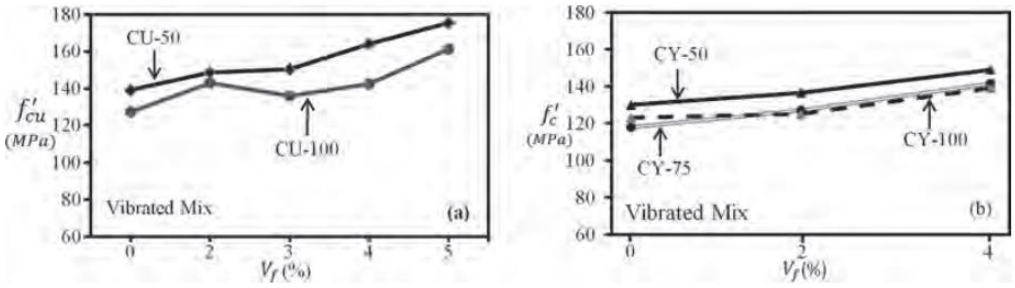

Figure 2.18 shows both the size and shape influence on compressive strength of UHPC. CU-cubes and CY-cylinder [118].

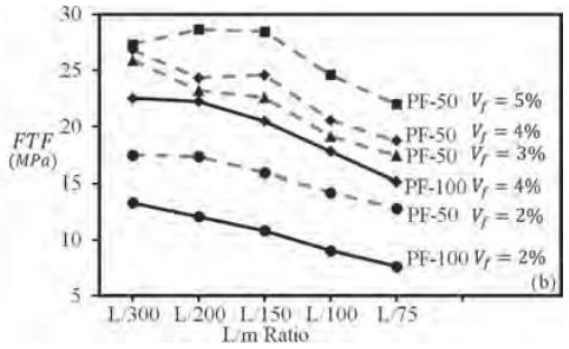

Figure 2.19 Influence of specimen size on flexural strength [118].

2.8 Properties of UHPC

2.8.1 Fresh properties

UHPC differentiates from conventional concrete in terms of its fresh properties. It has a higher viscosity than traditional concrete due to its high binder content, a large volume of fiber content, and low water-to-cement ratio. In order to lower the viscosity, a significant dose of SP is necessary to make UHPC self-consolidating [31], [120]. Since fresh properties influence hardened and mechanical characteristic performance, on-site casting, and workability, quantitative characterization of fresh UHPC mixtures is essential [31], [120], [121].

Similar test methods are typically used when assessing the flow performance, with or without modifications, for mortar, conventional concrete, and self-consolidating concrete. Some of the methods stated by Khayat et al. [122] are the V-funnel flow test, flow table test, and slump test. According to several studies [123]–[128], the test method typically used for UHPC is the flow table test to assess the flowability of the fresh mixture. Depending on the application, various spread flow testing standards have been utilized. The ASTM C143 "Standard Test Method for Slump of Hydraulic-Cement Concrete" may be suited for a non-consolidated UHPC. Moreover, the standard ASTM C1437, "Standard Test Method for Flow of Hydraulic Cement Mortar," is often utilized when the aim is to produce a self-consolidating UHPC [20]. This standard is suited to determine the flowability of fresh mortar. However, to cater to UHPC's specific features, ASTM C1856 modifies ASTM C1437 [120]. The flow measurement recommended in this standard is between 200-250mm [10]. In other research papers [20], [34], [40], [41] an acceptable range for flow between 175-300 mm is suggested. In order to release the majority of the air in the UHPC, Wille et al. [129] suggested that the flow table test spread measurement should be equal to or greater than 280mm.

In a study conducted by Alsalman et al. [123], the flow table test was employed for a mixture containing steel fiber ratios of 0 and 3 % by volume. In addition, mixtures comparing the effects of SCM such as fly ash and silica fume were investigated. SF demonstrated superior workability than FA in this investigation, with 215 and 195mm measurements, respectively. Furthermore, adding steel fiber to the mixture reduced the flowability from 190 to 185mm, according to the results of this investigation. The spread flow can be enhanced by dispersing nanoparticles or ultra-fine components into the mixes. By using 1% cement weight of nano-silica, Shakhmenko et al. [130] were able to obtain a 16 percent increase in flowability.

Several additional investigations [55], [126], [131]–[133] also had the same outcome as Alsalman et al. [123] when the steel fibers were employed in the mixture. Wang et al. [120] conducted one of these investigations, in which they tested steel fiber ratios ranging from 0 to 3 vol.% while maintaining all the other parameters constant. Flowability was significantly lowered by 22.3, 25.8, and 28.8%, respectively, in mixes containing 1%, 2%, and 3% steel fibers. One of the primary explanations for the reduction in flowability is the increased surface area of steel fiber. So, to cover the surface of the aggregates and the steel fiber, more cement paste is demanded as steel has a substantially greater specific gravity than cementitious mortar. Additionally, when the fibers are randomly placed in the matrix, they will eventually diminish the flow of the fresh UHPC. This is mainly because fibers will function as a skeleton in the mixture [31], [133].

Meng et al. [125] and Karim et al. [53] chose to establish a target measurement of flow value. Since they recognize that increasing steel fiber affects flowability, they increase the amount of SP material each time the steel fibers content were increased to obtain the value they desire. Karim et al. [53] reported that when the microfibers dosage was increased from 1 to 3%, the SP increased by more than 20%, while Meng et al. [125] tripled the amount of SP when they increased the fiber proportion from 2% to 5%.

2.8.2 Mechanical properties

Compressive strength

Compressive strength is an important quality to consider in the design of any concrete structure since it reflects the concrete's properties. This is because it provides information about the concrete's load-bearing capability before rupture. Moreover, compressive strength is the most often scrutinized trait as a result of this. Therefore, when associating compressive strength with UHPC, it is essential that a minimum of 120 MPa needs to be achieved.

Research has been done with varying fiber compositions ranging from 0 to 6% in the 16 publications that deal with compressive strength. Furthermore, depending on the fiber concentration of the concrete, diverse effects have been seen. In studies done by Le Hoang et al. [134] and Park et al. [135], steel fiber did not appear to impact compressive strength. The results of Le Hoang et al.[134] research, in particular, showed that steel fiber concentration of 1.5 to 3% had a negative impact on compressive strength.

In comparison, Ibrahim et al. [136]and Wu et al.[126] discovered that adding steel fiber to UHPC improves the compressive strength. Both acquired compressive strengths of 107 MPa and 105 MPa, respectively, without steel fibers. The compressive strength rose to 161 MPa and 150 MPa, respectively, with the addition of steel fibers. This represents a more than 40% increase in compressive strength. Furthermore, these two investigations corresponded well with other research [54], [131], [137]–[140], which indicated that when steel fiber content increased, the compressive strength increased as well.

Meng et al. [125] assessed the compressive strength when the steel fiber content exceeds 3 vol-percent. As a result of the high fiber content above 3% by volume, compressive strength was diminished due to entrapped air, and fiber clustering was observed. Meng et al. [125] attained compressive strength on 158MPa for 3vol- % steel fiber after 28 days. In comparison to 4% and 5%, they obtained 150MPa and 146MPa, respectively. Le Hoang et al. [134] observed fiber clustering with a steel fiber concentration of 3vol-%. This is a common occurrence in fibers with a high aspect ratio and a high volume content, which leads to reduced flowability and, as a result, fiber clustering. Although they observed fiber clustering, they still achieved a compressive strength of 207.62 MPa. Abbas et al. [131] and Erdogdu et al. [140] also investigated steel fiber above 3vol-%, and an increase in fiber content over 3% showed an increase in compressive strength.

Yoo et al. [54] and Karim et al. [53] investigated the hybridization of steel fibers. Both researchers discovered that deformed steel fibers had smaller compressive strength than micro straight fibers alone. However, mixing various types of fibers, such as straight steel fibers and twisted steel fibers, enabled them to attain the highest compressive strength for both studies.

Flexural tensile strength

Several studies investigated the impact fiber content has on flexural tensile strength. For example, Park et al. [135] evaluated fiber content ranging between 0.5-2 vol-%. As a result, post-cracking strength nearly rose linearly with fiber content in this investigation. The post-cracking strength of fibers with a composition of 2 vol-% was substantially higher than fibers with a content of 1.5 vol-%. Furthermore, Park et al. discovered that the post-cracking strength was affected by the aspect ratio and the volume fraction of the steel fibers, while the initial crack strength was only affected by the tensile strength from the matrix. This was also reported by other studies such as [126], [139]. Furthermore, Wu et al. [126] retained a flexural strength of 35MPa for a steel fiber content of 3 vol-%. Arora et al. [55] studied the effect of steel fiber

volume ranging from 0 to 3 percent by volume. The fiber content of 3 vol-% resulted in ultimate flexural strength of approximately 22MPa. Flexural strength of 12MPa was achieved without the use of fibers. This translates to a 45 % improvement in flexural strength from 0% to 3% [55].

Abbas et al. [131] observed a 64 % rise in peak load by raising the fiber content volume from 1% to 3%, indicating that flexural tensile strength rises with additional fibers. This is because the fibers are close together, which provides localized control of the formation of macro fractures, as mentioned earlier. Short steel fibers also showed stronger flexural strength than lengthy steel fibers. Significant gaps between the fibers can be established when utilizing long steel fibers at a low fiber concentration, such as 1-3 vol percent. Long fibers will function best if large cracks have formed [131].

[53], [54], [125], [128], [141]–[143] studied the influence of different kinds of steel fibers on flexural tensile strength. Meng et al. [125] and Zhang et al. [128] observed that flexural tensile strength rise till the deformed steel fibers reach 1 vol- %. Kim et al. [143] used three distinct types of deformed steel fibers, which illustrate the same effect as Meng et al. and Zhang et al. By employing deformed fibers up to 1 vol- %, flexural tensile strength improved by 20-40% when compared to micro steel fibers, according to the findings of this study.

For hooked and twisted steel fibers, Yoo et al. [142] studied the utilization of varied lengths and fiber content. Long hooked fibers of more than 1% by volume and twisted steel fibers of more than 1.5 % by volume significantly diminished the flexural strength. Straight Steel fibers were discovered to have the maximum flexural strength of 50.9MPa for the fiber content of 2% of the volume in this research. Similarly, Park et al. Similarly, Park et al. [135] investigated how the volume fraction and length of steel fibers impact flexural strength. The researchers discovered that the short straight steel fibers had a more minor impact on flexural strength than the long straight steel fibers at the lower fiber content.

Furthermore, compared to short and medium steel fibers, a 2 vol-% content of steel fiber led to a reduction in flexural strength for long straight steel fibers. The highest flexural strength of medium steel fiber was 49.5 MPa in this study for 2vol-%. This is 17% and 31% more than longer and shorter steel fiber, respectively.

A hybrid combination of different sizes and types of steel fibers was assessed by the following articles [53], [125], [128], [139], [141]–[143]. A study on a combination of hooked and straight steel fibers at a content of 2 vol-% was performed by Zhang et al. [128]. Furthermore, this

study resulted in the hybrid combination performing far better in flexural strength than those with single fibers hooked or straight. Ma et al. [141] obtained a similar result after doing a similar investigation using straight and hooked-end steel fibers. Karim et al. [53] investigated different hybrid combinations such as straight-twisted and straight-hooked fibers.

Furthermore, this study looked at which steel fiber concentration contributed to the highest flexural tensile strength. As a result of combining straight and hooked steel fiber, 0.5 % straight steel fiber and 1.5% hooked fiber provided the highest flexural strength. Furthermore, for the combination of straight and twisted steel fibers, 1.5% straight and 0.5% twisted produced the most remarkable results. Yoo et al. [142] did a hybrid combination of hooked steel fibers and straight steel fibers and suggested optimal values of 1.5vol-% medium straight steel fibers and 0.5vol-% long hooked steel fibers. When compared to other forms, the hooked-end performed better. This may be mainly because of its fiber-end, which can provide interlock and high bonding behavior between matrix and fibers [126].

2.9 Mixture designs

2.9.1 Main principles of mixture design

Due to the superior benefits that UHPC provides, it is employed as a structural material in a variety of constructions in a wide range of countries, as shown previously in Table 2.6 in Chapter 2.4. However, there has yet to be an idealized approach for the right constituent proportioning or mixture design. According to [50], most of the studies have endorsed the following key principles displayed in Figure 2.20 for the development of UHPC.

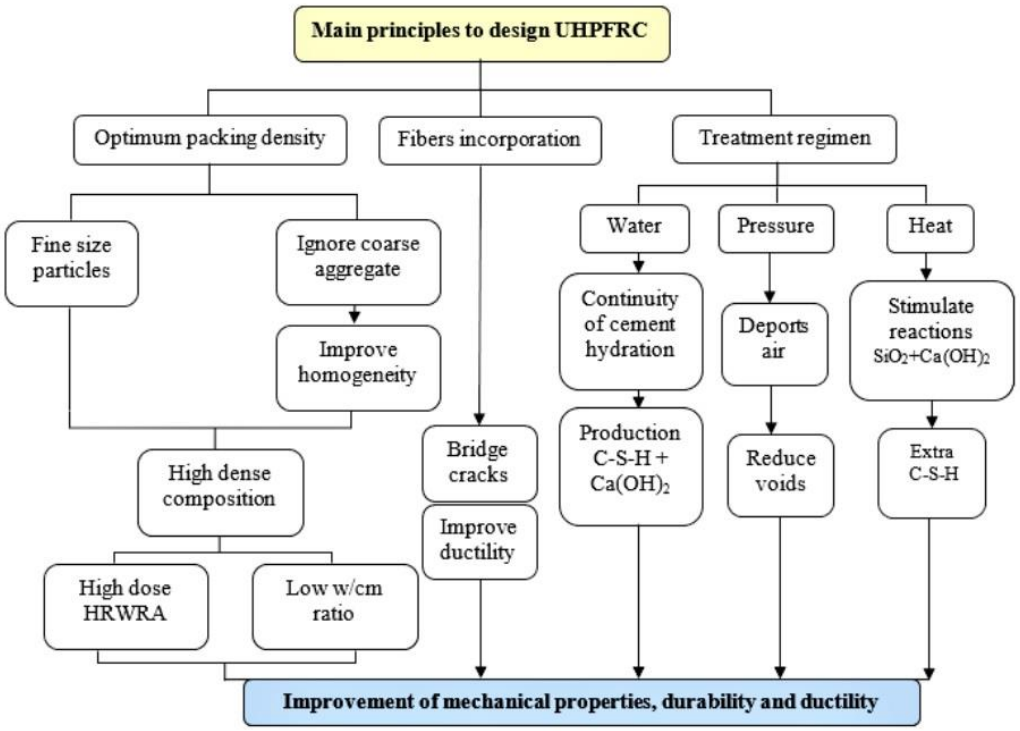

Figure 2.20 Main principles to design UHPC [50].

In brief, these fundamental principles revolve upon optimizing packing density, fiber incorporation, and treatment procedure. UHPC mixture designs need to be sustainable and cost-effective, as well as it generates optimum packing density. This is obtained by employing a high range of ultrafine particles, excluding coarse aggregates, and lowering the water to cement ratio. The denser matrix will enhance the internal microstructures as there is an improvement in the homogeneity and a reduction in porosity. As a result, the mechanical and durability attributes will be improved [7], [50]. For UHPC mixture designs, many

models have been presented throughout the literature, which address how to create a denser matrix. These models will be discussed in further depth in Chapter 2.9.2.

Fiber incorporation into a mixture helps improve the strength and ductility as the fibers bridge the cracks. Lastly, the selection of the treatment regime is an essential factor, as stated in Chapter 2.7. Adopting a high-temperature curing procedure has been demonstrated to increase compressive strength and tensile cracking strength in investigations [144]. E.g., the heat treatment speeds up the hydration product of cement with silica fumes pozzolanic reaction, resulting in far greater mechanical properties than the other treatments such as water curing [50].

Many research efforts have gone into generating different UHPC mixes. Table 2.12 shows the material proportions and properties of current commercially available UHPC mixtures and prior non-proprietary UHPC mixtures. The mechanical characteristics obtained in the research presented in Table 2.12 meet the minimal UHPC criteria.

Table 2.12 Commercially available and non-proprietary UHPC mixtures proportions and properties.

Publications	**Commercially available UHPC** [49], [108], [116], [144]	**Le Hoang et al.**[134]	**Yu et al. [12]**	**Meng et al.** [125]	**Gesoglu et al.** [145]	**Yoo et al.** [54], [142]
Year	-	2017	2015	2018	2016	2017
Unit	[kg/m^3]	[kg/m^3]	[kg/m^3]	[kg/m^3]	[kg/m^3]	[kg/m^3]
Materials						
Cement	712-1114	772-795	582-896	641-675	960	789
Fine Sand	730-1325	1134-1169	1256-1337	943-992	706-794	1104
Silica Fume	169-275	164-169	24	41-43	240	197
Other Binders	-	-	0-275	367-422	-	-
Superplasticizer	31-40	23-24	43-46	23-113	45-57	53
Water	109-211	182-188	153-179	228	234	160
Steel fiber	156-470	0-236	-	0-390	0-157	39-156
Other Parameters						
w/b	0.14-0.16	0.21	0.165-0.2	0.2	0.195	0.2
D_{max} [mm]	0.5-6	0.5	2	4.8	2.5	0.3
Material Properties						
Compressive strength [MPa]	180-225	199-219	100-117	140-166	137-162	185-220
E-modulus [GPa]	55-59	52-55	-	-	39-45	-
Flexural tensile strength [MPa]	40-50	-	12-19	10-27	7-14	34-49

2.9.2 Particle packing theory (PPT)

When it comes to the compositions of UHPC, the proportions of different grain sizes are vital. To achieve maximum particle packing density and mechanical homogeneity, the macro and micro characteristics of the components must be optimized [5]. Recipes for UHPC are frequently published without any explanation or theoretical context. As a result, it's safe to presume that UHPFRC will not make good use of a lot of binders and particles. Therefore, when employing a particle packing model, it is possible to alter the different particles to nearly whatever is needed in the mixture, ensuring that all the components are effectively engaged [146], [147]. According to various studies [146]–[149], it has been demonstrated that particle packing contributes to build a dense and uniform structure of UHPC with a reduced quantity of binder and reduced porosity. Strength, flowability, and workability have improved as a result of this, as the fine particles are filling the systems voids. Water is then ejected from the pores by the fine particles, leading to a more homogeneous distribution of water throughout the system [150]. The difference in matrix structure between UHPC and conventional concrete is depicted in Figure 2.21. The illustration shows that the particles in the UHPC structure are densely packed, with little space between them. On the other hand, conventional concrete has a less dense structure due to the presence of coarse particles and the inability to fill voids.

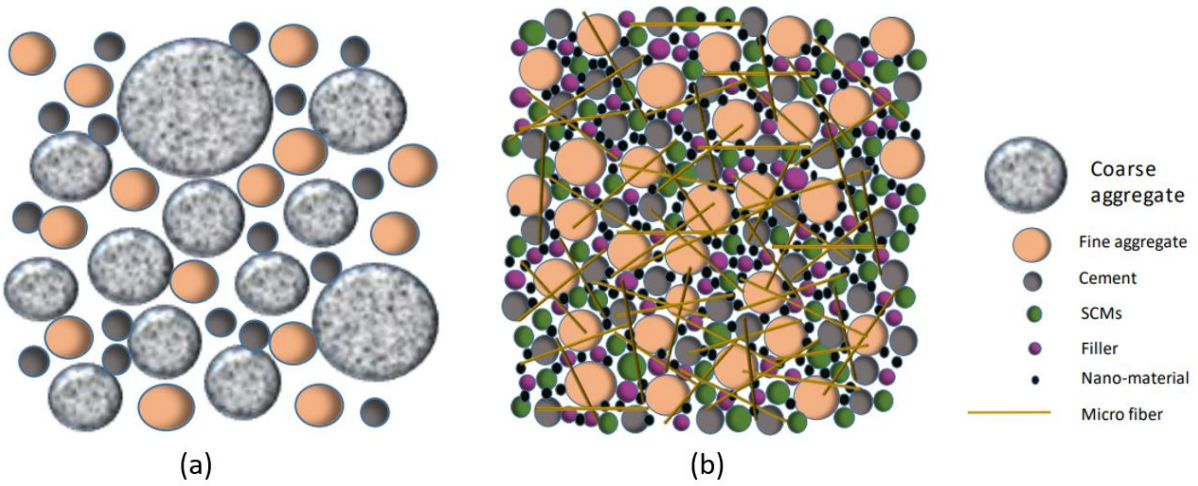

Figure 2.21 The packing system of: (a) Conventional concrete, (b) UHPC

However, regarding particle packing in UHPC, there are a variety of packing models to choose. A linear packing density model (LPDM) for UHPC mixture design was suggested by Larrad et

al. [151]. This model was proposed in the literature by Larrad et al. to forecast the ideal cement to mortar ratio and therefore based on how the different size groups of materials participate with one another. When estimating ideal amounts of cementitious materials, LPDM has displayed promising results. However, because of its linear behavior, it had an inherent flaw, as the model fails to describe the connection between packing density and material quantities [146], [147], [151].

Furthermore, Larrad et al. [151] upgraded the LPDM model to a Solid Suspension Model (SSM) by premising the principle of virtual density theory. This improved the particle density compared to LPDM. Virtual density is described as the largest density that could be obtained by placing the particles by hand one by one. [146], [149].

Based on the virtual packing density and compaction index notion, De Larrad et al. [152] enhanced the packing model to the Compressible Package Model (CPM). A compaction index was used in this model to account for the discrepancy in actual and virtual particle packing densities. As a result, it outlines the placement procedure. This model was proposed for use in the creation of ultra-high-performance concrete (UHPCs) [146].

Based on the models established by De Larrard and Sedran et al. [151], [152], Fennis et al. [153] created a mix-design approach for concrete. For these models, the packing fraction of the individual composite and the combination of the different combinations is the foundation for the mixture design approach. Moreover, employing these blend design methods has a drawback for extremely fine particles since it is challenging to determine the packing percentage and combinations of extremely fine particles. However, the principle of continuous grading is applied in this investigation's latest particle packing model. Incredibly small particles can be integrated with minimal exertion when continuously graded mixes are integrated using an integrated particle size distribution technique [146], [147]. This concept has existed for more than a century, as Fuller and Thompson [154] discovered in their investigations that the general characteristics of concrete mixes can be highly influenced by aggregate packing [146]. Andreasen and Andersen [155] later published a particle packing model supported by the findings of Fuller et al. [154], as presented in Equation 2.2. This model was developed by emphasizing that by optimizing the particle size distribution (PSD) of all the solid materials, the porosity diminishes, resulting in superior strength [149]. Equation 2.3 is presented as follows:

$$P(D) = (\frac{D}{D_{max}})^{q} \quad 2.2$$

Where,

P(D) = The percentage of particles accumulating with a size smaller than D

D = The particle size (μm)

D_{max} = The maximum particle size (μm)

q = Distribution modulus

Furthermore, the modified Andreasen and Andersen model was produced by Funk and Dinger [156], who refined the original model by considering the effect of the finest particles. The following equation is the basis for the modified particle packing model reported in [146]–[149].

$$P(D) = (\frac{D^{q} - D_{min}}{D_{max - D_{min}}})^{q} \quad 2.3$$

Here, D_{max} and D_{min} denote the maximum, minimum particle size, and D denotes the particle size. Furthermore, the fraction of coarse and fine particles in a mixture is governed by the distribution model coefficient q-value. The distribution model coefficient q tends to vary depending on what kind of concrete. A mixture rich in small particles is generated by a q value significantly lower than 0.25, while a q value significantly higher than 0.50 indicates a mixture of coarse content [149]. In a study conducted by Yu et al. [146], [147], a q value of 0.23 was utilized for the UHPC mixture. This was done in response to Hunter et al. [5] research, which advocated a q value between 0.22 to 0.25 for self-compacting concrete. Rizwan Karim et al. [149] and Borges used 0.37 as the distribution modulus for the target curve to achieve an optimal partial packing. However, Brouwers et al. [157] achieved an optimal particle packing by setting the q value below 0.28.

2.9.3 Mixing Procedure

Mixing energy

As previously indicated, UHPC requires significantly more mixing energy than conventional concrete, requiring a longer mixing time to achieve uniform particle dispersion. This is owing

to the low water to cement ratio, absence of coarse aggregates, and addition of ultrafine particle size [158]. According to El-Tawil et al.[159] the energy input varies depending on the mixer's size and paddles and the mixing rate. El-Tawil et al. evaluated the turnover time, which is the time it takes for a mixture to transition from a dry to a more consolidated state, and the flowability. According to the findings, the speed at which the fresh concrete was mixed had an influence on its performance. The workability improved marginally as the mixing speed increased, while the turnover time declined, which means a shorter mixing time. Schießl et al. [160] also accomplished this. However, increasing the speed ratio over 3 m/s did not engage in a further reduction in mixing time.

Sequence

In addition to mixing proportions, the mixing procedure is essential for the mechanical properties of UHPC to achieve the required fresh and hardened characteristics [48]. No standard specifies the technique for mixing the UHPC mixture. As a result, it was determined to go further into earlier investigations of experimental procedures to examine how they consistently blended UHPC. The mixing sequence for UHPC differs slightly from that of conventional concrete as UHPC comprises predominantly much finer components [20]. Since there are possibilities for the fine particles in UHPC to agglomerate and create chunks, dry mixing minimizes the amount of shear force essential to separate the fragments [158].

De Larrad and Sedran [84] commenced their mixing procedure by blending silica fume with a portion of SP and water. Furthermore, another portion of SP was added to the mixture, but this time with cement. Then, the remainders of the SP with the aggregates were appended. El-Tawil et al. [159] advised against adding the aggregate solely at the end of the mixture since silica sand aids in the dispersion of ingredients and inhibits fine particle agglomeration.

Numerous papers [54], [70], [131], [139], [145], [147], [161]–[163] concur that the most common trend is to mix all the dry materials first before adding water, superplasticizer, and lastly steel fibers. However, the mixing method for the dry components, the addition of SP and water, is approached differently by different investigations.

Some studies [15], [70], [129], [131], [164] proposed that the dry ingredients be mixed separately by mixing the silica fume and silica sand for about 5 minutes first. The silica fume particles are separated in this way, minimizing accumulation. Furthermore, cement and SCMs are incorporated, and the mixture is stirred for another 5 minutes. Then, while the mixer is still running, water and SP are progressively added until the desired consistency is reached for about

10 minutes before adding steel fibers. Finally, the fibers are added, and the mixture is stirred well for around 5 minutes to ensure that the fibers are equally distributed.

Other research [54], [139], [145], [147], [161], [162] advocated mixing all the dry ingredients at once for between 30 seconds to 10 minutes. Furthermore, water and SP were applied and mixed between 3 to 12 minutes. However, there were different approaches to adding water and SP. Gesoglu et al. [145] and Tafraoui et al. [162] blend water and half of the SP first before adding the remainder of the SP substant. While Yoo et al. [54], [139] and Chkheiwer [161] added SP that had been combined with water to the mixture. Finally, the steel fiber was mixed in until it was uniformly dispersed throughout the mixture.

2.9.4 Base Mixture

This study utilized an open recipe established by El-Tawil et al. [42] as the starting point for this investigation. This open recipe is based on field experience and research articles such as [70], which yielded excellent results in terms of mechanical properties. However, this recipe was eventually altered to see how the materials we had in the lab and the quantity we used affected the mechanical qualities. Table 2.13 displays the quantities and materials that were utilized in the open recipe.

Table 2.13 Materials and quantity used in the open recipe [43].

Materials	Quantity - [Ib/yd^3]	Quantity - [kg/m^3]
Ordinary Portland cement	653	391.8
Slag cement	653	391.8
Fine sand A (80-200 microns)	396	237.6
Coarse sand B (400-800 microns)	1586	951.6
Silica Fume	327	196.2
Water	272	163.2
HRWRA	26	15.6
Steel fibers	265	159

2.10 Digital Image Correlation (DIC)

Since UHPC is a heterogeneous cementitious material, it necessitates more sophisticated measurement techniques. This is significant in monitoring and assessing the detection of inhomogeneous crack propagation, strain localization, and deformation. [165]

Typically, the deformation of a single spot on a sample is determined by using traditional displacement measurement techniques such as the Linear Variable Differential Transformer (LVDT) [52]. However, Digital Image Correlation (DIC), which is high-speed photography, is one of these more advanced measuring techniques that is widely used to quantify deformation in quasi-brittle materials such as concrete. It combines optical measuring mechanics and contemporary digital image processing technology [166], [167].

This is a non-destructive technique that has been available since the 1980s and has shown to be highly efficient [166]. The foundation of this technique is based on speckle tracking, which involves tracking the movement of random spot patterns. These patterns are imprinted on the surface of a sample that is being loaded or deformed. The speckle patterns might be produced by the sample's intrinsic surface characteristics, applying laser speckle effect or paint [165], [167]. Other researchers [52], [53], [55] found that painting the surface of the specimen using white and black paint is the most straightforward approach for creating random speckles.

For DIC, multiple cameras (synched) or a single camera are used to record at different viewpoints. A single-camera can be employed to produce a two-dimensional deformation pattern in the material. However, multiple images are required to measure three-dimensional displacement. Therefore, two cameras are directed at the specimen from different angles to capture the deformation on any surface and in any direction [52].

Compared to an LVDT technique, this approach can detect the entire displacement field at every spot on the specimen's surface. Moreover, DIC acquires full-field surface deformations by sequential post-treatment of digital pictures recorded at a predefined time frame [52].

In an investigation of the flexural performance of micro steel fiber in UHPC, Rizwan et al. [53] utilized the DIC method. The aim of employing this approach in this study was to take images during the bending test to analyze flexural performance parameters and the crack pattern in terms of depth and width. The application of the DIC approach disclosed information on the impact of fibers on reducing the crack in UHPC samples.

A study conducted by Marina et al. [168] investigated vertical displacement and crack propagation. This was done in the midspan of three slab beams by utilizing the DIC technique

and LVDT sensor to compare the difference. The finding of this investigation shows that the DIC technique diverges about ±1% compared to the LVDT sensor. However, the variation might reach 3% at a lower load rate. In addition, the LVDT sensor and the DIC variers by up to 7% when it comes to crack width measurements. The variation may exceed 15% with a lower load level.

Arora A et al. [55] also used an LVDT sensor and DIC in a flexural test of a beam to demonstrate the effect of steel fiber on the UHPC response. The DIC findings in this study accurately detained the effect of matrix properties, distribution of the fiber reinforcement, crack propagation, and strain localization.

This approach is ideal for analyzing crack propagation and vertical deformation when it comes to investigating concretes, as demonstrated by various research. Therefore, in this study, the DIC technique is used to analyze and estimate the deformed specimen's vertical and horizontal displacement. With the correct cameras and software, this has the potential to increase research findings rapidly.

3 RESEARCH QUESTION

The main aim of this master thesis is to provide a small contribution to the concrete field and specifically on the topic Ultra-High-Performance Fiber Reinforced Concrete. The field of UHPFRC is vast, considering that this thesis was divided into two phases. Phase 1 was the data or research phase, where extensive research was done to build a fundamental understanding of the task at hand. This data acquisition phase that contributed to helping us build a solid understanding of UHPFRC's material and mechanical properties was achieved through a systematic literature review. This was necessary for phase 2 of this thesis which focused on the practical aspect of UHPFRC. Phase 2, which was relevant for the development aspect of UHPFRC and initially intended to solve the following questions:

- How can different constituents such as supplementary Cementing Materials (SCM), W/C ratio, and High Range Water Reducers (HRWR) contribute/influence the mechanical properties of UHPFRC?
- What are the contributions/influences of fiber type, fiber content, aspect ratio and fiber combination on the mechanical properties of UHPCFRC?
- Validation of our experimental work with the help of Digital Image Correlation (DIC) and numerical analysis.

However, due to countless limitations we have faced this past six months, which will be thoroughly reflected in the limitation sub-chapter in this chapter, this thesis was reduced to this simple research question:

- *How can different steel fiber content affect the fresh and mechanical properties of Ultra-High-Performance Concrete (UHPC)?*
- *How can different ingredients and factors influence flowability, compressive and flexural strength?*
- *Can we use DIC as a validation tool to compute displacement and crack width?*

3.1 Sub – questions

For clarification, some of the previously intended research questions, in the beginning, were considered for this purpose. The sub-questions were supposed to answer the following:

- Material and mechanical properties
    - The importance of mix optimization for UHPC.
    - Assessment of different constituents and their influence on properties of UHPC.
        - Additionally, observe different HRWR and their influence on compressive and flexural influence.
    - Assessment of the influence of the different curing methods and sequences on the mechanical properties of UHPC.
- DIC
    - Application of different DIC software (LaVision vs. GOM Correlate) for validation of our experimental program.

However, the current situation and limitations have led to incorporating most of these sub-questions into our main research question.

3.2 Limitations

NB! Our purpose here is not to assign any faults for varied factors that led to the achieved results; however, to shed light on how this has influenced our work!

Starting in this thesis, we hoped this sub-chapter would not exceed more than a single paragraph composed of four to five sentences. However, that is unfortunately not the case for this thesis. We chose to focus a little on this sub-chapter mainly because we want to communicate the shortcomings of having to work with this thesis and how greatly that has influenced our findings. Sadly, our overall findings and result that was intended to be shared initially had to be modified.

Honestly, we had no idea how to approach this and present the inadequacies that we faced during this thesis, so the best way we could think was to present our shortcomings.

Our first challenge was the resources or materials. The difficulty of acquiring the necessary materials within the intended timeframe led to compromises with the thesis. Some crucial examples of these compromises were the late arrival of intended materials led to the delay of our intended progress plan. The access to materials that, due to complications, never arrived;

in this case, it was different fiber ratios and types, led to re-editing our research questions about the influences of fiber types, aspect ratio, and combination (hybridization) from the thesis.

Furthermore, the lack of specific equipment affected the time and results of our work in experimental program. This will be expressed in the methodological chapter. This was crucial since certain aspects of the experimental testing plan are based on the prescribed standard (ASTM), and if not applied accordingly, this can affect the results. Finally, when it comes to testing our specimens, we also came across certain challenges in the application based on a certain standard. This, in short, was completely impossible because of the capacity of the machine available, and we ended up reconsidering and revising other test methods. This will also be reflected more in the experimental program under methodology.

As I have explained in the beginning, our aim here is not to assign faults, but we believe that it is crucial that we present the hindrance that led to providing these findings. So, moving forward, we redefined our research question and managed to deliver within that capacity. So, that been said, continuing from here on out, *we will be looking into the effects of steel fibers on the compressive and flexural strength of UHPC. Additionally, we also tried to incorporate DIC to see the behavior of our different prism specimens under the bending test*. This was initially intended to be used as a validation tool for our experimental program but ended up being used as a tool used to extract the necessary data.

4 CASE STUDY AND PRELIMINARY EXPERIMENTAL DESIGN

4.1 Case Study

As explained in the previous chapter, this thesis aims to investigate the effects of different constituents and fibers on the different properties of UHPC. However, due to the shortcoming we faced, the current investigation of this thesis will be on observing the effect of straight short steel fibers on the compressive and flexural strength of UHPC. To answer this question, we initially started with the material properties of UHPC and researched the importance of mix optimization. This led us to apply particle package theory within our thesis, which can help us create the optimal mix design. After carefully assessing and finding the optimal mixture "in theory," we proceeded to the next phase and applied this in a preliminary laboratory test. As per expectation, applying theory in practice was not as expected. Even though we have achieved the "optimized mix" in theory, this had to be further investigated through a course "Trial and Error" to achieve the final mixture for the final test.

This "Trial and Error" process was achieved with the help of an experimental program called "*Preliminary laboratory design*" and focused on identifying the "*Final Mixture*" through many iterations. More of the Preliminary laboratory test will come later in this chapter. Finally, after designing our Final Mixture, we created the intended test specimens (provided in Chapter 4.6) and tested them for compressive and bending tests to determine their compressive and flexural strength. Additionally, DIC cases were considered for validation purposes, but due to many complications, DIC analysis will only be used to showcase the crack propagation and placement. This is crucial for the credibility of the test results of your test specimen and for the sake of including or discarding them. Additionally, since this is valuable information, we also decided to use some of the results, such as strain development, displacement, displacement, and crack. The testing methods are thoroughly described in the methodology chapter, but the figure under shows the usual setup for different tests applied.

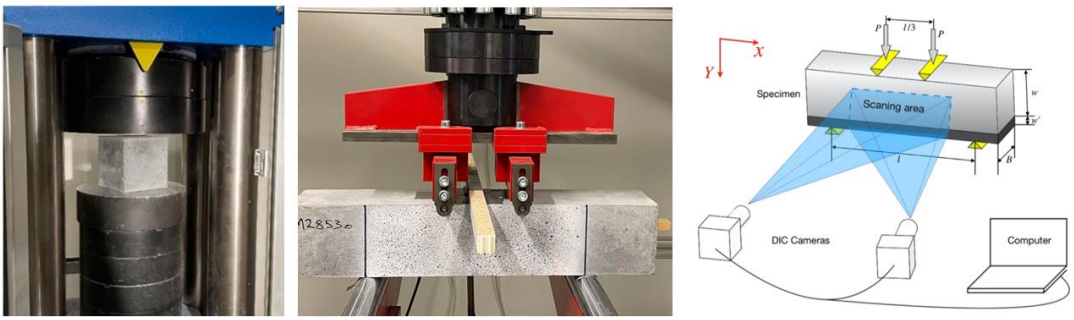

Figure 4.1: Left: Compressive test, Middle: Bending Test, Right: DIC-Setup [169].

4.2 Materials

UHPC mixture for this thesis is produced using cement (CEM), fine sand (FS) and coarse sand (CS), and silica fume (SF). The dry ingredients of the mix are divided into two components, those that constitute binder components (Cement and Silica fume) and those that constitute aggregate components (Fine and Coarse sand).

The materials that have been selected for this thesis are presented in Figure 4.2 below. Many considerations have been taken, and our choice is mainly due to their accessibility, according to what we have locally. That being said, those materials are ULTIPRO standard cement provided by Optimera, quartz sand (coarse 0.4-0.8mm and fine 0-0.4mm) provided by Mapei, Elkem micro silica, superplasticizers (SX-N by Mapei and MasterEase 2050 by Master Builder Solutions), water, and straight steel fiber provided by Dramix. Additionally, each material's chemical, physical and mechanical properties will also be presented accordingly.

Table 4.1 Material used for the development of UHPC mixture.

Constituents	Type	Supplier
Cement (CEM)	CEM II/B-M 42,5 R	Optimera
Silica Fume (SF)	Microsillica 940U	Elkem
Fine Sand (FS)	Quartz Sand (0.1 - 0.4) mm	Mapei
Coarse Sand (CS)	Quartz Sand (0.4 - 0.8) mm	Mapei
Fibers (SS)	Straight Steel Fiber	Dramix
Superplasticizers (SP) (HRWR)		Mapei
	MasterGlenium SKY 830	Master Builder Solutions
	MasterEase 2050	Master Builder Solutions
Water (w/c)	Tap/portable water	Oslomet

Figure 4.2 Materials used for developing UHPC recipe.

4.2.1 Cement

When considering binders, cement is the basic one of UHPC paste and is presented in a much bigger portion than traditional concrete. In this research, one type of cement is used, and that is a type CEM II produced by Norcem. However, the supplier is Optimera.

Table 4.2 Chemical properties.

Substituent (%)	Cement
Calcium Oxide (CaO)	57
Silicon Dioxid (SiO2)	24
Aluminum Oxide (Al2O3)	6,5
Iron Oxide (Fe2O3)	2,0
Magnesium Oxide (MgO)	5,3
Sulfur Trioxide (SO3)	3,0
Potasium Oxide (K2O)	0,65
Sodium Oxide (Na2O)	0,3
Sodium Oxide (Na2Oekv)	0,73
C3A	5,3
Chlorine (Cl-)	0,05

Table 4.3 Physical properties

Fineness (Blaine) – m2/kg	470
Density - g/cm3	3,08 g/cm3
Initial setting time (mins)	160
Soundness/Expansion (mm)	1

Table 4.4 Compressive strength properties.

16-hours (MPa)	10
1- day (MPa)	18
7-day (MPa)	28
28-day (MPa)	58

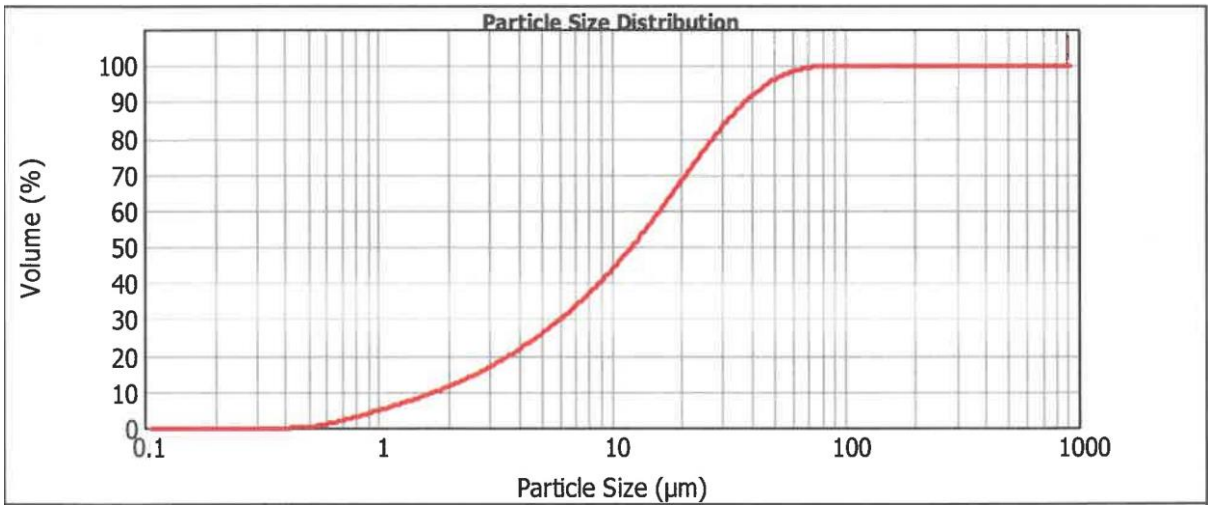

Figure 4.3 Particle size distribution of cement used in this project (Provided by Norcem)

4.2.2 Silica Fume

In this research program, one type of silica fume was used. This type was an undensified powder of color grey, a product of Elkem microsilica known as 940U. The manufacturer regarded this type as a highly reactive pozzolan and had a higher content SiO2 of more than 90%. The detail of the chemical and physical properties of the given material as specified by the manufacturer are given in the table below:

Table 4.5 Physical and chemical properties of undensified silica fume 940U.

Component	Value
SiO2 (%)	Minimum 90.0
H2O (when packed) (%)	Maximum 1.0
Loss of ignition (%)	Maximum 3.0
Retained on 45µm (%)	Maximum 1.5
Bulk density U (kg/m3)	200 - 350

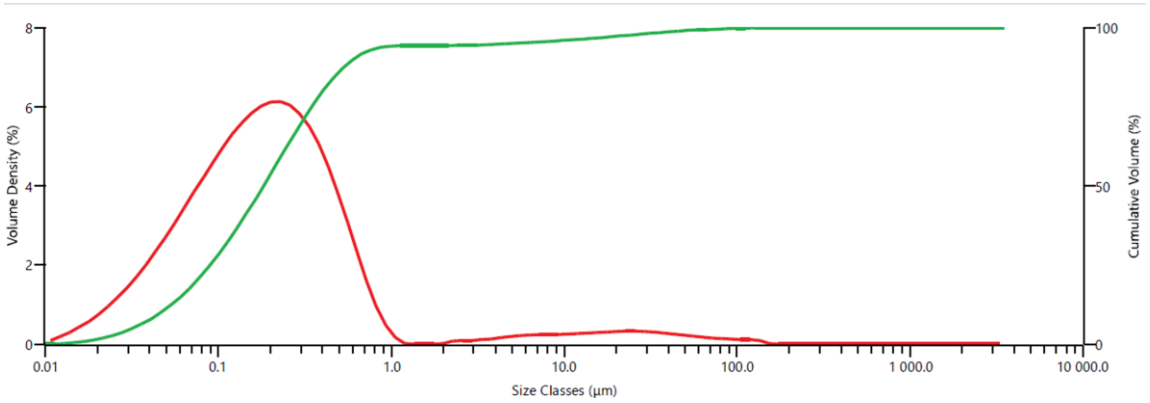

Figure 4.4 Particle size distribution of silica fume used in this project (Provided by Elkem)

4.2.3 Aggregates

Quartz sand of two different particle diameters was utilized to produce UHPC in this research. The first was categorized as fine sand with a diameter of 0.1 – 0.4 mm, and the second was coarse sand of 0.4 – 0.8 mm. The particle size distribution and other data related to both sand are provided in the Figure below.

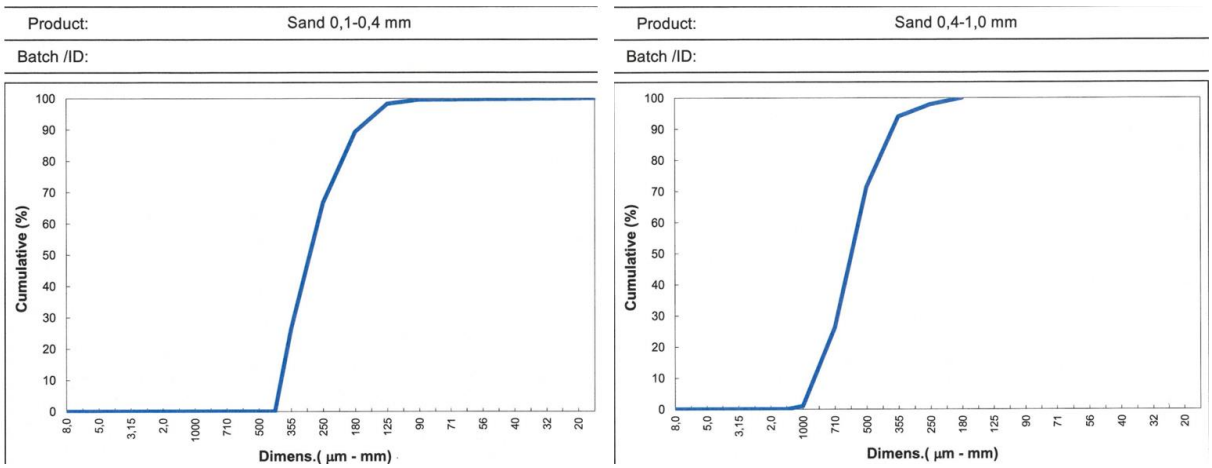

Figure 4.5 Particle size distribution of fine and coarse sand used in this project (Provided by Mapei)

4.2.4 Superplasticizer

Several superplasticizers have been considered for this thesis. This was mainly due to the accessibility and performance. As a result, we have used Dynamo SX-N (Mapei), MasterGlenium SKY 830, and MasterEase 2050 (Master Builder Solutions) in our thesis. The technical specification for each material used is in the table below.

Table 4.6 Technical data for different superplasticizers.

Product Identity	**Dynamo SX-N**	**MasterGlenium SKY 830**	**MasterEase 2050**
Appearance	Liquid	Viscous liquid	Liquid
Color	Yellow-ish Brown	Yellow	Light yellow
Active Ingredient		Polycarboxylate	Polycarboxylate
Viscosity	Easy flowing; < 30 mPa·s		
Solids content (%:)	18.5 ± 1.0	22 ± 1,0 %	25,0 ± 1,0 %
Density (g/cm3) / (kg/l)	1.06 ± 0.02	1,04 ± 0,02 kg/l	1,05 ± 0,02 kg/l
pH	6.5 ± 1	6,0 ± 1,5	10,0 ± 1,5
Chloride content (%)	< 0.05	< 0,01%	< 0,01 %
Alkali content (Na2O-equivalents) (%)	< 2.0	< 2,0 %	< 1,0 %

4.2.5 Steel fiber

Copper-coated straight steel fibers were utilized for developing our UHPC mixture. This type was the only one available for this thesis and was supplied by Dramix.

Table 4.7 Physical and mechanical properties of steel.

Type	**Density [g/cm3)**	**Length [mm]**	**Diameter [mm]**	**Modulus of Elasticity [GPa]**	**Tensile Strength [MPa]**
Straight Steel Fibers (Copper Coated)	7.85	13	0.2	200	≥2800

4.3 Mixture optimization

4.3.1 Design

Our focus for this project is the design/development of a non-proprietary UHPC mixture, also called “Open-recipe UHPC.” When designing a UHPC mixture, there are two crucial aspects one needs to consider: low water demand and high packing density. The first factor will be explored later within the experimental program chapter; however, achieving high packing density will be reflected in this chapter. For this part of our research and the development of our recipe, this was crucial, and a proper application of packing theory is essential. Mainly because this can help us control the fresh and hardened properties of UHPC, and the particle packing theory developed by Andreasen and Andreasen (A&A) is the most applied method. The theory, application of this method, and procedure are reflected in the theory chapter, and this knowledge has been applied to the optimization process of our mixture within this chapter. However, since the original model of A&A was unable to consider the effect of the smallest particle in this thesis, the modified A&A particle packing model was utilized. The equation for this model was presented earlier in the theory chapter, and based on that, the following values for particle size and the distribution modulus value “q” chosen for this thesis are presented in Table 4.8. The smallest and largest particle size was achieved with the help of particle size distribution of materials used for our UHPC mixture (Figure 4.6) and the “q” value from a scientific literature study.

Table 4.8 Smallest, largest particle size and the distribution modulus “q.”

D (µm)	**D_{min} (µm)**	**D_{max} (µm)**	**q**
0.076 - 1002.374	0.076	1002.374	0.25

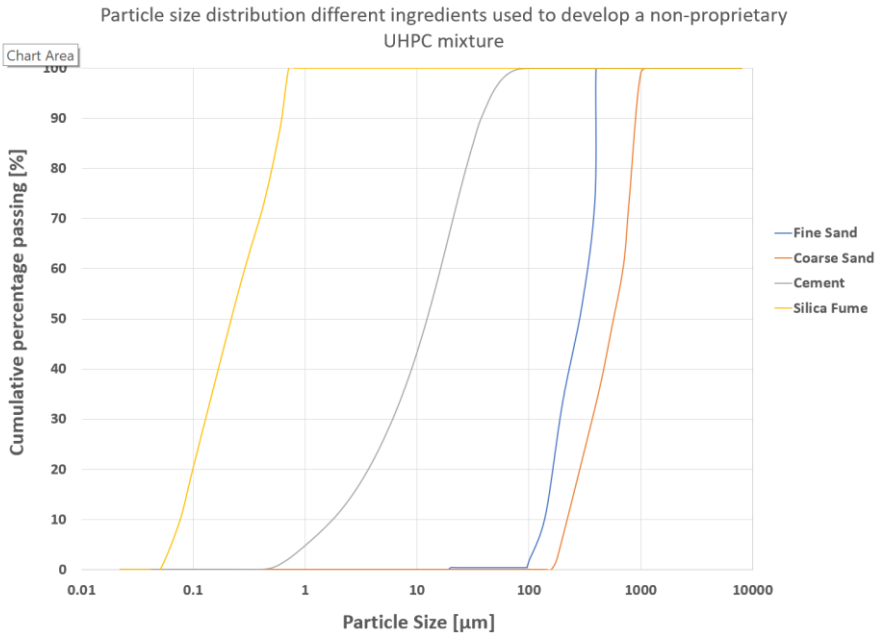

Figure 4.6 PSD of our different ingredients

As explained earlier, the distribution modulus "q" varies based on the type of concrete and is a constraint between 0 and 1. A&A found that the optimum packing is obtained when q = 0.37, but for mixtures that are very fine or have a high range of powder, a smaller value in a range of 0.22 to 0.25 is recommended. Both values have been utilized to achieve the target value for research purposes and can be observed in Figure 4.7. As for now, it might be difficult to assess these values, but this will be later used to optimize the cumulative passing percentage curve. To achieve this result, we first needed to build a reference mixture, and this was based on the "Open recipe." This mixture is referred to as "Preliminary Mixture 1" and will be first used to optimize our curve and modified to see if another mixture can be a better option. Different ratios chosen for Preliminary Mixture 1 are presented in Table 4.9.

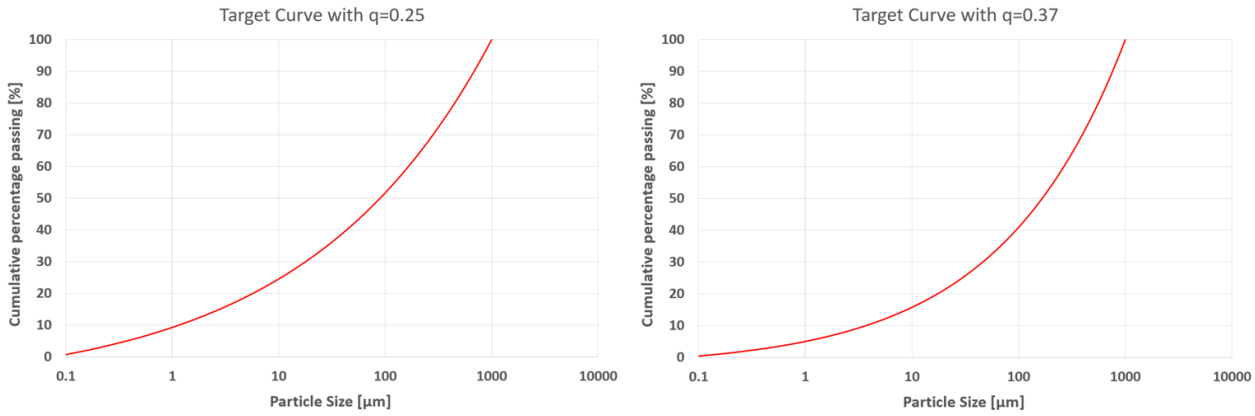

Figure 4.7 Target curves with (Left) q = 0.25 and (Right) q = 0.37.

Table 4.9 Mixture proportion for Preliminary Mixture 1 (PrM1), based on Open Recipe.

Mixture	Cement	Sand B: 0.1 – 0.4 [mm]	Sand A: 0.4 – 1.0 [mm]	SF [%]
Preliminary Mixture 1	1	1.21	0.3	0.25

Based on the particle size of our different ingredients and the mixture proportion of PrM1, we were able to produce the Preliminary Mixture 1 Curve (PrM1 curve). This modeled curve can be observed in the figure below.

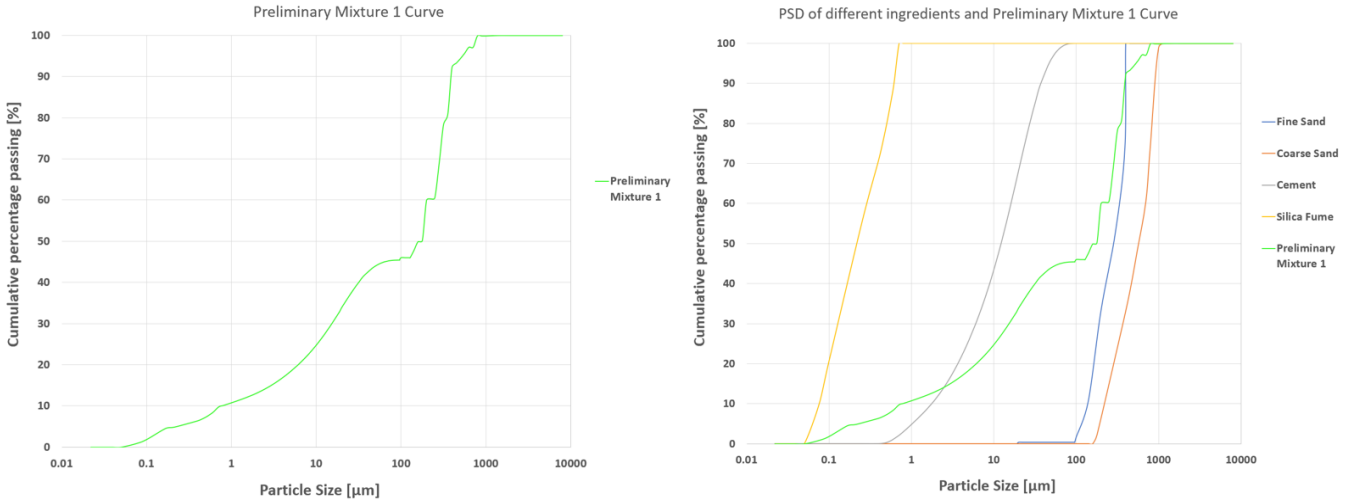

Figure 4.8 PSD (Left) Preliminary Mixture 1 and (Right) Different ingredients.

4.3.2 Mixture proportion

The proportioning of non-proprietary UHPC mixtures was developed using modified A&A curve to ensure that the maximum particle packing is achieved. The proportion of the Preliminary Mixture 1 was achieved by bringing the curve as close to the target value as possible. Since we have a target curve with two different q-values, both were assessed to see which is relevant for our mixture. This is a great way to compare with what is provided by different scientific literature studies. The result of our assessment can be observed in Figure 4.9 below and shows why we chose our q-value as 0.25.

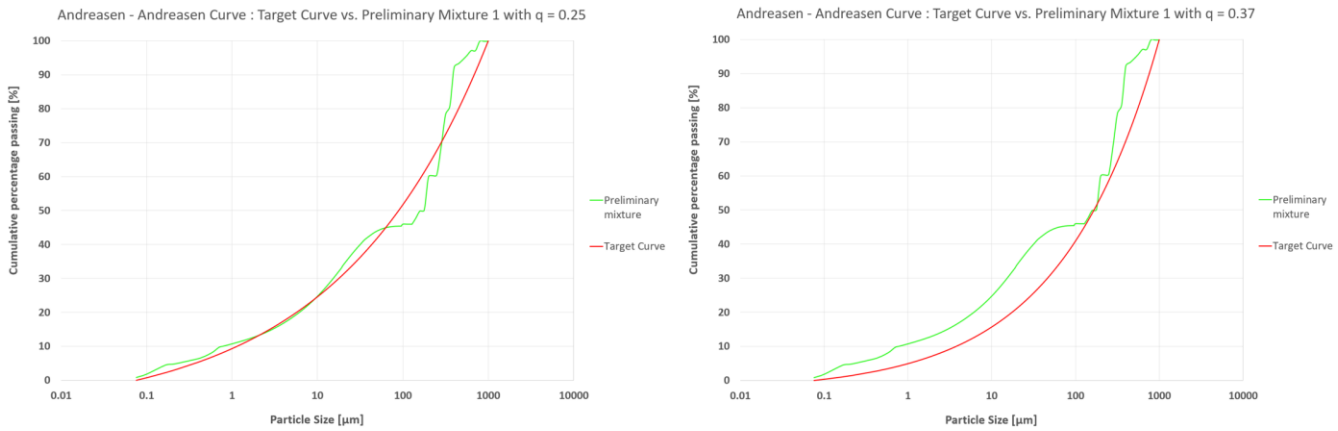

Figure 4.9 A&A Curve - Target Curve vs. Preliminary Mixture 1 (left) q = 0.25 and (right) q = 0.37.

Finally, after achieving our Preliminary design used in the experimental program, we also wanted to research other possibilities that might provide a better-mixed design. The aim of this was to observe the behavior and contribution of our different ingredients to our UHPC mix design, and for this purpose, six non-proprietary new mixtures were developed (Table 4.10).

First, we changed the different values for silica fume (SF – 5%,15%, 35%) and kept all other dry ingredients constant. In the second part, we investigated the sand-to-cement relationship. Here, the total sand-to-cement ratio was held at 1.5 and distributed with the necessary proportion throughout the different mixtures. The main idea here was to predict and observe which combination would provide a good for the target curve and a good outcome for our final mix design. The results of these trial experiments are presented in Figures 4.10 and 4.11.

Table 4.10 Development of six new non-proprietary mixture for the outcome of best mix design given by weight of cement.

Mixture	Cement	Fine Sand: 0.1 – 0.4 [mm]	Coarse sand: 0.4 – 1.0 [mm]	SF [%]
Mix 1	1	1.21	0.3	0.5
Mix 2	1	1.21	0.3	0.15
Mix 3	1	1.21	0.3	0.35
Mix 4	1	1.5	0	0.25
Mix 5	1	0	1.5	0.25
Mix 6	1	0.75	0.75	0.25

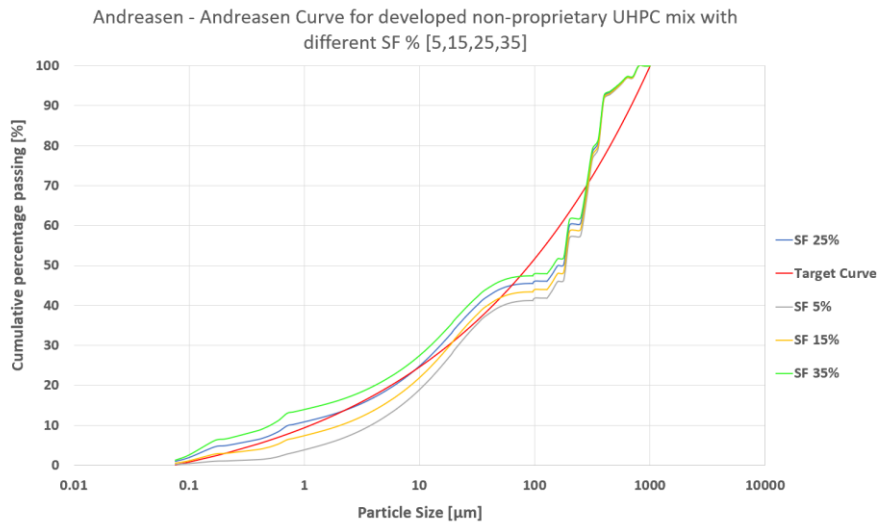

Figure 4.10 Andreasen - Andreasen Curve for developed non-proprietary UHPC mix with different SF % [5,15,25,35].

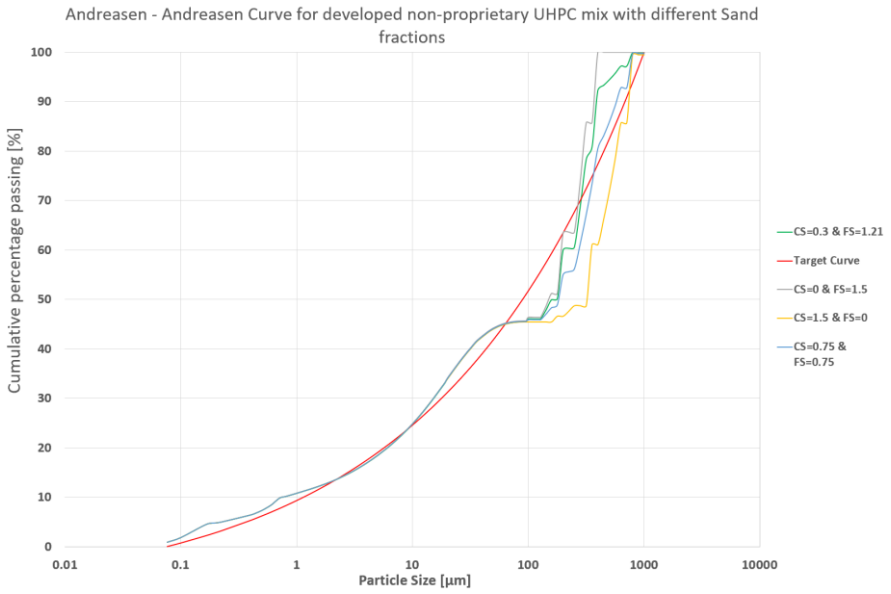

Figure 4.11 Andreasen - Andreasen Curve for developed non-proprietary UHPC mix with different Sand fractions.

In conclusion, the best qualifying mixture based on the target curve is silica fume of 0.25 (25%), fine sand of 1.21, and coarse sand of 0.3. These happen to be the ratios used for the Preliminary Mixture 1 (Preliminary Design). This will then be the reference mixture we will use for the preliminary laboratory test.

4.4 Preliminary laboratory test design

The next phase after the design of the preliminary mixture with the help of a modified A&A model was the preliminary laboratory test design. The mix optimization was designed to help us obtain a reference mixture based on the particle packaging model. So, we started our preliminary experimental trial by using this reference mixture (Preliminary Mixture 1). This trial was composed of 19 mixtures that went through a "trial and error" system/concept to achieve the intended result. The different 19 mixtures and the trial system are presented in Table 4.11 and Figure 4.12. The trial system (Figure 4.12) is a road map for achieving the best or final mixture used in this thesis. This consisted of creating the mixture, observing the workability and strength, and finally assessing if these mixtures provided us with acceptable performance. If this is the case, we achieve our result of designing the final mixture, and however, if this is not achieved, then the mixture must be re-adjusted and go through the same process.

When conducting a preliminary laboratory test, it is crucial to distinguish the determining factors. These factors are the minimum water to binder (w/b) ratio, workability (flow test), and compressive strength for this test. Therefore, before embarking on the preliminary lab test, we had to choose a form of a "reference mixture model." This was acquired from the mixture designs that corresponded to the lowest water demand and highest packing density. As previously stated under Chapter 4.3, the qualifying mixture based on the optimization process was "Preliminary Mixture 1". The combination of this together with different lowest water demands, was the pillar for the creating the bases for the preliminary laboratory test. This phase was crucial and provided us with a realistic expectation of how we could progress forward. After observing the behavior of the first six mixtures (Table 4.11), we continued with the second phase, where we cast thirteen more mixtures.

The preliminary laboratory tests' main intention was to provide the final mixture. Additionally, this test also included an investigation of the influence of different ingredients on our mixture's rheological (workability) and mechanical properties. This investigation provided insight into how the appropriate amount of different ingredients can help us achieve excellent properties for UHPC.

During this trial phase, the influence of the following components on the rheological and mechanical properties of our mixture was evaluated:

- Dosage of silica fume
- Influence of high coarse aggregate
- Influence of superplasticizer type and dosage
- Influence of different w/c ratios

If you take a closer look at Table 4.11, you can observe that we took this opportunity to research the influences of all these factors on the properties of our mixture in the first phase. Here the type of SP was held constant for the first nine mixtures, and after the first mixture, the same was applied for SF. Additionally, higher coarse aggregate content was also considered for three mixtures, and some of those were compared with those with high content of fine sand. This case can be seen for Mix 2 and Mix 5.

In phase two (Mix 7 – Mix 19), the influence of dry ingredients was held constant, and we focused on the influence due to SP and w/c. These variations of different dosages, types, and ratios can be observed for the rest of the thirteen mixtures.

After a thorough assessment of the following mixtures and their outcome, this thesis's recipe (final mixture) was developed. This was used in the final test of our specimen and is a form an extension part of the preliminary laboratory test. The final test will be presented in Chapter 6, under the experimental program.

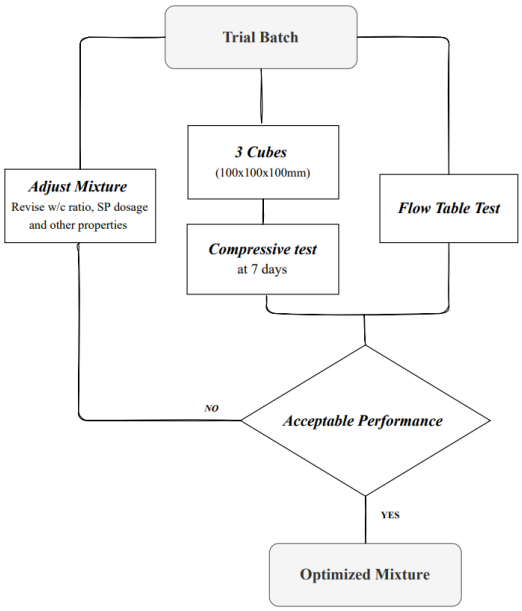

Figure 4.12 Mixture optimization process inspired by [33].

Table 4.11 Preliminary mixtures

Mixture	w/c	Cement	Silica fume [SF]	HRWRA [SP]	SAND A	SAND B	W/B	Steel fiber [%]	Type superplasticizer
1	0.21	1	0.15	5.0%	1.21	0.30	0.18	0	Dynamon SX-N
2	0.28	1	0.25	2.0%	1.21	0.30	0.22	0	
3	0.28	1	0.25	4.0%	1.21	0.30	0.22	0	
4	0.21	1	0.25	5.0%	1.21	0.3	0.17	0	
5	0.28	1	0.25	2.0%	0.30	1.21	0.22	0	
6	0.28	1	0.25	8.0%	0.30	1.21	0.22	0	
7	0.23	1	0.25	6.5%	1.21	0.30	0.18	0	
8	0.24	1	0.25	6.5%	1.21	0.30	0.19	0	
9	0.25	1	0.25	6.5%	1.21	0.30	0.20	0	
10	0.23	1	0.25	6.5%	1.21	0.30	0.18	0	MasterGlenium SKY 830
11	0.25	1	0.25	6.5%	1.21	0.30	0.20	0	
12	0.24	1	0.25	8.0%	1.21	0.30	0.19	0	Dynamon SX-N
13	0.25	1	0.25	8.0%	1.21	0.30	0.20	2%	
14	0.25	1	0.25	6.5%	1.21	0.30	0.20	0	MasterEase 2050
15	0.24	1	0.25	8.0%	1.21	0.30	0.19	0	
16	0.25	1	0.25	6.5%	1.21	0.30	0.20	0	
17	0.25	1	0.25	8.0%	1.21	0.30	0.20	0	
18	0.25	1	0.25	10.0%	1.21	0.30	0.20	0	
19	0.25	1	0.25	12.0%	1.21	0.30	0.20	0	

4.5 Recipe

The development of the mix recipe for the thesis has used “Open Recipe” as a reference model. Furthermore, we modified the recipe through theoretical and practical means to obtain the Final Mixture. Particle Packaging Theory was applied to find the optimal mixture design for our mixture. Furthermore, the theoretical model was evaluated experimentally to observe its credibility and achieve the final mix design. After incorporating these two applications and evaluating different trial mixes, we finally developed a UHPC mixture for this thesis. We have provided the material proportion and the final UHPC recipe in the tables below.

Table 4.12 Proportion of materials in the UHPC mixture by weight of cement.

CEM	SF	FS	CS	SP	W	SS
1.0	0.25	1.2	0.3	0.055	0.25	0 – 2% by vol

Table 4.13 UHPC Recipe (Final Mixture)

No.	CEM [kg/m3]	SF [kg/m3]	FS [kg/m3]	CS [kg/m3]	SP [kg/m3]	W [kg/m3]	SS [kg/m3]
1	783.6	196.2	951.6	237.6	23.4	196.2	0
2	783.6	196.2	951.6	237.6	23.4	196.2	39.25
3	783.6	196.2	951.6	237.6	23.4	196.2	78.5
4	783.6	196.2	951.6	237.6	23.4	196.2	117.75
5	783.6	196.2	951.6	237.6	23.4	196.2	157

4.6 Casting and test program

The test or casting program was mainly based on fiber availability. Therefore, the initial plan was adapted to different ratios, types, and combinations. However, this was modified to adapt to the availability, and the final casting/mixture program used for this thesis is presented in Table 4.14. To summarize, we had two types of specimens, depending on the test type. Cubes were used for compressive and beams for the flexural test. The test was dependent on fiber content, consisting of five variations (0 – 2 % by vol), and three samples were used for each mixture. In other words, we had three samples for each cast/mixture representing different fiber content. Additionally, the testing of the specimens for compressive strength was divided into 2 phases, 7 days and 28 days. However, the beams were only tested after 28 days.

Table 4.14 Number of specimens and test program.

Number of specimens and test program					
Mixture	**Steel ratio (%)**	**Curing and Test days**			
		7		**28**	
		Specimen		Specimen	
		Cubes		**Cubes**	**Prisms**
		Compressive Test		***Compressive Test***	***Flexural Test***
Number of Specimens					
1	0%	3		3	
2	0.50%	3		3	3
3	1%	3		3	3
4	1.50%	3		3	3
5	2%	3		3	3
Sum		**15**		**15**	**15**
Total samples		**45**			

5 METHODOLOGY

This chapter will reflect on the different tools and methods used to provide an answer to our research questions. Several options had been considered, such as numerical simulations, but this was limited to the two approaches due to different issues. The background information and knowledge about UHPC were first obtained with the help of a systematic literature study. This was a crucial aspect in helping us navigate and map our expectations towards the topic. Additionally, a qualitative and quantitative approach was implemented in the form of experimental or laboratory tests. This chapter will present the procedures undertaken to help us achieve our results by applying these different approaches.

5.1 Literature review

A thorough investigation was conducted to achieve a broader and deeper knowledge of the research topic. Furthermore, this will aid in analyzing the findings of the experimental investigation. An emphasis was made throughout this investigation on previously published scientific studies in the field of UHPC. The objective of this systematic review was to identify relevant studies that may aid us with our research topic.

The strategy utilized in literature searches was inspired by [170], which is an article conducted with a systematic review that our supervisors offered us to familiarize ourselves with the process. Furthermore, the following steps which were inspired by this article have been implemented within this research study and shown below.

- Search strategy and search terms
- Keyword search
- Applying filters
- Full-text analyses
- Analyses and data extraction

Research questions

The aim of this systematic literature study is to determine the impacts of material composites, steel fiber reinforcing, and other parameters such as curing regime, specimen size and shape on compressive and flexural strength. The contribution of particle packing theory will be analyzed in this study. Finally, Digital Image Correlation (DIC) is incorporated to validate some of the results within the thesis based.

These set of questions were therefore assessed:

1. *How does the different material composites impact the compressive and flexural strength?*
2. *What are the main factors or parameters that affect the compressive and flexural strength in UHPC?*
3. *What different fiber types, combinations and volume contents affect the compressive and flexural strength of UHPC.*
4. *Assessment of particle packing theory*
5. *Assessment of DIC as validation tool within UHPC.*

Search strategy and search terms

By reviewing and analyzing suggested literature studies provided by the project supervisors [5], [15], [39], [53], [171], the authors got more acquainted with terminology and general knowledge of the research field. As a result, the authors also discovered the experts in the topic of UHPC, whose work is frequently cited by other researchers such as Wille et. al. [129] and Russell et. al. [20].

Database

Scopus was utilized in this thesis to conduct a systematic literature search, which yielded significant research papers. A database like this is used extensively by engineering researchers, as there is availability for essential and cutting-edge research of the highest quality in a certain study subject.

Keywords and concept development

Next, by analyzing significant terminology utilized in several articles and their sources provided by the supervisors, it was possible to establish different sets of keywords for different research question as shown Tables 5.1, 5.2 and 5.3. Different categories for the different literature searches were established as shown in the tables and Boolean operators such as "OR and “AND” were used to combine the keywords into developing a search string for each literature search by combining these concepts.

Table 5.1 literature search for the impact of material composition, steel fibers, and factors on mechanical properties.

Concept 1	Concept 2	Concept 3
UHPC	Steel fibers	Flexural
Ultra-high-performance concrete	Experiment	Tensile
UHPFRC	Fiber type	Compressive
Ultra-high-performance fiber reinforced concrete	Fiber ratio	
	Numerical	
	Microfiber	
	Macrofiber	
	Hooked fiber	
	Straight fiber	
	Twisted fiber	

Table 5.2 literature search keyword for particle packing theory

Concept 1	Concept 2
UHPC	Particle Packing
Ultra-high-performance concrete	Andersen particle packing
Ultra-High-Performance Fiber Reinforced concrete	Anderson & Anderson packing model

Table 5.3 Keyword for literature search of DIC

Concept 1	Concept 2	Concept 3
UHPC	DIC	Flexural
Ultra-high-performance concrete	Digital image correlation	LVDT
Ultra-High Performance Fiber Reinforced concrete	DIC camera	Linear variable differential transformer
Concrete		

Criteria for data selection

The papers that were only limited for English-language publications, journal articles and journal articles published during the last two decades (2000 -2021). The review of publications over the past two decades is due to the fact that different nations have invested heavily in research programs to expand understanding within the UHPC since the early 2000s [5]. Full text review was then performed and many of the publications turned out to be either unrelated or extremely particular to other disciplines of study, such as Earth and planetary sciences, medicine, physics, and astronomy, among others. Additionally, other publications addressed unique themes such as structural components such as slabs, and loadings such as impact and explosion, and the utilization of different types of fibers. Since these studies fall outside of the scope of this study's research question, they were omitted. Only the papers that satisfied the criteria in Table 5.4 was kept for the thesis.

Table 5.4 Exclusion and Inclusion criteria for literature search

Excluded	Included
Structural elements (e.g., bridge girders, slabs, walls)	Experimental paper
Other loading than tensile and compressive strength (e.g., blast and impact)	Compressive and flexural tensile strength
Non- steel fibers reinforcement	Investigation of material composition effect on compressive strength and flexural strength
	Investigation of other UHPC factors (e.g., specimen size and shape and curing regime)
	Usage of DIC technique on flexural bending test
	Investigation of steel fiber reinforcement

5.2 Experimental program

5.2.1 Test specimens

Cubes and prisms are the only molds accessible in the lab, and therefore they are employed in this experiment shown in Figure 5.1. The cubes are 100mm x100mm x 100mm in dimension and are composed of plastic. On the other hand, the prisms are 100mm x100mm x 500mm in dimension and are composed of steel. In terms of form, both of the mold measurements meet the requirements set out in the NS-EN 12390-1 standard. Furthermore, both types of forms are non-absorbent materials, which is also required. The same forms are utilized for all the mixtures, consisting of six cubes and three prisms.

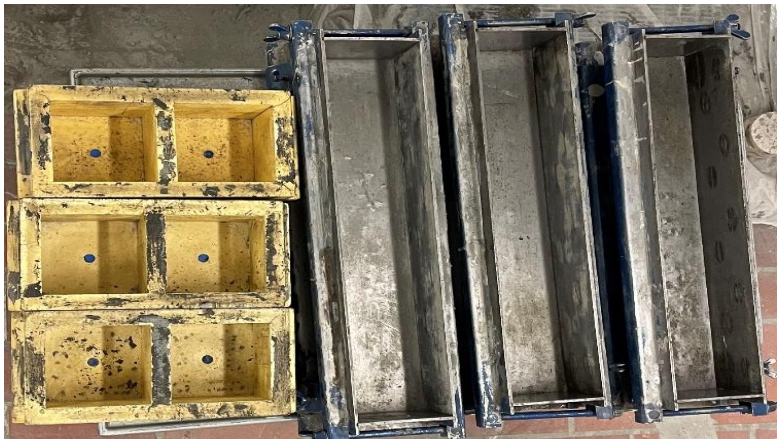

Figure 5.1 Specimen molds available at the lab

5.2.2 Mixing procedure

Based on minor adjustments to the previous studies mentioned in Chapter 2.9.3 two types of mixing processes were investigated in this paper to evaluate which provided the optimum flowability. Water and SP substances are the main difference between the two mixing processes.

Prior to mixing, the mixing machine was thoroughly cleaned to ensure that no particles from earlier experiments remained, which could affect the results. The mixing of the UHPC was performed using Zyklos ZK 30 E, and the speed of the machine was held constant for all the mixtures.

Figure 5.2 Zyklos ZK 30 E mixer used in this experiment

Preliminary mixtures mixing procedure

The trial mixtures were made in small batches, as there were three cubes for each mixture being tested for compressive strength. Figure 5.3 outlines the mixing process comparable to that employed by Chkheiwer et al. [161].

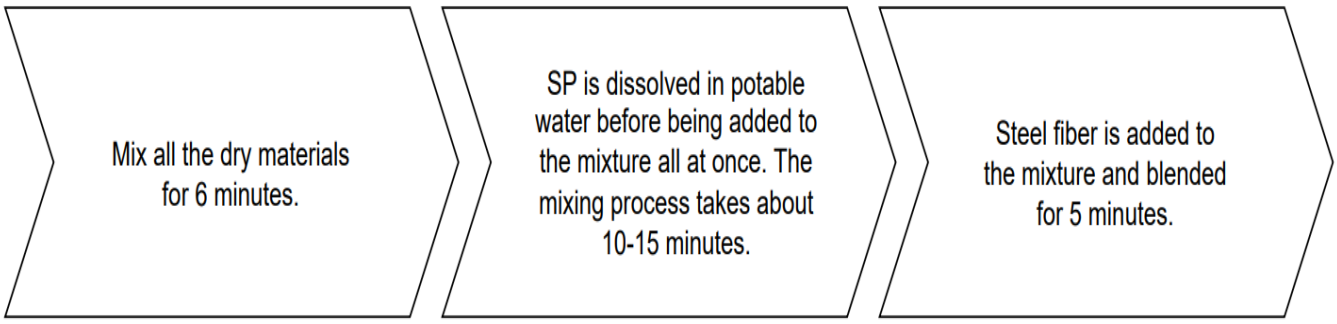

Figure 5.3 Mixing process for the trial mixtures

Optimized mixtures mixing procedure

A step-by-step mixing procedure for the optimal mixture was devised after a series of preliminary experiments were completed. Since multiple specimens were needed for both compressive and flexural tests, the optimized mixtures were made in large batches.

At the initial stage, all the recipe's ingredients stated in Table 4.13 were weighed using a scale to an accuracy of ±1 gram. Furthermore, the two types of sands and the silica fume were put into the mixer first and then dry mixed for 3 minutes. Then cement was then added to the mixture and mixed for another 3 minutes. This is done to ensure that the silica sands and silica fume, which are very fine materials, were disseminated evenly throughout the cement particles. Additionally, it prevents any agglomerations that could otherwise arise. The addition of the dry components to the mixture and the condition of the mixture after each mixing phase are depicted in Figure 5.4.

Figure 5.4 (a-f) Weigh-in and addition of the dry ingredients

Furthermore, water and superplasticizer were applied after a total of 6 minutes of dry mixing. For this study, it was preferred to add half of the water and 20% of the SP to the mixture first. Moreover, water and SP were gradually added while the mixer was spinning based on a lab trial experiment and literature review. The dry ingredients are mixed for 15 minutes with water and SP, and only 20% of the SP material is set aside for later use while all water is added. Furthermore, steel fiber is added to the mix in a slow manner. This ensures that there is no accumulation and segregation and that there is even dispersion. The mixing process is repeated for another 5 minutes while gradually adding the remaining 20% of the SP. This is then observed after 5 minutes if the steel fibers are thoroughly distributed, and the UHPC mixture has achieved an acceptable consistency. If this is not the case, additional 2-5 minutes of mixing time would be considered.

The UHPC mixture will then be investigated for flowability in the following phase. Figure 5.5 and Figure 5.6 display the addition of water, SP, and steel fiber to the mixture and the state of the mixture after each mixing phase.

g) In the center of the dry mixture, half of the water and some SP substance is added.

h) Water is gradually added to the mixture while the mixer is running.

i) While the mixer is running, SP is gently incorporated into the mixture.

j) All of the water and 80% of the SP are added to the mixture.

Figure 5.5 (g-j) Addition of water and superplasticizer

k) Addition of steel fibers to the UHPC mixture in a well-distributed manner.

l) The remaining 20% of the SP material is added to the mixture.

m) The UHPC mixture's final state when steel fiber is incorporated.

n) Demonstrate the flowability of the UHPC mixture's final phase.

Figure 5.6 (k-n) Addition of steel fibers and the remaining superplasticizer

5.2.3 Casting and curing regime

Once the flow test has been completed and verified within an acceptable range, the UHPC mixture is ready to be cast inside the molds specified in Chapter 5.2.1. However, prior to casting, oil was smeared on the surface of the cubes, and prism forms to achieve a smooth surface on the bottom and the sides. Additionally, it also helps with reducing friction so that UHPC does not stick to the molds. Furthermore, the cubes are filled in one layer into the molds without any internal vibrations or consolidation. This is done as the UHPC produced for this report is a self-consolidating, and, therefore, it is no need for vibrations in accordance with ASTM C1856. However, the casting procedure for the prisms, on the other hand, is done in accordance with EN 14651 [172]. This standard specifies the casting technique for metallic concrete samples and is followed thoroughly, except for skipping the taming of the samples. Figure 5.7 depicts the method for filling the mold, which consists of phases one and two. In phase one, UHPC is filled in one layer in the middle of the mold up to approximately 90% of the height. The mold is then topped up slightly over-mold height at both ends, as shown in

phase 2 in Figure 5.7, before being leveled out with a trowel. The total time for the whole casting procedure was about 15-20 minutes after the mixing. As per ASTM C1856, the tops of all the samples were promptly covered with polythene after casting to prevent water evaporation of the top surface.

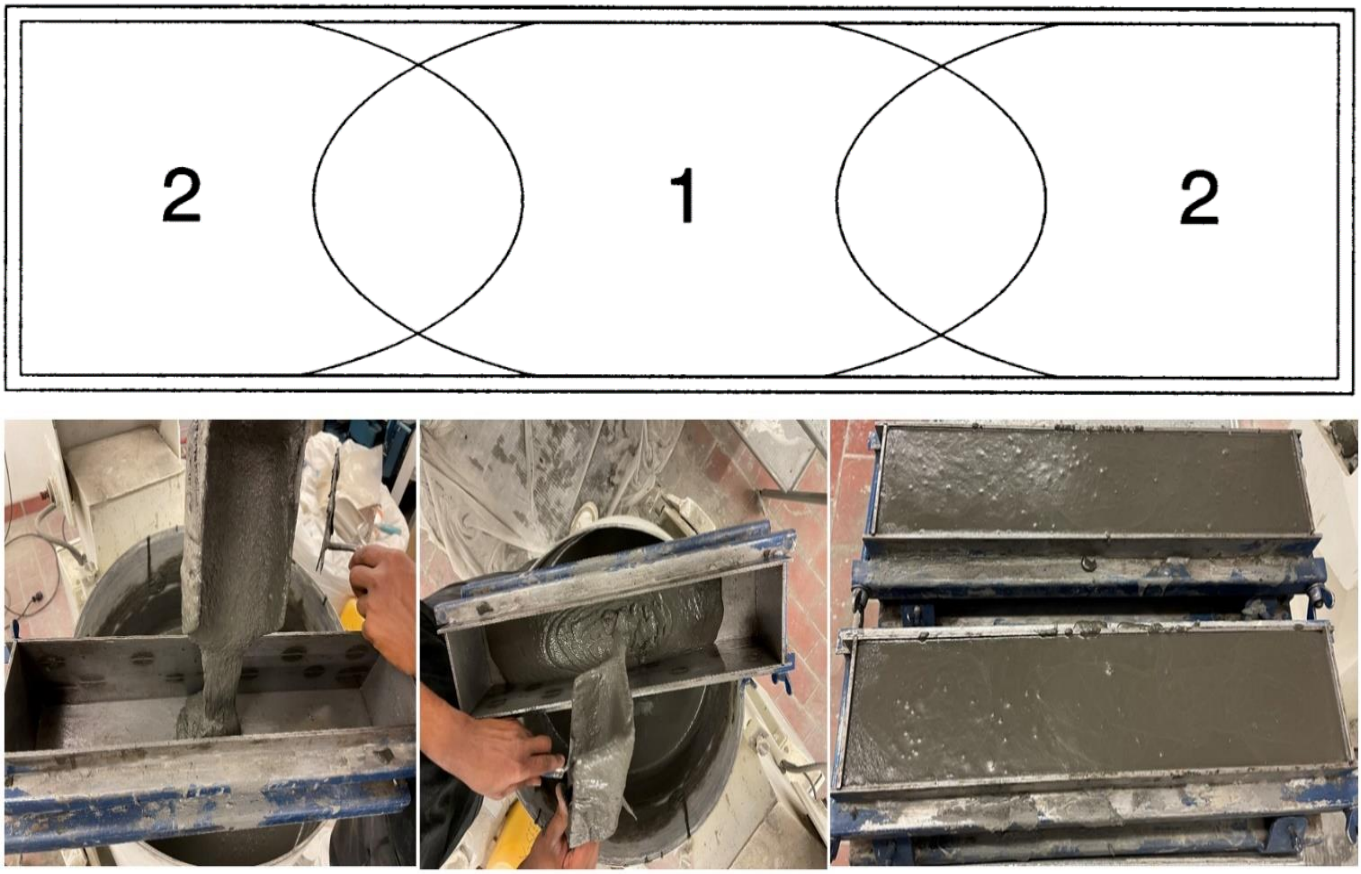

Figure 5.7 Casting direction of the beams [173]

For the curing of UHPC specimens, no unique technique is used due to the lack of equipment. After casting, the specimens are set aside for 24 hours at a room temperature of 20±5 degrees Celsius with a plastic cover on the surface. After 24 hours, the specimens were all de-molded and placed into the water chamber. The water utilized in the water chamber had around 20±2 degrees Celsius. Seven and 28 days are the two curing regime periods for UHPC samples counting from the day there were cast. All samples are then piled inside the water chamber, as shown in Figure 5.8.

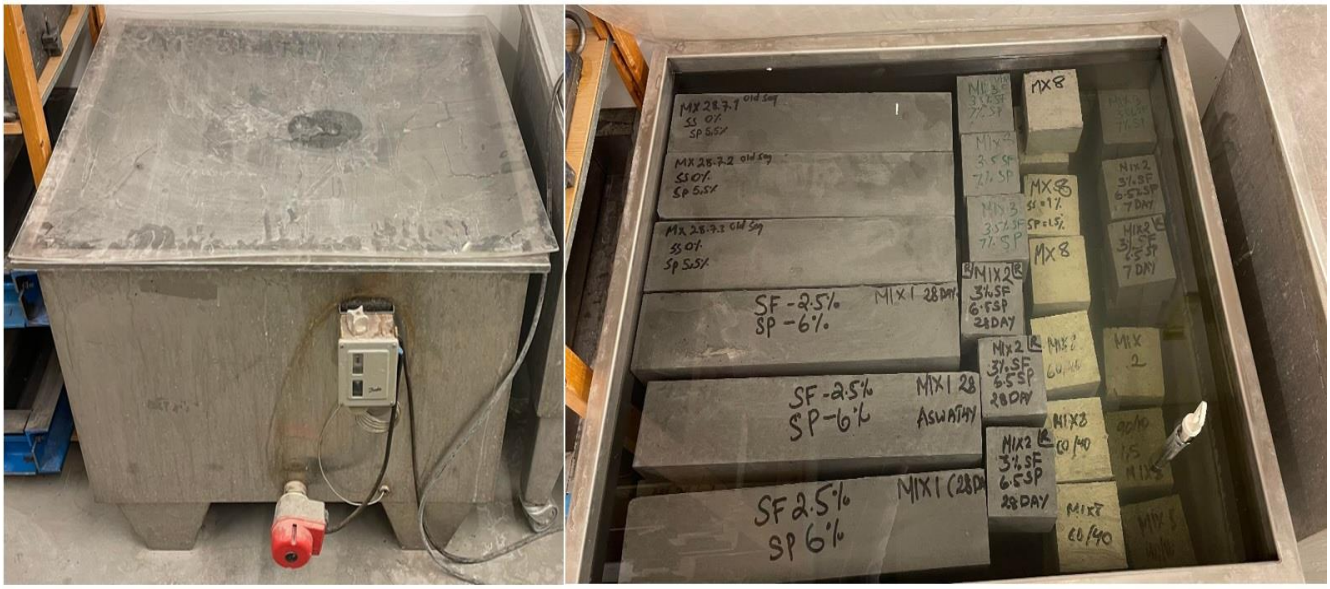

Figure 5.8 Water chamber used for the curing regime.

5.2.4 Test Methods

Flowability

The quality of the newly mixed UHPC is determined by performing the spread test as suggested in the literature. For this study, the spread test is performed in accordance with the standard ASTM C1437 "Standard Test Method for Flow of Hydraulic Cement Mortar" [174]. According to the specification, the flow table must be a circular steel plate and have at least a diameter of 300 mm. The mini cone utilized must also have the following diameter of 70mm at the top, 100mm at the base, and a height of 50mm (depending on the American or European standard, this height can vary between 50 and 60mm).

Figure 5.9 Flow table apparatus required in ASTM C1437 [33].

However, if such equipment is unavailable as it was for this thesis, other solutions and materials were utilized to perform the test. This was the case with the assessment of workability at the initial stage of the preliminary test (Mixture 1 to 6). For these mixtures, a slump cone test was applied to assess the workability in accordance with ASTM C1611 [175]. This consideration was done due to the presence of a slump cone as the only testing equipment available at the lab. The dimensions of the slump cone are 100mm at the top, 200mm at the base, and a height of 300mm, as displayed in Figure 5.10.

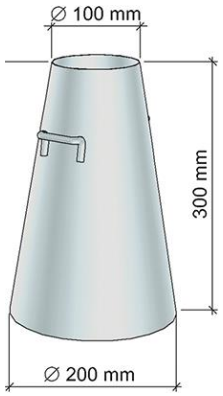

Figure 5.10 Cone used in the slump test for the initial preliminary test (Mixture 1 -6) [176].

After consulting with the right party to gain access to the proper equipment and realizing this was unachievable, we had to consider other options. We had the only option to create part of the testing equipment ourselves, as this was essential for the upcoming flow test. In this case, one has to consider that the equipment to be utilized is made of a non-water-absorbent material. As a result, a steel bottom plate suitable for slum-testing is utilized in this research. Furthermore, a 3D printer was also used to create a mini cone with the measurements described above, as shown in Figure 5.11.

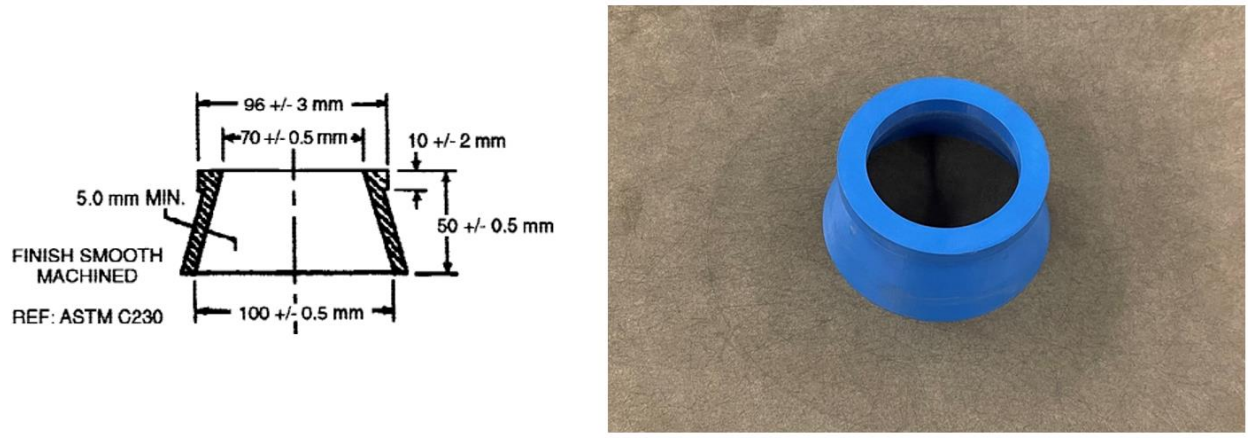

Figure 5.11 Mini cone and steel plate used.

The method for this test commences with moistening and drying the mini cone and the steel bottom plate with a damp cloth. A laboratory worker places the cone on the bottom plate and keeps the cone securely in place while the cone is filled until it reaches the upper rim. The cone is filled up in one cycle without any compacting or table drop since it is a self-consolidating UHPC. Finally, any residue and spilled concrete are removed from the bottom plate.

Next, the mini cone is raised gently in a vertical motion, and as it spreads, the residual material attached to the cone is wiped off and added to the spread test on the bottom steel plate. Lastly, the spread diameter is measured after 2 minutes have passed in two orthogonal directions. The spread value is then determined using the average diameter of d1 and d2 shown in Figure 5.12. As stated in the literature in Chapter 2.8.1, a spread value ranging between 175-300mm is acceptable, but in this report, a target spread value of 200mm was set as the minimum requirement for all mixtures.

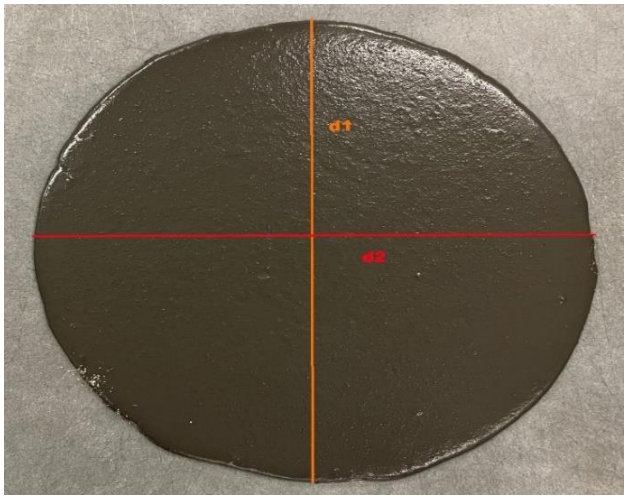

Figure 5.12 Flow measurement is determined by using average diameter of d1 and d2.

Compressive Strength test

Compressive strength is measured in line with this report's standard NS-EN 12390-3 [177]. This experiment aims to determine the compressive strength of the hardened concrete specimen by loading it until it fractures. This is accomplished by employing a universal testing machine in compliance with NS-EN 12390-4 [177]. Furthermore, the compressive strength is computed using the peak load measured when the sample is fragmented. The compressive strength test is performed in the following approach; first, the test specimen must be moistened during testing since it must be tested within 10 hours after being withdrawn from the curing process. Moisture and filth are removed from the surfaces of the test specimens and the bearing test equipment in order for the testing results to be unaffected.

Nest, the test specimen is put in the compression testing machine in the center, with a precision of ± 1mm for cubes. Finally, the specimen is loaded at a constant velocity of 0.6 MPa/s without being shocked for this research.

The ultimate compressive force is termed as the maximum load at failure. This value is used to determine the compressive strength in the following equation:

$$f_c = \frac{F}{A_c} \ [MPa] \qquad 5.1$$

Where F [N] denotes the maximum load at failure and Ac [mm^2] denotes the sample's cross-sectional area where the compressive force operates.

Figure 5.13 Compressive strength test

Flexural tensile strength test

Flexural strength for our specimen was supposed to be determined in with the standard ASTMC1609. For fiber reinforce specimens, it is crucial to evaluate the flexural performance after the first peak. However, to perform this evaluation, the right testing machine is needed. This was not the case for this research study since the testing machine was not a displacement - but a load-controlled one. This meant that the test machine was designed for conventional concrete and based on the European standard (NS-EN 12390-5). This led to revising the test method for this thesis and adapting to the only method we had available.

In this case, the flexural strength is determined in line with the standard NS-EN 12390-5 [178] by utilizing a four-point bending apparatus. This experiment aims to determine the specimen's flexural strength by supporting it on the bottom surface and loading it on the top surface with load-controlled force. Then, the maximum load achieved is used to calculate flexural strength.

Flexural strength is measured using a testing machine that is compliant with NS-EN 12390-4 [177]. Two top rollers are required on the test machine, which evenly distributes the load applied, and two support rollers at the bottom. The procedure commences with placing the top and lower rollers correctly. The spacing between the bottom roller supports is set to 3d, and the spacing between the upper roller supports is set to d, where d is the width of the test sample. Furthermore, moisture and filth are also cleaned from the test specimens' surfaces and the machine's rollers, ensuring that the testing outcomes are unaffected. It is critical to test the samples within 10 hours after their removal from the curing process to ensure that moisture loss is avoided. The specimens are centered in the machine, with the load applied perpendicular to one of the specimen's surfaces. Here it is wise to have the loading on one of the smooth surfaces (not the casting surface). Moreover, the test specimen is loaded by utilizing load control, where the loading rate is calculated as follows:

$$R = \frac{s \times d_1 \times d_2}{L} \ [N/s] \qquad 5.2$$

Where, s [MPa/s] signifies the stress rate, and L [mm] denotes the span between the lower rollers, while d_1 and d_2 [mm] represent the dimension of the lateral sides of the samples.

For this research, the parameters presented in Table 5.5 are employed to investigate the flexural strength.

Table 5.5 Parameter used to achieve the flexural strength

Parameters	Values	Units
lateral dimension [d1=d2=d]	100	mm
Stress rate [s]	0.5	MPa/s
The span of lower rollers 3d, [L]	300	mm
Load rate [R]	1.67	N/s

The flexural strength is then calculated in accordance with the following equation:

$$f_{cf} = \frac{PXL}{b * d^2} \ [MPa] \qquad 5.3$$

Where, P [N] denotes the maximum load at failure, and L [mm^2] denotes the span between the lower supporting rollers, while b and d [mm] denote the width of the specimen and the span depth.

Figure 5.14 Flexural tensile strength test.

5.3 DIC technique

In this study, the Digital Image Correlation approach is used to obtain a sequence of images during the flexural bending test. Furthermore, the strains and vertical displacement sustained by the UHPC beam specimen were assessed using the images. This chapter will go more into the procedure of employing DIC in this investigation.

5.3.1 Surface preparation

The preparation of the surface is an essential factor that influences the precision of the DIC results. The DIC technique is based on detecting the movement of random spot patterns that are imprinted on the surface of the testing specimen using paint, as previously indicated.

Before the DIC test, a random speckle pattern must be developed on the specimen surface to offer the best surface texture. For that reason, the random speckle in this investigation is created by spraying white and black paint (Figure 5.15) on the surface of the specimen.

However, the preparation procedure in this investigation was done in two stages. The sample's surface with the fewest porosity and defects was selected for our tests. The area of the interest surface of the prism was sprayed with white paint in the first stage. Then, the white paint was allowed to dry out for 1 hours.

Moreover, the dry white surface of the specimen was then sprayed with black paint in the second phase. This leads to the formation of a randomly dispersed pattern of black dots on the surface of the specimen. To obtain the ideal random pattern and small diameter of the black speckles, black paint is sprayed from a distance. Furthermore, another hour was allotted to allow the specimen to dry. Figure 5.16 depicts the final surface preparation, in which the prism is coated with white featuring black dots.

Figure 5.15 The speckle pattern is achieved with these spray paints.

Figure 5.16 The final surface preparation of the prism coated with white paint and black dots.

5.3.2 Image acquisition system

In this investigation, two-dimensional displacement measurements were obtained using two cameras. This was conducted using “Imager X-lite 29M GigE,” which is a DIC camera product of LaVision. These cameras feature a sensor resolution of 10 megapixels. Furthermore, the camera tripod was set up and leveled in the image acquisition region. This was done in order to keep the camera in a stationary point and reduce vibrations during testing. As designated in the schematic setup in Figure 5.17, once the tripod was installed, the surface of the camera lens was oriented towards the specimen from different angles. The camera lens is positioned approximately half a meter away from the specimen. It was adjusted like that so that the interest area of the sample is viewed in the camera. In this investigation, images were collected every second until the failure of the sample, and they were recorded with a resolution of 6600 x 4400 pixels.

Lighting on the surface under investigation is essential as it helps enhance the capturing process. Furthermore, small shifts in ambient light intensity can be avoided by providing even light for the sample surface. This is accomplished by maintaining continuous illumination in the room during the testing period. Two additional LED linear lighting illumination lamps were also put on the tripod, making it easier for the cameras to record and determine the displacement fields.

Figure 5.18 displays the actual experimental test setup of the DIC approach and the four-point bending test.

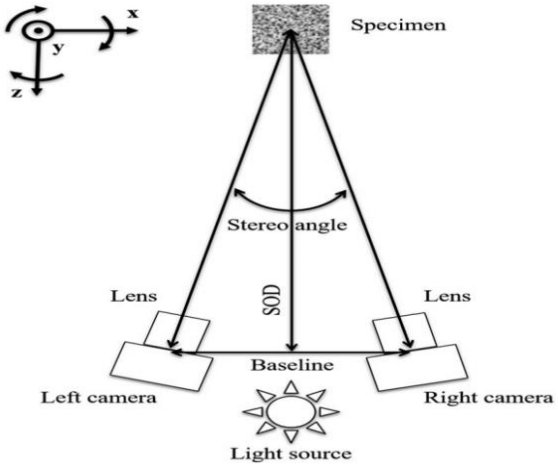

Figure 5.17 Schematic presentation of DIC setup [167].

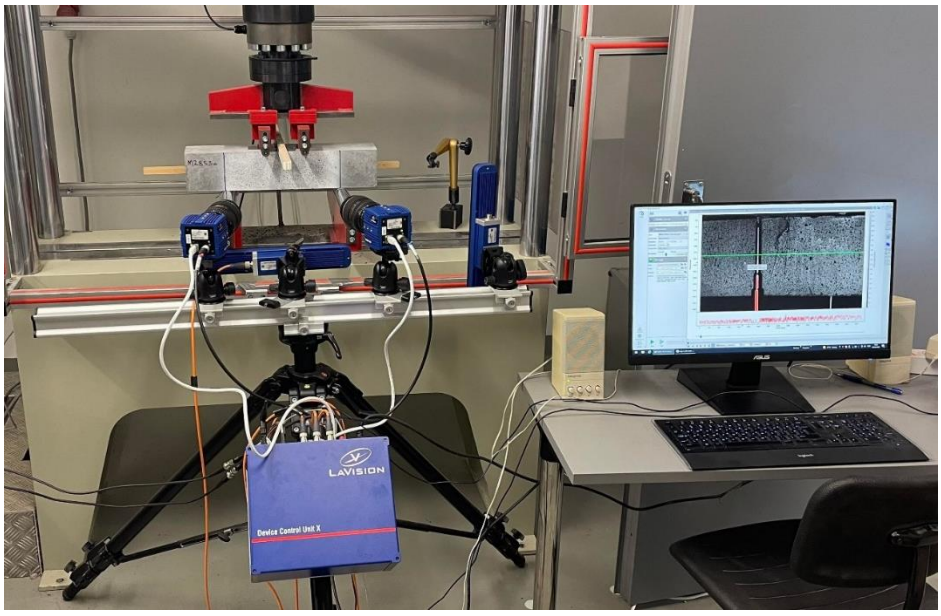

Figure 5.18 Actual DIC setup

5.3.3 Camera settings and software

During the experiment, the DIC camera was paired to a computer. The camera setting was controlled manually by using the software DaVis. Table 5.6 shows some of the features that was used in the camera setup, and they were held constant throughout the investigation. The focal length was as it exhibits a minimum amount of distortion, and the value of the aperture of F/16 was selected to ensure the highest lens sharpness.

Table 5.6 Features used in the camera setup.

Resolution	6600 x 4400 pixels
Aperture	F/16
Focal length	40 mm

When the camera is linked to a computer, DaVis is used to capture images. For the processing of the digital images captured, this software may also be used. This program, however, was just too complicated to use. It is quite resource-intensive since many problems occur frequently, and one must spend money to receive assistance from the support system. As a result, it was chosen to do the processing of the images on the commercial software tool called GOM Correlate.

6 RESULTS AND DISCUSSION

6.1 Experimental Test

6.1.1 Preliminary Test

As previously stated, the preliminary mixture design considers the impact of various material components by assessing mechanical characteristics via compressive strength and rheological properties via flow testing. Thus, different amounts of the mixture's components and different types of material compositions were tried in these experiments. A comprehensive description of the outcomes of the numerous tests performed is provided in the following sub-chapters below.

Flowability

The flow measurement data for the first six combinations were not documented using a mini cone due to a shortage of testing equipment in the laboratory, as described in Chapter 3.2, “Limitations”. Therefore, the first six mixtures utilized a slum cone to evaluate the flow property, and the results stand out significantly as compared to the mixtures that used a mini cone. Table 6.1 displays the flow measurements obtained by utilizing a slum cone, and these flow values are compared separately from the other mixtures.

Table 6.1 Flow measurement for the preliminary test with the use of slump cone

Mixture	Flow measurement [mm] (slump test)
1	325
2	--
3	335
4	280
5	--
6	340

The flow tests using slump cone results were not satisfying for a self-consolidating UHPC compared to previous research conducted by [132], [134]. In these studies, a flow ranging between 600-1000 mm was obtained to have a self-consolidating UHPC.

The best flow results when using the slump cone were from mixtures 3 and 6, which produced flow values of 335mm and 340 mm, respectively. Compared to mixture 2 and mixture 5 with less SP, no flow was observed as these mixtures were too dry.

When it comes to deciding whether UHPC should comprise a majority of fine or coarse sand, it turns out that it has minimal effect on the flow in this circumstance. The result in mixtures 2 and 3 are nearly identical to mixtures 5 and 6, respectively, and it was decided to employ the majority of the fine silica sand materials in the UHPC since it was closest to our target curve based on the particle packing model. In addition, it was the fine silica sand that we had the most available in the laboratory compared to the coarse silica sand.

Mixture 1 attained a flow result of 325 mm when 15% silica fume by cement weight was used. Compared to mixture 4 where 25% silica fume by cement weight is utilized, a flow result of 280mm was obtained. This shows that as the amount of the silica fume increased, the flow decreased, and in this case, it decreased by approximal 15%.

Chan et al. reported similar outcomes [179] and Wu et al. [180]. The reason for the declination of flow is that silica fume is a considerably finer substance than cement in the mixture. Therefore, increased silica fume content leads to a high surface area and to break the flocculation action, and it would demand a substantially larger volume of water or SP. With smaller silica fume content, the flowability is improved as silica fume helps flocculated cement particles disperse as ultra-fine particles, allowing more entrapped water to escape [180], [181].

The flow measurement data for the various mixtures tested using the flow table are displayed in Figure 6.1 and Table 6.2. Furthermore, a flow of 200 mm was the target for the mixes that used the flow table as indicated in ASTM C1856. This was attained in some of the mixtures as shown in Figure 6.1, since some of the columns have graced over the red dotted line that refers to the required flow value.

Table 6.2 Flow measurement for the preliminary test with the use of flow table

Mixture	Flowability [mm] (mini cone)
7	162.5
8	175
9	190
10	160
11	160
12	210
13	190
14	205
15	187.5
16	210
17	218.5
18	230
19	245.5

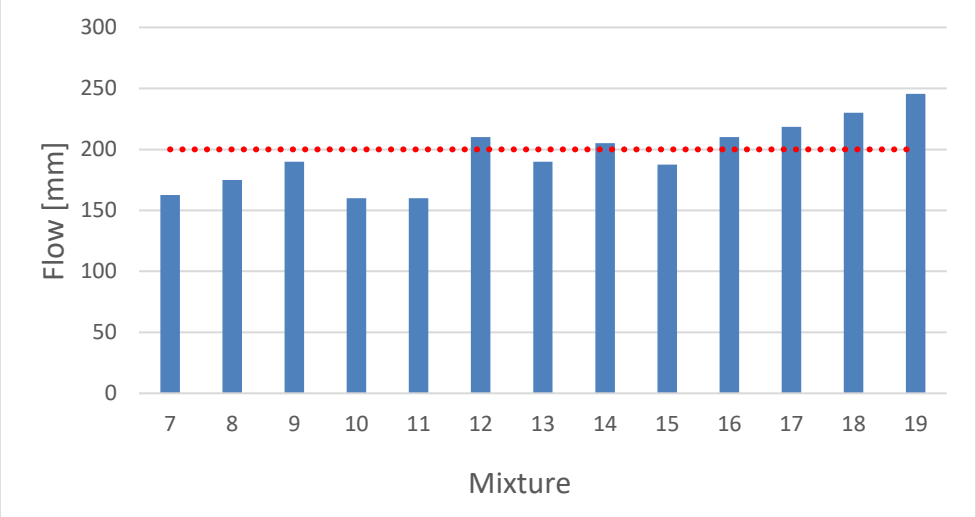

Figure 6.1 Flow spread values for preliminary mixtures using mini cone where the red line shows the target requirement at 200mm.

In mixtures 7, 8, and 9, the SP remained constant at 6.5%, while the w/c ratio fluctuated between 0.23-0.25 in order to achieve a water to binder ratio less than or equal to 0.20, as suggested in the literature. The flow result showed an 8% enhancement from mixture 7 to mixture 9. Moreover, increasing the SP content rather than the w/c as done in mixture 12 resulted in a far greater improvement, with 210mm of flow achieved with 8 % SP as opposed to mixture 8. Nonetheless, this resulted in an approximately 18% increase in flow spread. Following an acceptable flow spread over 200mm, a flow of 190 mm was observed in mixture

13 with the addition of 2% steel fiber. This implies that the SP level needs to be increased by more than 8% to achieve 200mm flow with the addition of steel fiber.

Previous research by El-Tawil et al. [159] employed about the same ratio of the various materials as us with an even lower w/c ratio. In this investigation, a w/c ratio of 0.22 was adopted with an optimal proportion of 1:0.25 between cement and silica fume. To ensure adequate workability, however, an SP concentration of 2 to 3% by weight of cement was recommended.

So, as a result of investigating the different types of SP, the MasterGlenium SKY 830 SP in mixtures 10 and 11 resulted in a reduction in flowability as 160mm flow was detected for both mixtures. Compared to mixtures 7 and 9, which employed Dynamon SX-N SP, a decrease of 1.5 and 17% is noted, respectively. However, it was expected that MasterGlenium SKY 830 would outperform Dynamon SX-N since this type of SP has less water and much more solid material, as indicated in Table 4.6. The inferior outcome might be attributed to the fact that it was discovered that the MasterGlenium SKY 830 had expired and was no longer usable, owing it did not function effectively.

Therefore, a new SP "Masterease 2050" was purchased and utilized for the remaining six mixtures. Mixture 14 demonstrated a 7.6% increase in flow spread while using Masterease 2050 compared to Dynamon SX-N in mixture 9. The identical mixture was created again as mixture 16, where a flow of 210 mm was achieved. This was done to validate mixture 14, as mixture 15 was less workable with the new Masterease 2050 material than mixture 12, which utilized Dynamon SX-N.

Furthermore, for mixtures 17 to 19, the w/c ratio was held constant at 0.25 while increasing the SP ratio by 8, 10, and 12%. This was done since mixtures 14 and 16 with less SP content achieved over 200mm spread flow as opposed to mixture 12. Respectively, measurements of 218.5, 230, and 245.5 were obtained in mixtures 17, 18, and 19, which is encouraging in contrary to mixture 13 were adding steel fiber resulted in a 10% decline, putting us below the needed target flow.

In summary, the more solid content in the SP, the better the flow is achieved in the UHPC mixture, according to Li et al. [101]. Among the several SP substances employed in this thesis, Masterease 2050 delivered the greatest result in terms of flowability.

Compressive strength

The average value and standard deviations of the compressive strength of cubes after 7 days of curing regime at 20 degrees are presented in Table 6.3 and Figure 6.3. In addition, standard deviations are depicted in Figure 6.3 as the black bars. At seven days, most of the mixes acquired a compressive strength of 80 MPa, while prior research [125], [134] and the typical values displayed earlier in Table 2.2 sought a compressive strength of 100 MPa was achieved in some of the mixtures. The standard deviation between the mixtures is in the range of 1-8.46.

Table 6.3 Compressive strength measured for the preliminary test

Mixture	Compressive Strength [MPa]	Standard deviation
1	70.5	8.1
2	78.8	3.98
3	96.6	8.46
4	113.2	1.00
5	79.1	3.31
6	97.1	5.34
7	104.3	4.57
8	100.3	8.08
9	97.0	2.16
10	108.9	2.87
11	102.2	3.42
12	93.0	2.57
13	93.0	4.63
14	105.5	3.40
15	99.5	3.30
16	104.9	2.43
17	96.0	5.95
18	93.9	2.12
19	80.2	5.24

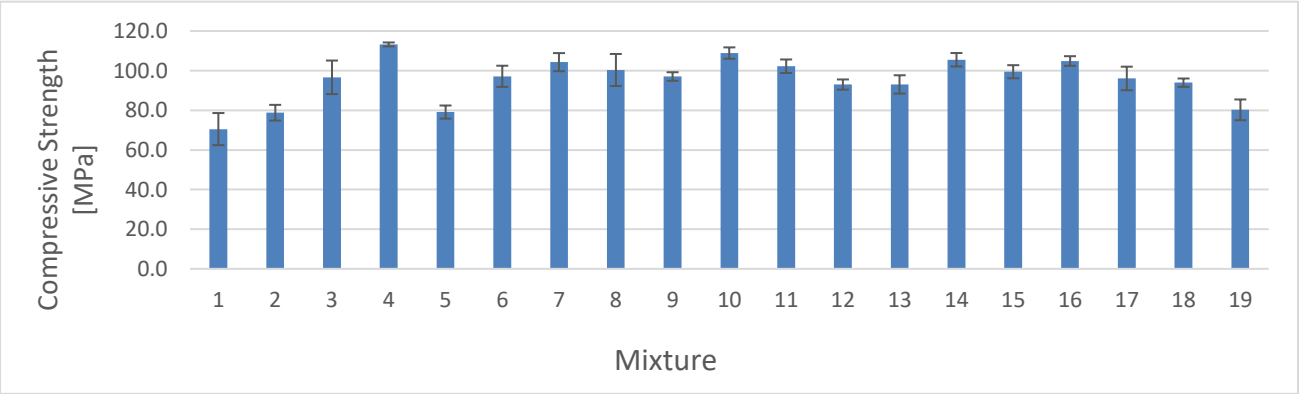

Figure 6.2 Compressive strength of the preliminary test and standard deviation.

As discussed in Chapter 2.5.3, the influence of silica fume concentration on compressive strength differs throughout the literature. Some research demonstrated that raising the concentration of silica fumes above 15% reduces compressive strength, while other research stated that raising the amount of silica fumes up to and above 25% enhances compressive strength [70], [86]. The last claim was observed in this investigation, where mixture 4 with 25% silica fume concentration attained 113.21 MPa in compressive strength, as contrasted to mixture 1 with 15% silica fume concentration attaining 70.5MPa. This showed approximately a 46% growth in compressive strength by applying a 25% silica fume compared to 15% silica fume content.

Furthermore, the effect of the fine and coarse sands volume fractions did not indicate any significant variations in compressive strength for mixtures 2 and 3 compared to mixes 5 and 6. The difference in compressive strength was less than 1% for this investigation.

Compressive strength of 97.1 MPa and 96.6 MPa was achieved with w/c content of 0.28 and SP of 4%. Therefore, by only increasing SP by 2%, an enhancement of approximately 20% was obtained for compressive strength between mixtures 2 and 3 and between 5 and 6. However, the flow of these mixtures was too poor to be used as the optimal mixing.

Once the w/b ratio was held within the recommended range, increasing the w/b ratio from 0.18 to 0.20 while holding the SP constant decreased compressive strength, as demonstrated in mixtures 7, 8, and 9. The strength of the various mixtures drops by around 3% whenever the amount of water is increased. A similar outcome was documented in the literature where mechanical properties decreased with an increase in water to binder ratio, while the porosity of the concrete was enhanced [109], [110], [147]. Although mixes 7, 8, and 9 achieved compressive strengths of 104.3MPa, 100.3MPa, and 97 MPa, respectively, the various mixtures' flowability was insufficient since it was below the intended objective.

Furthermore, only increasing the SP substance to a higher content of 8% in mixture 12 led to a reduction from 100.3MPa in mixture 8 to 93 MPa. When the concentration of the SP material is increased to this level, surplus water is produced that is not required for hydration. As a result, cavities will form in the concrete mixture, increasing the porosity and lowering the concrete's strength.

The compressive strength of Masterglenium sky 830 was 108.9 MPa and 102.2 MPa, respectively, for mixtures 10 and 11, although this was due to the dryness of the mixes and the fact that the SP material had expired and had extremely poor processability.

However, using Mastereaser 2050 SP, we achieved the best compressive strength at mixtures 14 and 16 with an average value of 105.5MPa and 104.9MPa. In contrast, by increasing the SP above 6.5%, a reduction in compressive strength was obtained in mixtures 15,17,18, and 19.

Summary of the preliminary trial result

Furthermore, for this research, it has been chosen to proceed with mixtures 14 and 16 as the optimized mixture. This mixture provided the best value for flow, achieving over the minimal requirement of 200mm set for this research. Moreover, it exceeded 100MPa in compressive strength, which is above the typical values for 7 days of compressive strength displayed in Table 2.2. What influenced this choice is the quantity of silica fume content, water and binder ratio equal to or lower than 0.20, the dosage of the SP, and the type of SP material employed. The factor that affected the flowability most was the SP content and the type of SP substant. The higher SP content used and most solid content in the SP led to the best flowability measurement, which was observed by using the Masterease 2050 SP. Furthermore, the compressive strength was affected by keeping the mixture as dense as possible by using 25% silica fume and a low w/b ratio of 0.20.

6.1.2 Optimized Mixture Test

Once we established an optimal mixture that demonstrated to have the properties we were searching for, the recipe was developed to explore the influence of varied fiber content on the mechanical properties of UHPC. This subchapter will present the results and further discuss the outcome of the final test. Additionally, the focus of this chapter will be mainly on Mix 1 – Mix 5. The other two mixtures (Mix 6 and Mix 7) are to begin cast with 0% steel fiber content and included so we can observe their behaviors on other factors such as mixing sequence, the lowest rate of superplasticizer needed to achieve our target value of 20cm flow.

Flowability

Figure 6.3 and Table 6.4 presents the flow outcomes achieved for the optimized final mixtures. Additionally, a physical illustration of the mixture flows taken immediately after mixing and during the flow test process can be observed in Figure 6.4. Furthermore, just as we chose 200mm (20cm) flow as a target value for our preliminary test, the same target value was also set for the optimized mixture test. As presented in Table 6.4 and Figure 6.3, this target value was achieved by all our mixtures. The red dotted line in Figure 6.3 shows the required flow for the target value.

Table 6.4 Flow measurement of the optimized mixture

Mixture	Steel Fiber ratio [%]	Flow measurement [mm]
1	0	260
2	0.5	247.5
3	1	240
4	1.5	235
5	2	225
6	0	232.5
7	0	195

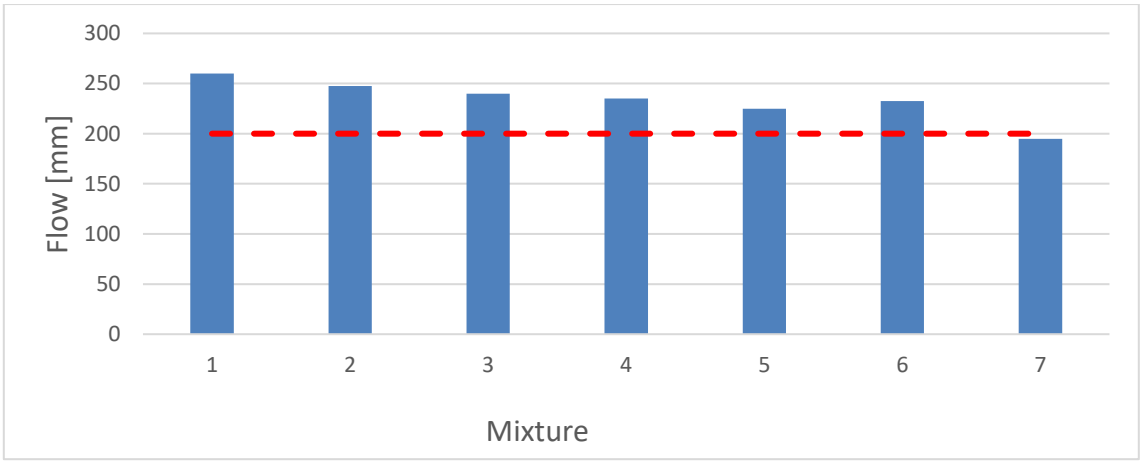

Figure 6.3 Flow measurement of the optimized mixture where the red line shows target requirement at 200mm.

.

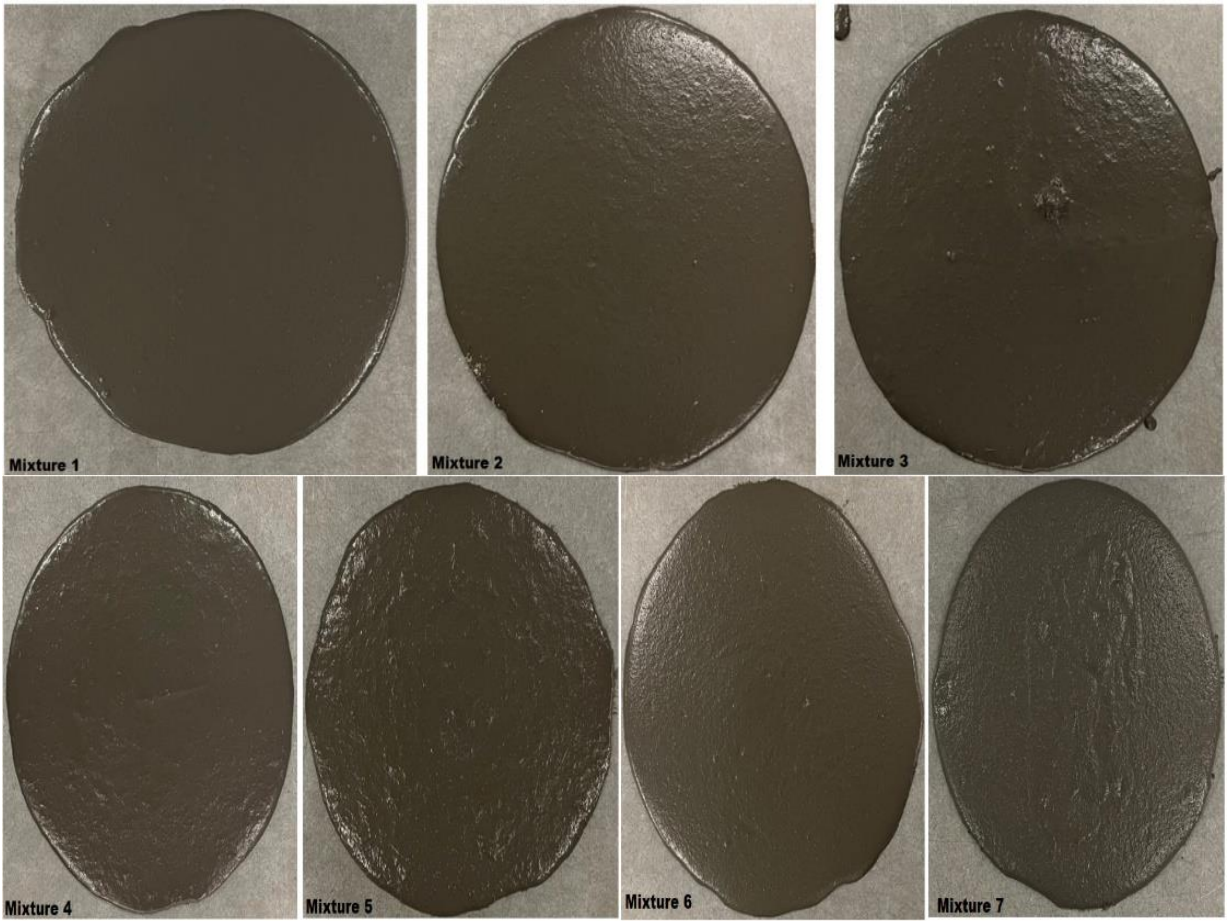

Figure 6.4 Image of the flowability for the different mixtures after measuring the diameters.

To investigate the influence of steel fibers on UHPC, all parameters were kept constant, as previously mentioned, and only the steel fiber content was altered. The results demonstrate that the flowability of all the mixes with varying fiber contents (mixtures 1-5) declines with increasing steel fiber content. In mixture 1, which is the reference mixture without the presence of fiber reinforcement, a flow value of 260 mm was obtained. What is very interesting to observe here is the decrease of flowability with the increase of fiber content. The addition of 0.5% has resulted in a major reduction in flowability compared to Mix 1(0% SS). However, when we observe the decrease of flowability from 0.5% to 2%, only a slight decrease occurs compared to that of Mix 1. For instance, between Mix 1 and 2, we observe a reduction of close to 12.5 mm in diameter, and for the rest of the fiber content, this does not go beyond 10 mm. The main reason for this behavior can be related to the increased surface areas of steel, which would lead to a higher demand for cement paste for covering the surface of fiber and aggregates. Another reason can be that the random distribution of steel fibers in the mortar can cause the steel fibers to act as a skeleton and eventually prevent the flow of the fresh mixture.

Additionally, the mixtures 6 and 7 were cast for two purposes. In the observation above, the influence of steel fibers has been discussed. However, the intended purpose with Mix 6 and 7 was to observe the lowest value of SP we needed to achieve the target flow value of 20cm and the influence of different mixing sequences on flowability.

The results from Mix 6 show that by reducing the SP value from 5.5% to 4.5%, we were well over our target value of 20cm. This shows that there is a potential to use a lower value but eventually will force us to consider having a varied SP value (instead of constant) as we increase the fiber content. This can be an interesting investigation and possibility for future work. Similarly, Mix 7 shows that we observe a major reduction in flowability by using our “old” mixing sequence while keeping everything else the same as Mix 1. This has mainly to do with the interaction of the different ingredients and order of application.

Finally, another interesting observation we also came across was the mass of the batch, small compared to large once of mixing batch. This was one factor we did not consider, but throughout the experimental program, we saw how huge impact this can have on flowability. Another interesting topic for future work as well. The result of this can be observed between the Preliminary laboratory test results of the 19 mixtures and the optimized mixture test compromised of 7 mixtures.

Compressive strength

Figure 6.6 and Table 6.5 and 6.6 presents the compressive strength achieved for the optimized final mixtures. Furthermore, as explained earlier, a minimum of 120 MPa for the compressive strength was set as the target value for the test. This was a value associated with 28days of curing, and as presented in Table 6.6 and Figure 6.5, this target value was achieved by all our mixtures.

The general observation when it comes to the contribution of steel fibers is its great influence on the failure mode of UHPC mixtures. Without steel fiber, UHPC specimens have a typical brittle failure under uniaxial compression. Under the testing process, you can observe the loud noise that occurs upon failure, and the physical state of the specimen will be in pieces; sometimes, some specimens will also be intact. However, the addition of steel fibers will increase the ductility of UHPC. Our steel fiber reinforced specimens were all intact after the compressive test, with only a few minor cracks on the surface. This can be observed in Figure 6.5.

Figure 6.5 Failure appearance for UHPC specimen under uniaxial compression with (left) 0% steel fibre and (right) 0.5% steel fibre.

Figure 6.6 and Table 6.5 and 6.6 shows the change in compressive strength for different curing days of our UHPC mixture. Our general assessment based on previous scientific articles is to have an increasing pattern of compressive strength with the increase of steel fiber. This kind of pattern is not achieved for our research study; instead, we have an increasing pattern until 1% fiber content, then the compressive strength decreases and increases again. Generally, since the increase of fiber content can cause the average

distance/space between fibers to decrease, this will eventually lead to more fibers sustaining the load. In addition, the increase of fibers will also delay the formation and propagation of cracks, resulting in an increase in strength. However, this is not the case for our results. For our specimens, Mix 5 (2.5%) did not have a higher value than Mix 3 (1%), and the sudden decrease of compressive strength of Mix 4 (1.5%) could be categorized under the influence of steel agglomeration. This, in return, have a negative effect on the compressive strength. Another aspect is the effect of entrapped air within the specimen; however, we can see from the physical illustration of the different mixtures presented under the reflection of flowability that we did not experience any reduced workability. So, making a professional assessment remains a bit difficult when factors such as curing condition, workability, and specimen size are also other aspects in addition to fiber effect. Nevertheless, the highest compressive strength for this research study was achieved with a fiber content of 1% for Mix 3.

The next interesting observation was for mixtures 6 and 7. As explained in the previous sub-chapter, this was casted with the intention to see the influence of SP and of course, different mixture sequences.

From comparing Mix 1 and 6 we observed that the reduction of SP from 5.5% to 4.5% had no effect on short time term (7 days) test results. However, this was different for long-term results as we experienced an increase of compressive strength for Mix 6, higher than that of Mix 1. Another interesting research question, at least for us. Similarly, mixture 7 also had the same trend for the short-term and long-term effects on the compressive strength based on the mixture sequence.

Table 6.5 7-days compressive strength

Mixture	No.	Fiber content	Aspect ratio (Lf/df)	Casting date	Curing conditions	Testing date	Compressive strength [MPa]	Average value of compressive strength [MPa]	Standard deviation
	1.1						99.1		
	1.2				20°C		105.7		
1	1.3	0.0%	--	24.03.2022	Water tank	31.03.2022	107.6	104.1	4.5
	2.1						106.5		
	2.2				20°C		107.7		
2	2.3	0.5%	13/0.2	23.03.2022	Water tank	30.03.2022	105.7	106.6	1.0
	3.1						108.9		
	3.2				20°C		112.7		
3	3.3	1.0%	13/0.2	22.03.2022	Water tank	29.03.2022	111.2	110.9	1.9
	4.4						107.3		
	4.2				20°C		108.4		
4	4.3	1.5%	13/0.2	23.03.2022	Water tank	30.03.2022	109.8	108.5	1.3
	5.1						110.1		
	5.2				20°C		109.9		
5	5.3	2.0%	13/0.2	24.03.2022	Water tank	31.03.2022	108.8	109.6	0.7
	6.1						100.0		
	6.2				20°C		108.8		
6	6.3	0.0%	--	24.03.2022	Water tank	31.03.2022	103.4	104.1	4.5
	7.1						99.0		
	7.2				20°C		99.4		
7	7.3	0.0%	--	25.03.2022	Water tank	01.04.2022	98.8	99.1	0.3

Table 6.6 28-days compressive strength

Mixture	No.	Fiber content	Aspect ratio (Lf/df)	Casting date	Curing conditions	Testing date	Compressive strength [MPa]	Average value of compressive strength [MPa]	Standard deviation
	1.1				20°C		120.103		
	1.2				Water		127.092		
1	1.3	0.0%	--	24.03.2022	tank	21.04.2022	128.68	125.3	4.6
	2.1				20°C		132.123		
	2.2				Water		132.287		
2	2.3	0.5%	13/0.2	23.03.2022	tank	20.04.2022	128.003	130.8	2.4
	3.1				20°C		127.999		
	3.2				Water		136.993		
3	3.3	1.0%	13/0.2	22.03.2022	tank	19.04.2022	138.684	134.6	5.7
	4.4				20°C		128.783		
	4.2				Water		131.507		
4	4.3	1.5%	13/0.2	23.03.2022	tank	20.04.2022	133.255	131.2	2.3
	5.1				20°C		130.136		
	5.2				Water		135.866		
5	5.3	2.0%	13/0.2	24.03.2022	tank	21.04.2022	133.165	133.1	2.9
	6.1				20°C		129.9		
	6.2				Water		133.6		
6	6.3	0.0%	--	24.03.2022	tank	21.04.2022	120.0	127.8	7.0
	7.1				20°C		124.9		
	7.2				Water		128.0		
7	7.3	0.0%	--	25.03.2022	tank	22.04.2022	124.8	125.9	1.8

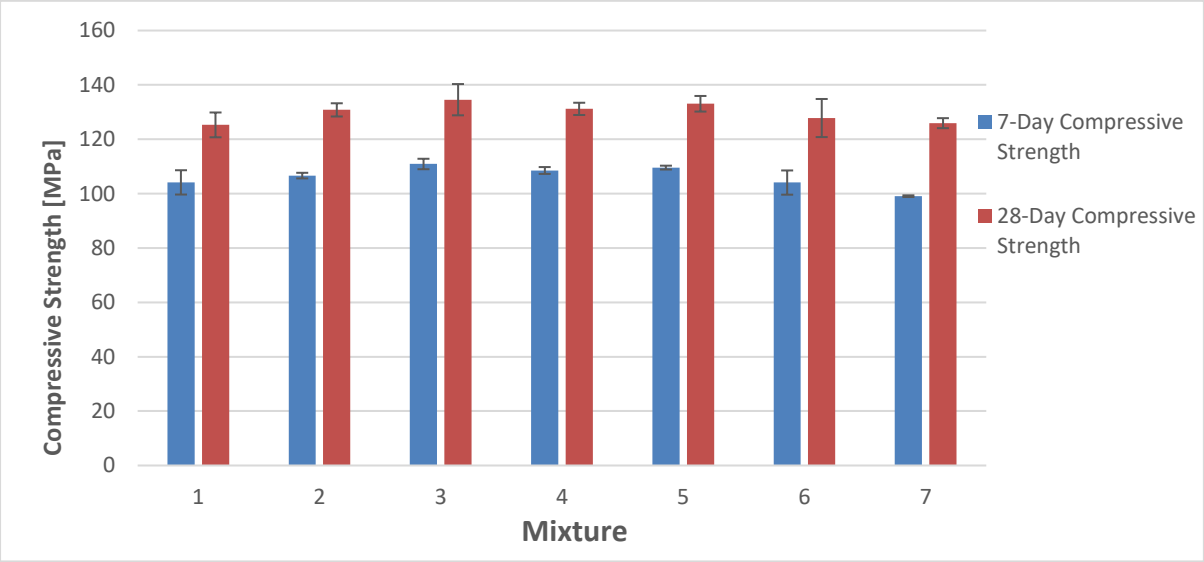

Figure 6.6 Compressive strength at 7-days and 28-days curing condition.

Flexural strength

The flexural strength results for our different mixtures are presented in Tables 6.7 and 6.8 and Figure 6.7 below. The first interesting reflection here is the comparison of fiber content contribution to the different strengths of compressive and flexural. Earlier, we observed that Mix 3 had the highest compressive strength compared to the other fiber-reinforced specimens. However, here Mix 3 had the lowest value for flexural strength compared against the other mixtures.

The addition of 0.5% fiber content throughout our entire mix has increased flexural strength of about 9.2%, 7.7%, 14%, and 50.7%, respectively. Additionally, we can observe that 2% steel fiber had a significant increase in flexural strength. This is clearly because of the crack-bridging effects of higher fiber content, which will lead to an increase in the flexural load carrying capacity. In addition, we also have the mechanical interlock and friction at the fiber matrix that can contribute to the suppression of propagation and crack development.

Table 6.7 Flexural strength measurements for 28 days

Mixture	No.	Fiber content	Aspect ratio (Lf/df)	Casting date	Curing conditions	Testing date	Flexural tensile strength [MPa]	Average value of flexural tensile strength [MPa]	Standard deviation
	1.1				20°C		15.489		
	1.2				Water		13.917		
1	1.3	0.0%	--	24.03.2022	tank	21.04.2022	13.317	14.2	1.1
	2.1				20°C		16.17		
	2.2				Water		15.627		
2	2.3	0.5%	13/0.2	23.03.2022	tank	20.04.2022	14.685	15.5	0.7
	3.1				20°C		14.802		
	3.2				Water		15.648		
3	3.3	1.0%	13/0.2	22.03.2022	tank	19.04.2022	15.507	15.3	0.5
	4.4				20°C		16.758		
	4.2				Water		14.568		
4	4.3	1.5%	13/0.2	23.03.2022	tank	20.04.2022	17.127	16.2	1.4
	5.1				20°C		18.921		
	5.2				Water		21.111		
5	5.3	2.0%	13/0.2	24.03.2022	tank	21.04.2022	24.171	21.4	2.6
	6.1				20°C		15.8		
	6.2				Water		16.0		
6	6.3	0.0%	--	24.03.2022	tank	21.04.2022	15.2	15.7	0.4
	7.1				20°C		15.1		
	7.2				Water		16.4		
7	7.3	0.0%	--	25.03.2022	tank	22.04.2022	16.1	15.9	0.7

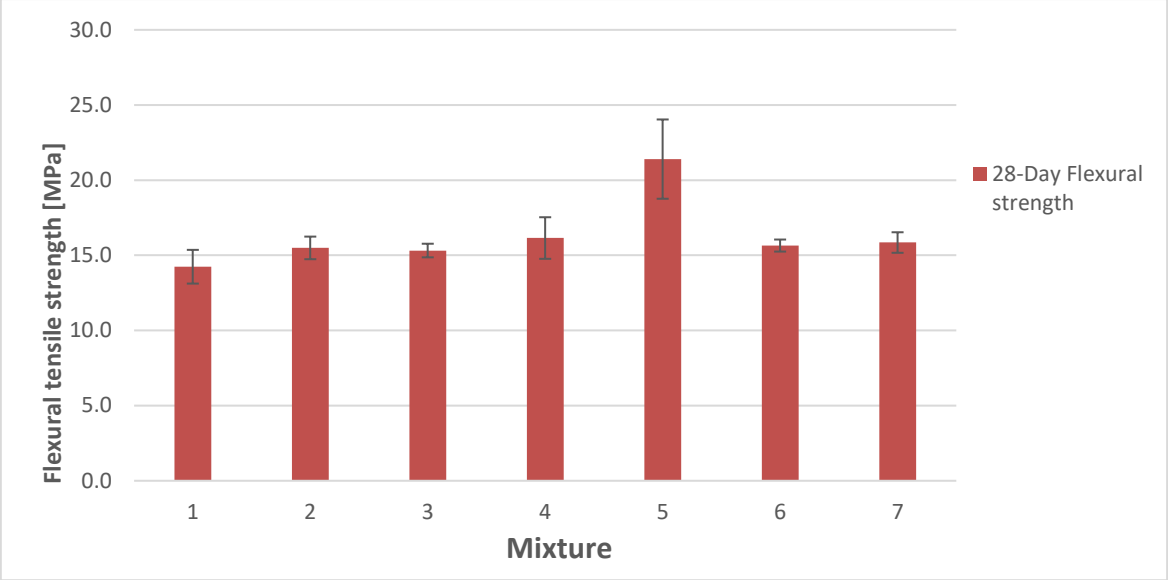

Figure 6.7 Flexural measurements

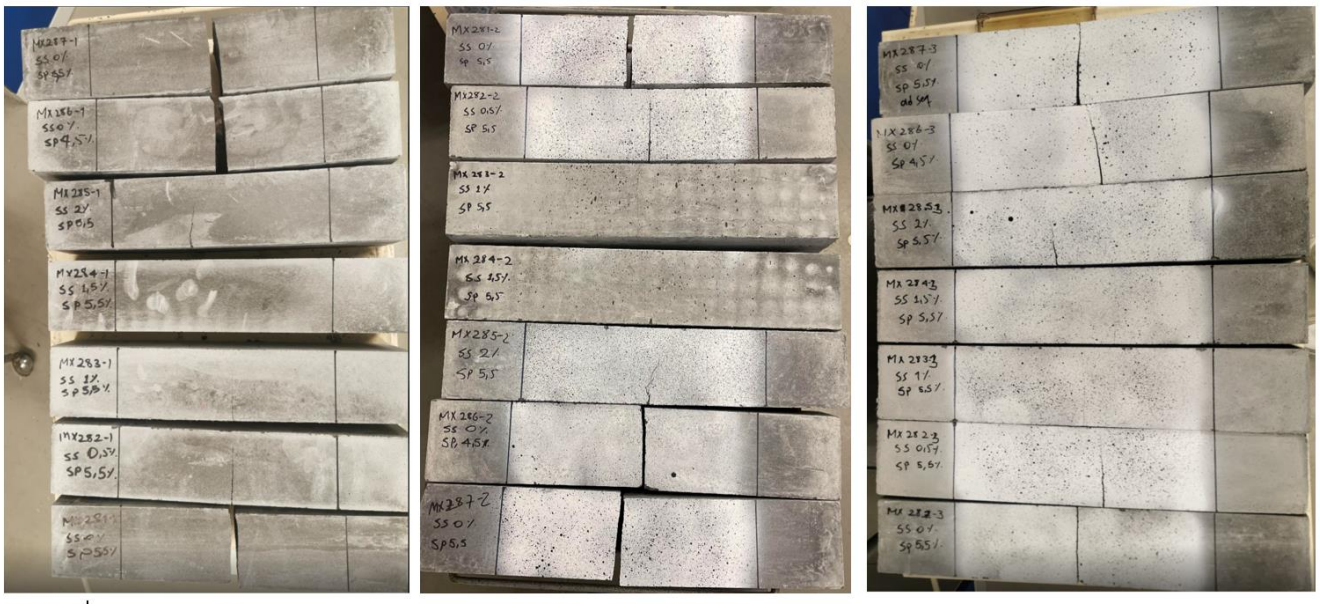

Figure 6.8 Crack development for our entire mixture samples under 4-point loading test.

DIC technique Results

The DIC results for this research study were achieved with the help of a two-dimensional method. As explained initially, DaVis software from Lavision was supposed to be the main component used to analyze our specimen. However, due to the complication and shortcomings explained under limitations in Chapter 3.2, this had to be combined with another software called GOM correlate. This process goes as follows: DaVis software was used to capture the testing process, and the analysis was performed with GOM correlate.

The idea about the two-dimensional DIC method can perform a post-processing analysis, and it can provide us with the deformation field for a region of interest selected by the user. The region of interest for this research study was chosen based on the location of the crack, which naturally is located between the loading roller under the 4-point bending test.

For the assessment of our specimens with GOM, a default value of 19 pixels for facet size, 16 pixels for point distance, and high accuracy for computation was chosen. The pattern quality was initially controlled to ensure a sufficient intensity level, which can be observed in the figure below.

Figure 6.9 Region of interest.

For the analysis of our specimen, all the calculations are based on the comparison of each stage with a so-called "Reference Image." That is why for the two-dimensional analysis, the user needs to introduce a reference image. In GOM correlate, the first image within the timeline is chosen as the reference image, and every stage was compared to that. Usually, there are no activities at the reference image or stage, and this can be observed in the figure below.

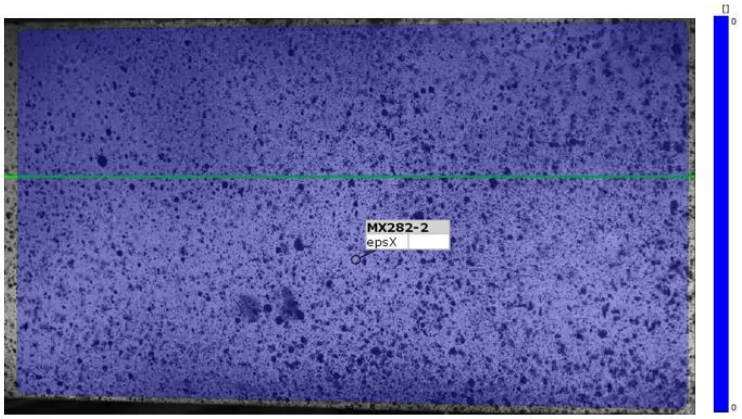

Figure 6.10 Reference image where all other stages will be compared to.

The aim with the application of GOM correlate at this phase now manly stands for illustration crack propagation and localization. Additionally, to the best of our abilities, we are also aiming to present the full-field strain mapping, measurement of vertical displacement, and maybe measurement of crack width with the help of a virtual extensometer.

Before we can dive into the analysis of each specimen, a description of each mixture and its abbreviation will be presented in Table 6.8. This will simplify the representation and illustration of each specimen. Additionally, the DIC analysis was conducted for two samples from each mixture. So, to separate these two samples within the same mixture, each sample has been labeled with 2 or 3 at the end of their label/identity.

Table 6.8 Identification of different mix samples.

Mixture	Fiber content [%]	Sample 2	Sample 3
Mix 1	0	MX281-2	MX281-3
Mix 2	0.5	MX282-2	MX282-3
Mix 3	1	MX283-2	MX283-3
Mix 4	1.5	MX284-2	MX284-3
Mix 5	2	MX285-2	MX285-3

Crack behaviors and localization for each mixture

This sub-chapter will present the crack localization and behaviors for our different mixtures. The illustration will compare the deformation or strain field (however one decides) of the reference image with that at the onset of cracking for 4-point bending test. For this case, we have only analyzed all fiber-reinforced specimens. Mainly because of their ductile behavior.

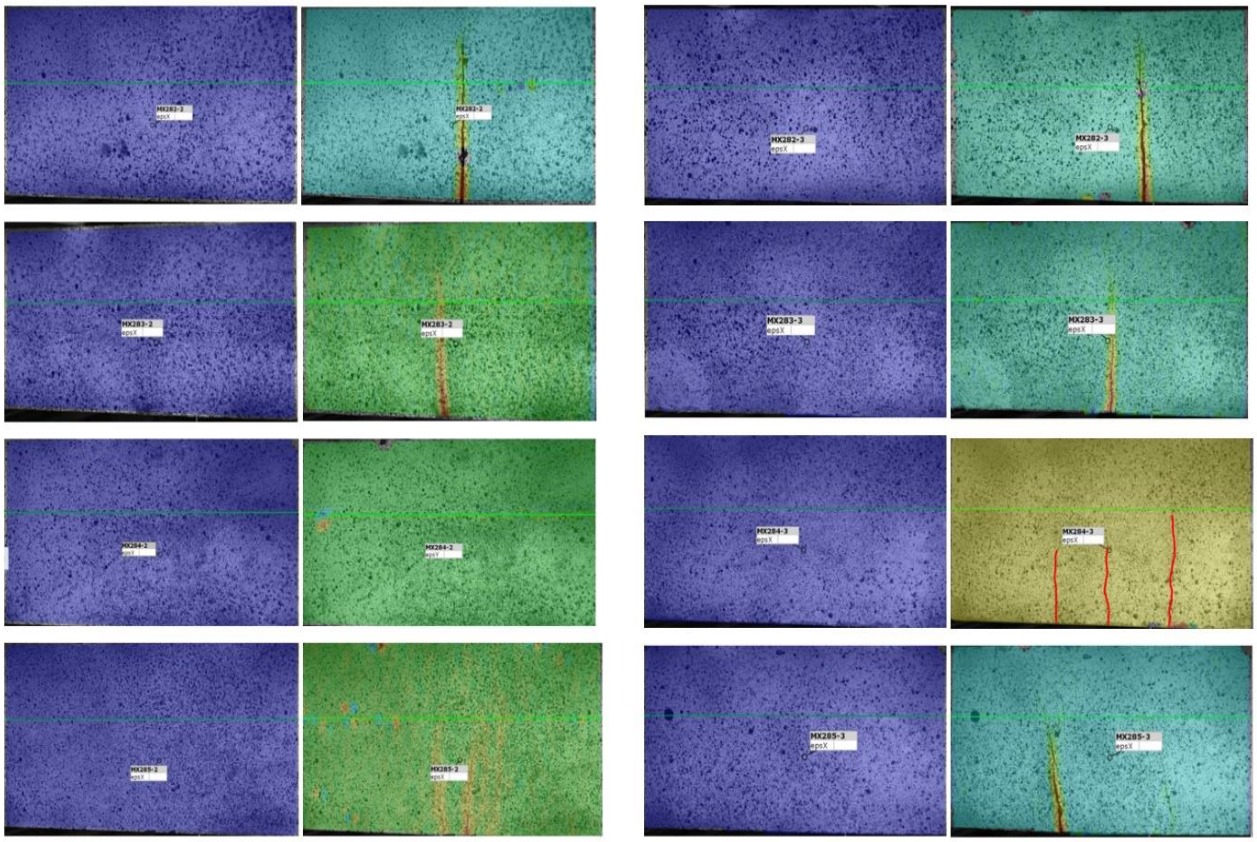

Figure 6.11 Illustration of crack development and localization compared to their reference image: (left) sample 2 and (right) sample 3.

Full-field strain development and fracture mechanism analysis

It is crucial to integrate deflection-load-time curves for each specimen of interest to fully utilize this analysis. By defining key stages of the specimen and implementing a full-field strain mapping, we can better understand our specimen behavior. However, due to the limitations we face within this research study, this sub-chapter will reflect only on the development of strain in both X – and Y directions and are represented by ε_x (epsx) and ε_y (epsx). Furthermore, only those of interest will be investigated instead of taking all our specimens. In this case, Mix 1(MX281-2), Mix 1(MX281-2), and Mix 1(MX281-2) are chosen for analysis. Our choice is based on the following reasons:

- Comparison of specimens with and without fiber reinforcement
- Analysis of the reduction of flexural strength for Mix 3
- Analysis of the optimal fiber content compared with the recommended values in many scientific literatures.

When we talk about strain, GOM has a different representation, and those can be chosen to illustrate any assessment. The illustration of our analysis is presented with the help of technical strain. Additionally, one can also have an inspection option, and this is divided into two. You can either choose inspection against a "Fixed value" the software computes or again "reference stage." It was logical to use inspection against a reference stage since our strain is the quotient of the length change and the reference length. Based on these choices, the full-field strain development for each specimen will be presented and reflected. These different mixtures are analyzed at three different test stages (beginning, middle, and onset of the crack). This will provide us with three different results, as seen in the figures below, and the analysis of two different strains, one in each direction.

In the case of mixture 1, since there is no presence of fibers, the behavior of our specimen is very brittle. Due to this reason, the camera could not capture the onset of cracking as it happens very fast. However, what was interesting here was that the ε_x of this specimen was distributed throughout the specimen. Additionally, we also observed localized strains which might have been mainly due to the clumping of concrete. However, in the case of ε_y it stays constant throughout the test, localized at the neutral axis. This again might have been due to the clumping referred and that this might have created a strain zone at that point.

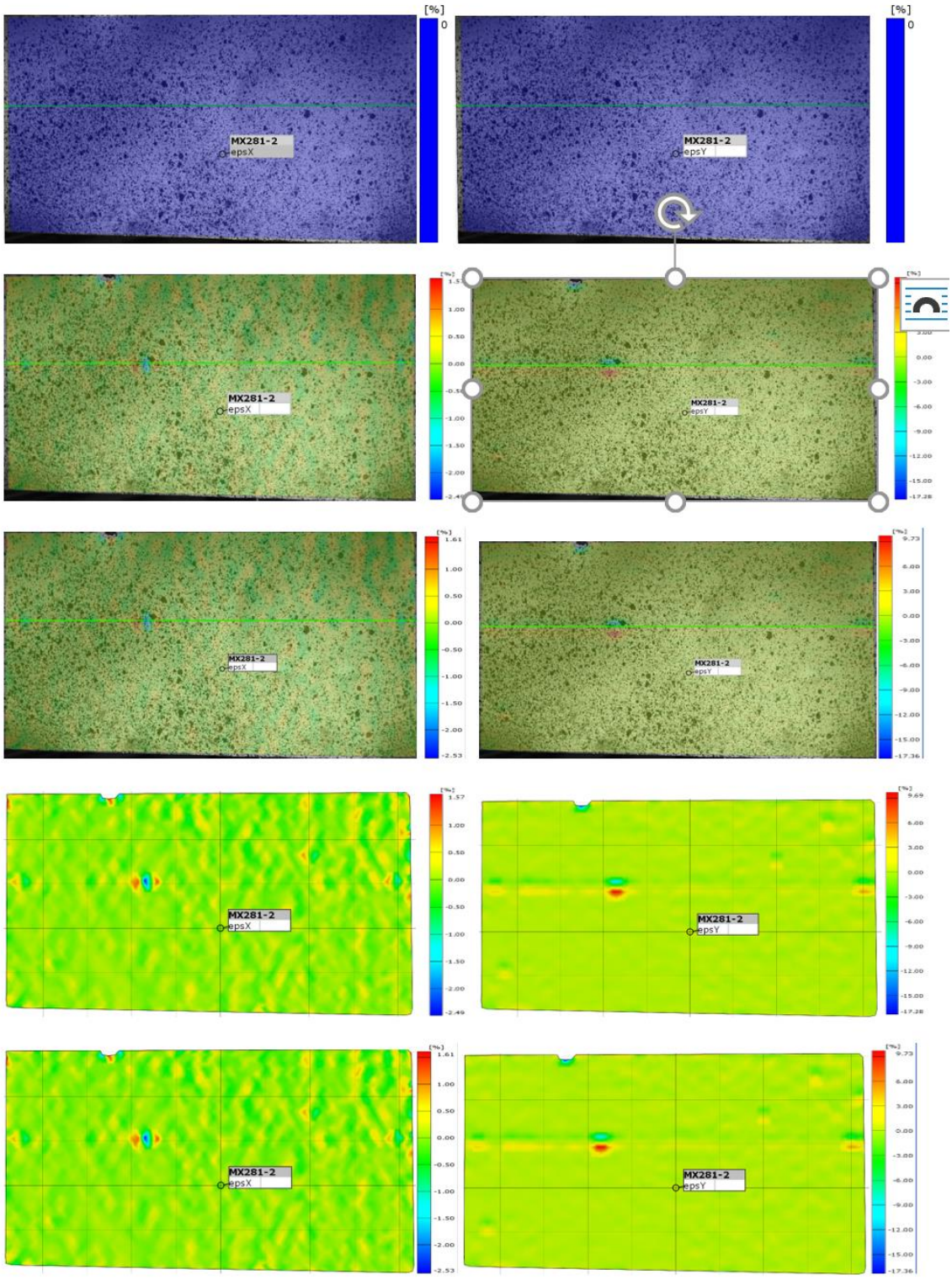

Figure 6.12 Strain development for Mixture 1 in each direction (X and Y) represented by εx (epsx) and εy (epsx).

Mixture 3 was a point of interest mainly due to its reduction in flexural strength compared to mixture 2, which has less fiber content. However, even at 1% fiber content, it is very difficult to distinguish the strain at the crack formation ($\varepsilon_{c,x}$) from the ultimate strain ($\varepsilon_{u,x}$). In other words, even thou we have a fiber-reinforced specimen, it still has a behavior of the ductile-brittle type. This is exhibited in Figure 6.13, where in a short time, we have a strain concentrated near the main crack where $\varepsilon_{c,x} = \varepsilon_{u,x} = 4.17\%$. However, in terms of ε_y we see a strain distribution in both the compressive and tensile zones. After the onset of crack, this strain is then released.

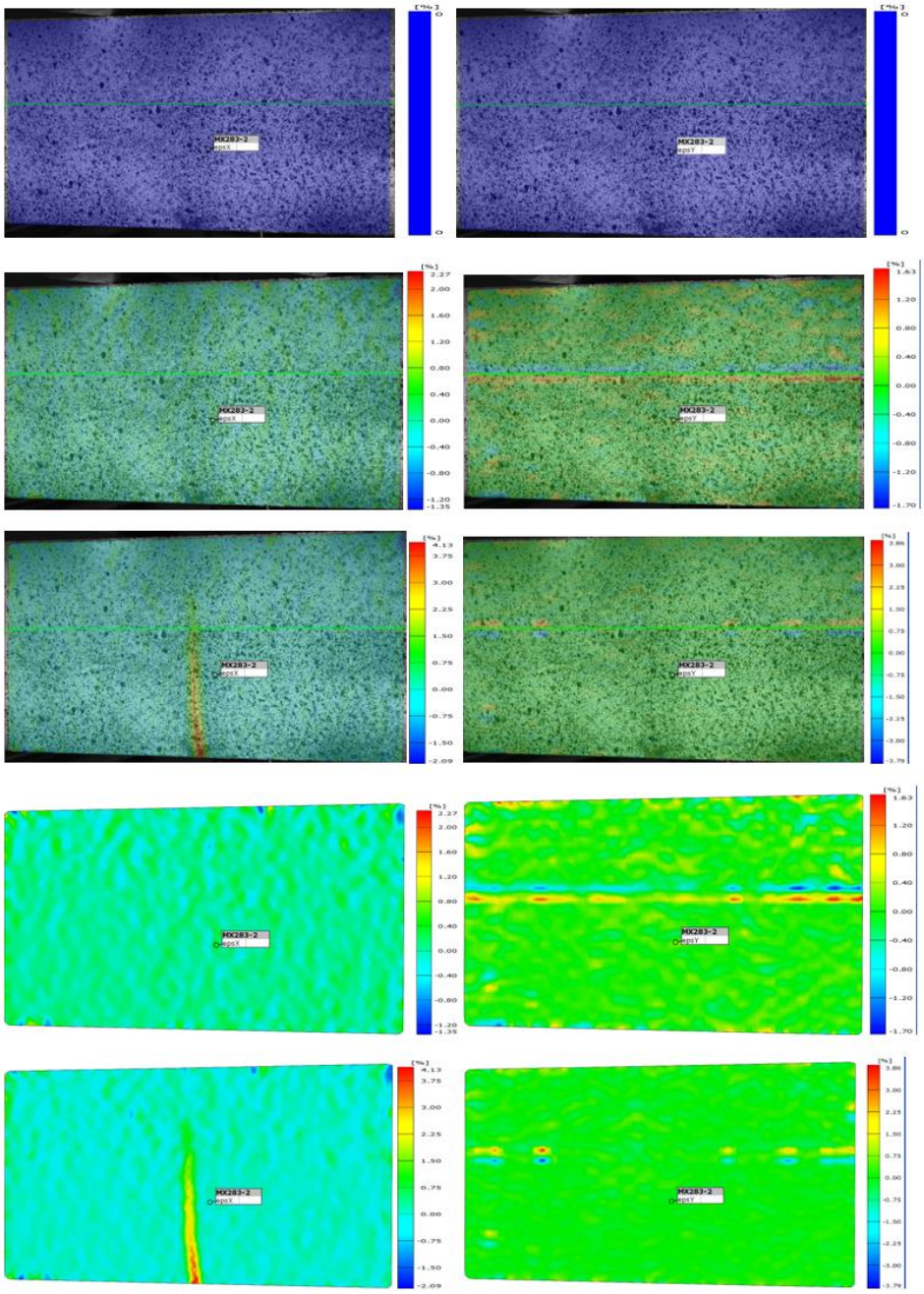

Figure 6.13 Strain development for Mixture 3 in each direction (X and Y) represented by εx (epsx) and εy (epsx).

In this case, there is also a very small development of ε_x and very less change in ε_y. It can also be that we have a late ε_x development, and since we have chosen three different stages to represent the development, the middle part could not achieve that. In this way, we only experience strain development at the onset of crack. Like the previous 2, we see that ε_y is heavily localized at the neutral axis and remains fairly constant throughout the test.

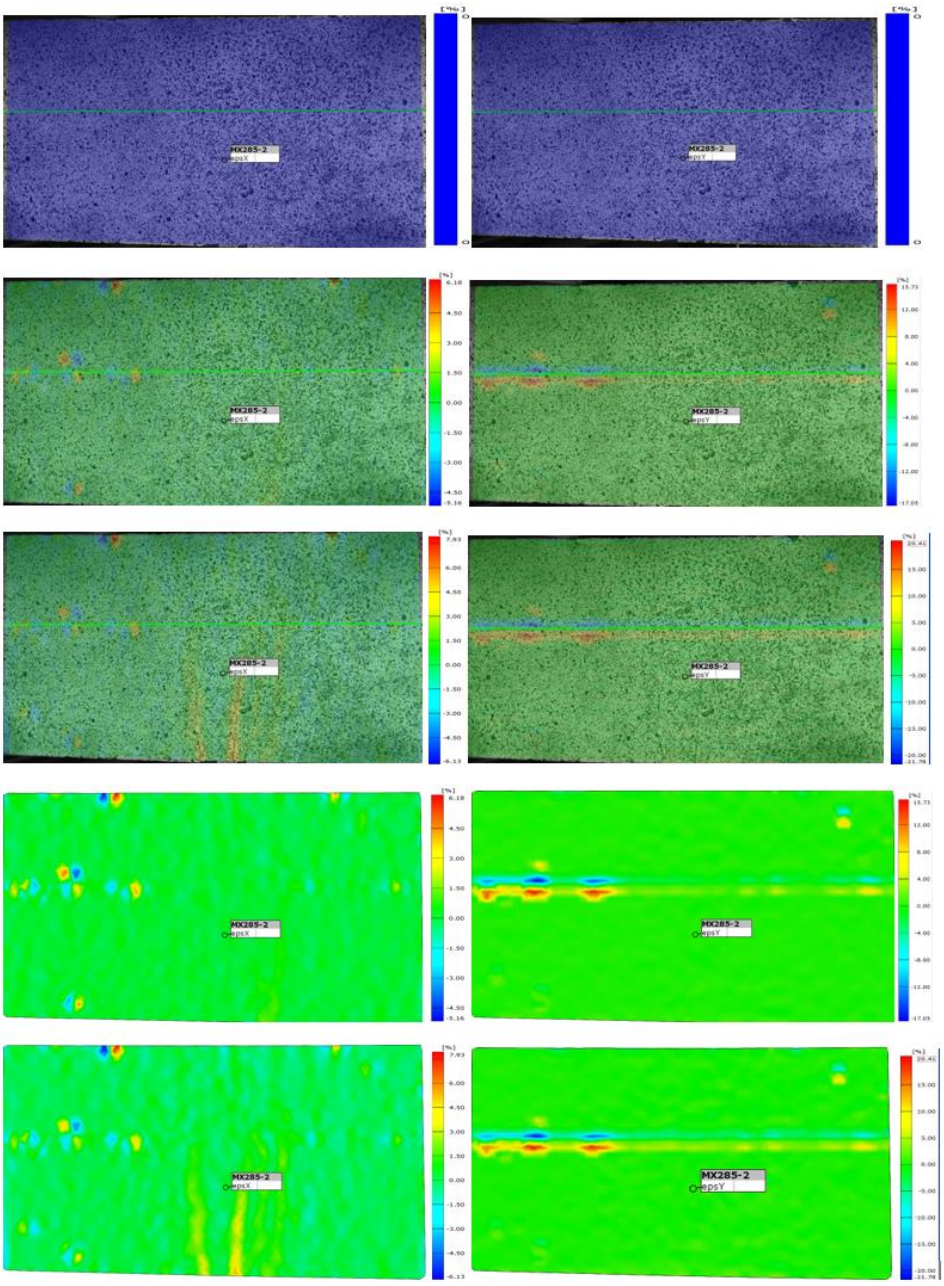

Figure 6.14 Strain development for Mixture 1 in each direction (X and Y) represented by εx (epsx) and εy (epsx).

Analysis of the deformation field

Here the main aim is to observe both vertical and horizontal displacement. The observation of vertical displacement within GOM can be compared with an external displacement transducer (LVDT) and used to validate the results. For this research study, we were unlucky because the testing machine did not have the possibility to register the external displacement acquired from LVDT. Nevertheless, with the help of a dial gauge, we tried to measure the displacement of

the test specimens. The dial gauge was placed in the middle of the span and on the back side of the specimen, so it does not interfere with the preparation/calibration of DIC. The maximum displacement achieved for each mixture is presented in Table 6.9

Table 6.9 Vertical displacement acquired with a dial gauge

Mixture	Sample 2	Sample 3
Mix 2	0.35	0.33
Mix 3	0.3	0.33
Mix 4	0.55	0.65
Mix 5	1	1.5

For comparison and validation purposes, the same displacement was also analyzed with the help of GOM. This will be presented in Figure 6.15. The displacement analysis is achieved with the help of "Point inspection." In this case, a point is placed at the exact point where we placed our dial gauge on the surface in GOM and then analyzed to compute the max displacement.

Table 6.10 Vertical displacement acquired from GOM.

Mixture	Sample 2	Sample 3
Mix 2	1.12	1.23
Mix 3	0.15	0.39
Mix 4	0.04	0.41
Mix 5	1.14	1.14

As we can observe from Tables 6.9 and 6.10 above, we see a big deviation between most mixtures. Only mixture 5 shows a hint of similarity, but even that is very hard to extract a conclusion. The reflection here is that using an analogy dial gauge may not be the best option since pre-calibration is needed before the test begins. So, if the gauge is tampered with in any way, it would need to be recalibrated. This was one of the problems we faced during pre-loading. The loading rollers sometimes need to be leveled up and down manually for adjustment and preparation of the test, and during this phase, the gauge might register a slight application of load. Nevertheless, if conducted properly, with the right tools, this would be the best way to compare and validate our experimental results with DIC.

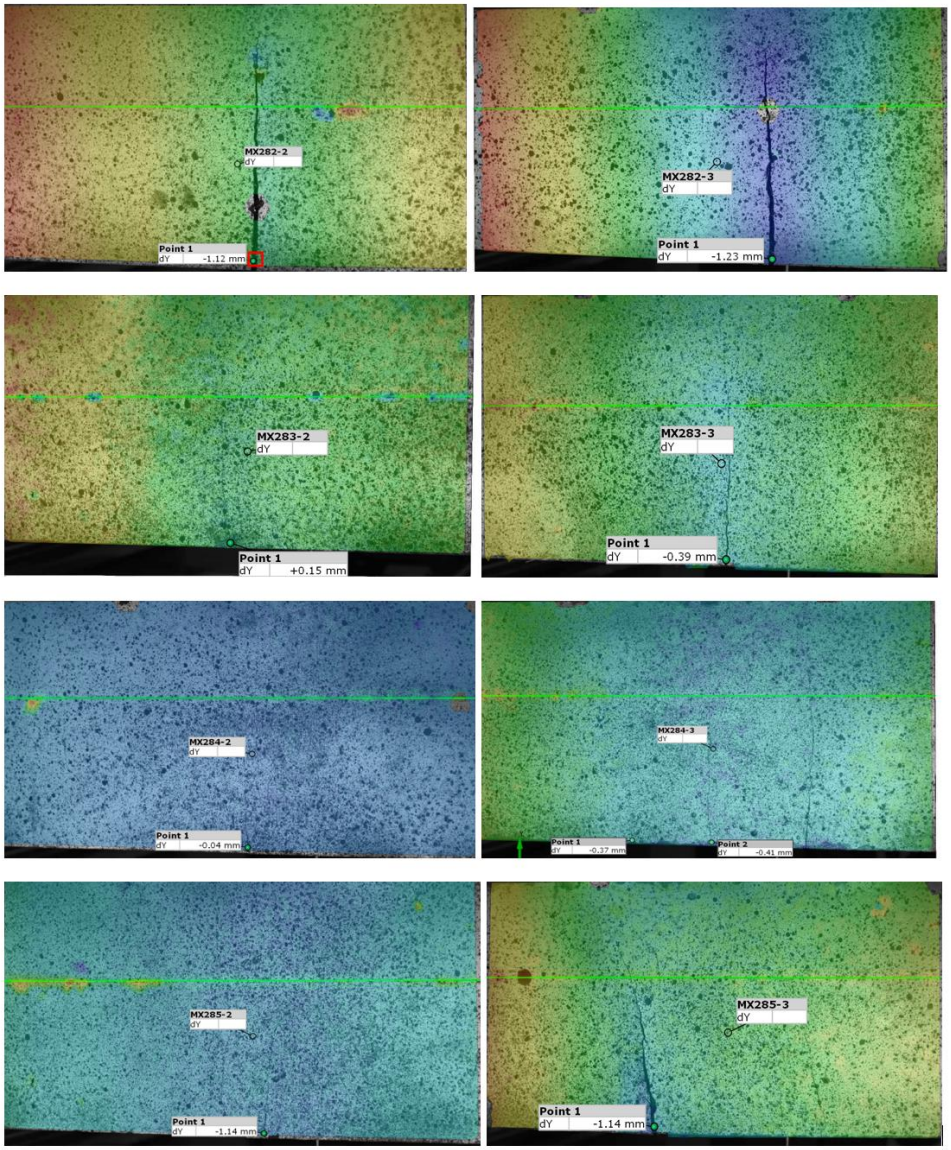

Figure 6.15 Vertical Displacement achieved from GOM.

Just as the field of strain, we also have a displacement field within GOM. This can be utilized to obtain the crack width since the crack width can be calculated from the relative horizontal displacement of points across the crack surface. One of the challenges with plastic strain in concrete is that they tend to be significantly small, and all the post-crack deformation we have on our crack surface is mostly due to crack displacement. So, by utilizing the relative horizontal displacement, the different points across our crack surface can be translated into crack width.

Figure 6.16 shows the displacement field at the onset of cracking and horizontal displacement of points across our crack surface.

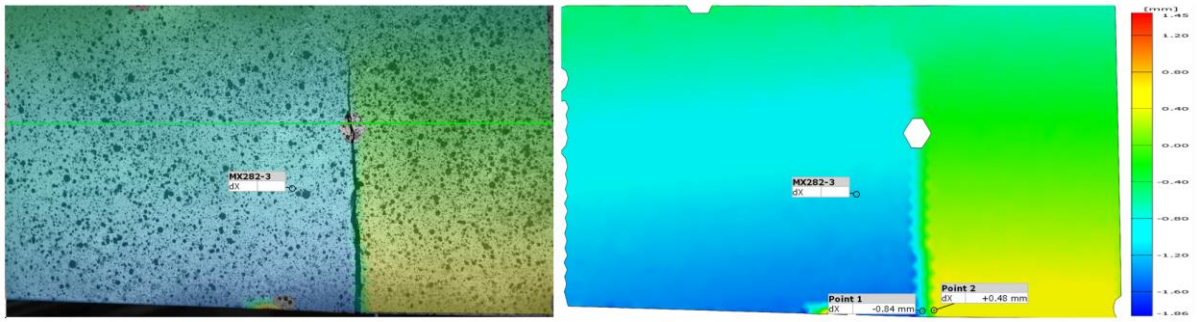

Figure 6.16 (left) displacement field at the onset of cracking and (right) horizontal displacement of points across our crack surface.

The next part would be the calculation of crack width, and as explained, this can now be achieved by computing the distance between these two points. However, the same can also be achieved by using a virtual extensometer. By placing this across the crack section on our test surface, you can compute the change in length in the direction needed (X-direction for horizontal displacement). In Figure 6.17, we can observe the change of length with respect to its reference length, which is expressed in percentage. Even thou the diagram shows an increased change in length, this is not the case for this specimen. Since we are observing the initial crack, some of the crack width as we progress with the height of the specimen can be wider than those in the bottom. However, the crack development would usually have an increasing pattern after we have tested the specimen into failure.

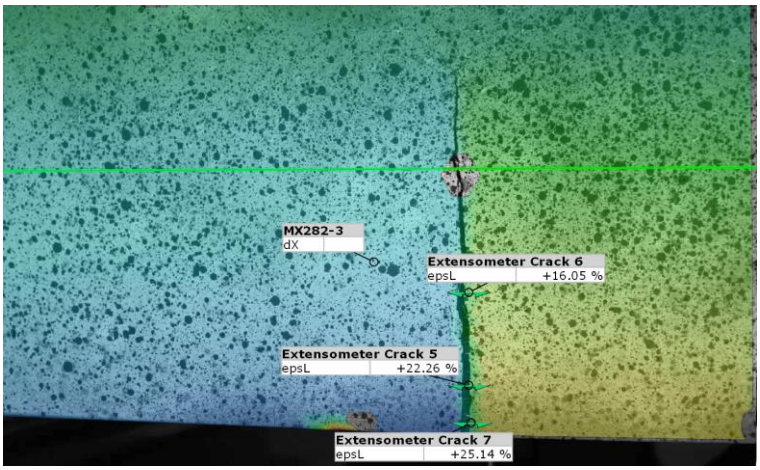

Figure 6.17 Crack width computation with virtual extensometer

7 CONCLUSION

Flowability

The outcome of steel fiber influence on flowability was almost as predicted since we expected to see a decreasing pattern with an increase in fiber content. Another interesting observation was the notable reduction when comparing Mix 1 and 2 to the rest of the mixtures. Some of our reflection on this behavior can be related to the increase in specific surface areas of steel, which would lead to a higher demand for cement paste covering the surface of fiber and aggregates. Another reason can be that the random distribution of steel fibers in the mortar can cause the steel fibers to act as a skeleton and eventually prevent the flow of the fresh mixture.

Additionally, the effect of superplasticizer reduction and different mixture sequences has also been assessed. The reduction led to a reduction in flowability, which was well within the target value for our minimum requirement for flowability. However, utilizing a mixture sequence where you take less consideration to the interaction between each ingredient can reduce flowability. The last consideration to be noted here is also the "batch size." For the preliminary laboratory, a smaller batch was utilized for our specimen, but for the final optimized mixture, a large batch was utilized to help with the effectivity and production of more specimens. The conclusion was that we achieved better flowability with a large batch/mixture compared to small batches.

Compressive Strength

Our general assessment based on previous scientific articles is to have an increasing pattern of compressive strength with the increase of steel fiber. This kind of pattern is not achieved for our research study; instead, we have an increasing pattern until 1% fiber content. After that, the compressive strength decreases and increases again. However, this is not the case for our results. For our specimens, Mix 5 (2.5%) did not have a higher value than Mix 3 (1%), and the sudden decrease of compressive strength of Mix 4 (1.5%) could be categorized under the influence of steel agglomeration, which can in return have a negative effect on the compressive strength. Another aspect is the effect of entrapped air within the specimen; however, we can see from the physical illustration of the different mixtures presented under the reflection of flowability that we did not experience any reduced workability. Nevertheless, the highest compressive strength for this research study was achieved with a fiber content of 1% for Mix 3. The addition of 0.5% throughout our entire mix has provided an increase in compressive strength of about 4.4%, 7.4%, 4.7%, and 6.2%, respectively

Flexural strength

Regarding the flexural strength, we observed that Mix 3 had the highest compressive strength compared to the other fiber-reinforced specimens. However, flexural Mix 3 has the lowest value for flexural compared to the other mixtures.

The addition of 0.5% throughout our entire mix has provided an increase in flexural strength of about 9.2%, 7.7%, 14%, and 50.7%, respectively. However, here we see that the addition of 2% steel fiber had a big increase in flexural strength. The reason behind this is clearly because of the crack-bridging effects of higher fiber content, which in return will lead to an increase in the flexural load carrying capacity. Additionally, we also have the mechanical interlock and friction at the fiber matrix that can contribute to the suppression of propagation and crack development.

Digital Image Correlation (DIC)

2D-DIC, when compared with conventional means, it offers many advantages in measuring crack width and displacement. The advantage of DIC within crack width is that it can allow the measurement of every crack separately, no matter their location. Another advantage is also the cost problems. Conventional measurements with LVDT sensors are much more expensive because of the price of the equipment and a data acquisition system. However, with DIC, all that you need is a digital camera, a personal computer, and a photo processing program.

The initial aim of this research study was to use DIC software to validate and evaluate the accuracy of 2D DIC results. However, due to many complications, some administrative and technical, a revision of this was necessary. So, in this study, DIC is used to evaluate and compare the vertical displacement achieved from a dial gauge. Which we found showed a big deviation.

In addition, the analysis of the full field of strain development is also presented. This gave us a small understanding of the stress distribution based on the load. However, to present a clear reflection was difficult due to the lack of equipment, such as load reading capabilities of the test machine, which can be crucial for any specimen.

8 RECOMMENDATION/FUTURE WORK

The work presented in this research study has proven to be satisfactorily assessed and managed to reach the overall goal even with the limited resources at hand. So, on that premises, we would recommend this type of study for future work, however, with minor adjustments. This adjustment will help elevate this topic to a higher level with the help of the following recommendations.

Mixtures and Resources

When working with experimental work/program, with development recipes and mix optimization, it is crucial to understand the importance of resources. This can be simply solved by introducing a small commercial mixture such as a Hobart countertop mixer. In addition, if one can integrate this with small forms certified by different standards, such as (50mmx50mmx50mm) for cubs and (40mmx40mmx160mm), this would provide higher efficiency and effectivity of the task at hand.

Laboratory essentials

Before embarking on a research study like this, it is also crucial to have an overview of the availability of all the proper equipment necessary to carry out the task. The lab is fully equipped to do an experimental program of a concrete specimen, but not ultra-high-performance concrete. Even thou we could be a bit creative and provide ourselves with the necessary equipment, that should not be the case for future work. This is mainly due to the time students have and the availability of resources. So, to simplify this, the following recommendation needs to be taken into consideration concerning lab essentials.

When working with flowability, UHPC has a set of equipment that needs to be available under testing. This is very crucial due to the behavior of UHPC mixtures, so either such equipment can be borrowed for a duration of time or invested.

Finally, when working with testing equipment, all necessary tools must be accounted for. For future work, it is important that the system is updated and able to perform the task at hand when it comes to the bending test. This was not possible for this research study, and for future work, this needs to be addressed and taken into consideration.

The different points above have been our primary concern and recommendation regarding the administrative aspect for future work. However, with our research study as a reference model or a form of a guideline, this process can be less demanding for future work.

So, to summarize and conclude, our recommendation would be to use the a or our pre-developed recipe to produce UHPC mixtures based on different fiber types and content. This will provide a better understanding of the fiber's influence on UHPC in a short time, and based on that assessment, an optimization process can be integrated. Another aspect is to observe the influence of different fiber combinations (hybridization) on UHPC. In addition to an experimental program, one can also incorporate a numerical analysis and Digital Image Correlate as validation tools. We believe combining all these would provide the best outcome for a master thesis.

9 REFERENCES

[1] A. M. Brandt, ‘Fibre reinforced cement-based (FRC) composites after over 40 years of development in building and civil engineering’, *Compos. Struct.*, vol. 86, no. 1, pp. 3–9, Nov. 2008, doi: 10.1016/j.compstruct.2008.03.006.

[2] I. H. Yang, C. Joh, and B.-S. Kim, ‘Structural behavior of ultra high performance concrete beams subjected to bending’, *Eng. Struct.*, vol. 32, no. 11, pp. 3478–3487, Nov. 2010, doi: 10.1016/j.engstruct.2010.07.017.

[3] P. Rashiddadash, A. A. Ramezanianpour, and M. Mahdikhani, ‘Experimental investigation on flexural toughness of hybrid fiber reinforced concrete (HFRC) containing metakaolin and pumice’, *Constr. Build. Mater.*, vol. 51, pp. 313–320, Jan. 2014, doi: 10.1016/j.conbuildmat.2013.10.087.

[4] P.-C. Aïtcin, ‘Cements of yesterday and today: Concrete of tomorrow’, *Cem. Concr. Res.*, vol. 30, no. 9, pp. 1349–1359, Sep. 2000, doi: 10.1016/S0008-8846(00)00365-3.

[5] N. M. Azmee and N. Shafiq, ‘Ultra-high performance concrete: From fundamental to applications’, *Case Stud. Constr. Mater.*, vol. 9, p. e00197, Dec. 2018, doi: 10.1016/j.cscm.2018.e00197.

[6] I. L. Larsen and R. T. Thorstensen, ‘The influence of steel fibres on compressive and tensile strength of ultra high performance concrete: A review’, *Constr. Build. Mater.*, vol. 256, p. 119459, Sep. 2020, doi: 10.1016/j.conbuildmat.2020.119459.

[7] S. Abbas, M. L. Nehdi, and M. A. Saleem, ‘Ultra-High Performance Concrete: Mechanical Performance, Durability, Sustainability and Implementation Challenges’, *Int. J. Concr. Struct. Mater.*, vol. 10, no. 3, Art. no. 3, Sep. 2016, doi: 10.1007/s40069-016-0157-4.

[8] C. Shi, Z. Wu, J. Xiao, D. Wang, Z. Huang, and Z. Fang, ‘A review on ultra high performance concrete: Part I. Raw materials and mixture design’, *Constr. Build. Mater.*, vol. 101, pp. 741–751, Dec. 2015, doi: 10.1016/j.conbuildmat.2015.10.088.

[9] S. El-Tawil, M. Alkaysi, A. E. Naaman, W. Hansen, and Z. Liu, ‘Development, characterization and applications of a non proprietary ultra high performance concrete for highway bridges’, Michigan. Dept. of Transportation, 2016.

[10] ‘Standard Practice for Fabricating and Testing Specimens of Ultra-High Performance Concrete’, *ASTM C1856C1856M*, 2017.

[11] Y. Dong, ‘Performance assessment and design of ultra-high performance concrete (UHPC) structures incorporating life-cycle cost and environmental impacts’, *Constr. Build. Mater.*, vol. 167, pp. 414–425, Apr. 2018, doi: 10.1016/j.conbuildmat.2018.02.037.

[12] R. Yu, P. Spiesz, and H. J. H. Brouwers, ‘Development of an eco-friendly Ultra-High Performance Concrete (UHPC) with efficient cement and mineral admixtures uses’, *Cem. Concr. Compos.*, vol. 55, pp. 383–394, 2015, doi: 10.1016/j.cemconcomp.2014.09.024.

[13] N. Randl, T. Steiner, S. Ofner, E. Baumgartner, and T. Mészöly, ‘Development of UHPC mixtures from an ecological point of view’, *Constr. Build. Mater.*, vol. 67, pp. 373–378, Sep. 2014, doi: 10.1016/j.conbuildmat.2013.12.102.

[14] R. F. Zollo, ‘Fiber-reinforced concrete: an overview after 30 years of development’, *Cem. Concr. Compos.*, vol. 19, no. 2, pp. 107–122, Jan. 1997, doi: 10.1016/S0958-9465(96)00046-7.

[15] A. E. Naaman and K. Wille, ‘The path to ultra-high performance fiber reinforced concrete (UHP-FRC): five decades of progress’, *Proc. Hipermat*, pp. 3–15, 2012.

[16] D.-Y. Yoo and N. Banthia, ‘Mechanical properties of ultra-high-performance fiber-reinforced concrete: A review’, *Cem. Concr. Compos.*, vol. 73, pp. 267–280, Oct. 2016, doi: 10.1016/j.cemconcomp.2016.08.001.

[17] P. Richard and M. Cheyrezy, ‘Composition of reactive powder concretes’, *Cem. Concr. Res.*, vol. 25, no. 7, pp. 1501–1511, Oct. 1995, doi: 10.1016/0008-8846(95)00144-2.

[18] A. Sadrekarimi, ‘Development of a Light Weight Reactive Powder Concrete’, *J. Adv. Concr. Technol.*, vol. 2, no. 3, pp. 409–417, 2004, doi: 10.3151/jact.2.409.

[19] M. Schmidt, ‘Sustainable building with UHPC - Coordinated Research Program in Germany’, *UHPC Nanotechnol. Constr. 3rd Int Symp UHPC*, pp. 17–25, 2012.

[20] H. G. Russell, B. A. Graybeal, and H. G. Russell, ‘Ultra-high performance concrete: A state-of-the-art report for the bridge community.’, United States. Federal Highway Administration. Office of Infrastructure …, 2013.

[21] M. Schmidt, T. Leutbecher, S. Piotrowski, and U. Wiens, ‘The German guideline for ultra-high performance concrete’, in *Proceedings of the FGC-ACI-fib-RILEM Int. Symposium on Ultra-High Performance Fibre-Reinforced Concrete, Montpellier, France*, 2017, pp. 2–4.

[22] V. Perry and K. Habel, ‘STANDARDIZATION OF ULTRA-HIGH PERFORMANCE CONCRETE THE CANADIAN PESPECTIVE’, *Reinf. Concr.*, p. 10, 2017.

[23] R. MCS-EPFL, ‘Ultra-high performance fibre reinforced cement-based composites (UHPFRC) construction material, dimensioning und application’, *Lausanne Switz.*, 2016.

[24] J. No, ‘9: Guidelines for Concrete, Recommendation for design and construction of ultra high strength fiber reinforced concrete structures (Draft)’, *Jpn. Soc. Civ. Eng. JSCE Jpn.*, 2006.

[25] N. Gowripalan and R. I. Gilbert, ‘Design guidelines for ductal prestressed concrete beams’, *Ref. Artical Univ. NSW*, 2000.

[26] J. A. López, P. Serna, and J. Navarro-Gregori, *Advances in the development of the first UHPFRC Recommendations in Spain: Material classification, design and characterization*. RILEM Publications SARL, 2017, pp. 565–74.

[27] M. K. Tadros, D. Gee, M. Asaad, and J. Lawler, ‘Ultra-high-performance concrete: A game changer in the precast concrete industry’, *PCI J*, vol. 65, pp. 3–06, 2020.

[28] A. Association Françoise de Genie Civil, ‘French interim recommendations of ultra-high performance Fiber reinforced concrete (UHPFRC)’, 2002.

[29] N. P18-470, *Concrete-Ultra-High Performance Fiber-Reinforced Concrete-Specifications, performance, production and conformity*. AFNOR-French standard institute, 2016.

[30] A. (Association F. de Normalisation), *National addition to Eurocode 2—Design of concrete structures: Specific rules for ultra-high performance fibre-reinforced concrete (UHPFRC)*. AFNOR Paris, 2016.

[31] W. Meng, ‘Design and performance of cost-effective ultra-high performance concrete for prefabricated elements’, 2017.

[32] W. Meng, M. Valipour, and K. H. Khayat, ‘Optimization and performance of cost-effective ultra-high performance concrete’, *Mater. Struct.*, vol. 50, no. 1, p. 29, Aug. 2016, doi: 10.1617/s11527-016-0896-3.

[33] E. Shahrokhinasab and D. Garber, ‘Development of “ABC-UTC Non-Proprietary UHPC” Mix’, Final Report# ABC-UTC-2016-C2-FIU01-Final, 2021.

[34] B. Graybeal, ‘Design and construction of field-cast UHPC connections. Rep. No’, FHWA-HRT-14-084. Washington, DC: Federal Highway Administration, 2014.

[35] ACI Committee 239, ‘Ultra-high-performance Concrete: An Emerging Technology Report (ACI 239R-18)’, 2018.

[36] M. Tadros, ‘Implementation of Ultra-High-Performance Concrete in Long-Span Precast Pretensioned Elements for Concrete Buildings and Bridges’, *Precast. Concr. Inst. PCIJanuary 2020 Doi*, vol. 10, 2020.

[37] Canadian Standards Association, *Concrete Materials and Methods of Concrete Construction: Test Methods and Standard Practices for Concrete*. Canadian Standards Association, 2009.

[38] S. Merkblatt, ‘2052: 2016: Ultra-Hochleistungs-Faserbeton (UHFB), Baustoffe, Bemessung und Ausführung’, *Schweiz. Ingenieur- Archit. SIA Zür.*, 2016.

[39] M. Alkaysi and S. El-Tawil, ‘Effects of variations in the mix constituents of ultra high performance concrete (UHPC) on cost and performance’, *Mater. Struct.*, vol. 49, no. 10, pp. 4185–4200, 2016.

[40] D. Garber and E. Shahrokhinasab, ‘Performance Comparison of In-Service, Full-Depth Precast Concrete Deck Panels to Cast-in-Place Decks’, Accelerated Bridge Construction University Transportation Center (ABC-UTC), 2019.

[41] B. A. Graybeal, ‘Material Property Characterization of Ultra-High Performance Concrete’, p. 188.

[42] O. Mishra and S. Singh, ‘An overview of microstructural and material properties of ultra-high-performance concrete’, *J. Sustain. Cem.-Based Mater.*, vol. 8, no. 2, pp. 97–143, 2019.

[43] S. El-Tawil, Y.-S. Tai, J. A. B. Ii, and D. Rogers, ‘Open-Recipe Ultra-High-Performance Concrete’, *Concr. Int.*, vol. 42, no. 6, pp. 33–38, Jun. 2020.

[44] M. Gesoglu, E. Güneyisi, G. F. Muhyaddin, and D. S. Asaad, ‘Strain hardening ultra-high performance fiber reinforced cementitious composites: Effect of fiber type and concentration’, *Compos. Part B Eng.*, vol. 103, pp. 74–83, Oct. 2016, doi: 10.1016/j.compositesb.2016.08.004.

[45] ‘Influence of steel fiber content and aspect ratio on the uniaxial tensile and compressive behavior of ultra high performance concrete - ScienceDirect’. https://www.sciencedirect.com/science/article/pii/S0950061817314733 (accessed Dec. 05, 2021).

[46] W. Meng and K. Khayat, ‘Effect of hybrid fibers on fresh, mechanical properties, and autogenous shrinkage of cost effective UHPC’, *J. Mater. Civ. Eng.*, vol. 30, Apr. 2018, doi: 10.1061/(ASCE)MT.1943-5533.0002212.

[47] D. Yoo, S. Kim, G. Park, J. Park, and S. Kim, 'Effects of fiber shape, aspect ratio, and volume fraction on flexural behavior of ultra-high-performance fiber-reinforced cement composites', 2017, doi: 10.1016/J.COMPSTRUCT.2017.04.069.

[48] D.-Y. Yoo, M. Kim, S.-W. Kim, and J.-J. Park, 'Development of cost effective ultra-high-performance fiber-reinforced concrete using single and hybrid steel fibers', *Constr. Build. Mater.*, vol. 150, pp. 383–394, Sep. 2017, doi: 10.1016/j.conbuildmat.2017.06.018.

[49] N. Azmee and N. Shafiq, 'Ultra-High Performance Concrete: From Fundamental to Applications', *Case Stud. Constr. Mater.*, vol. 9, Sep. 2018, doi: 10.1016/j.cscm.2018.e00197.

[50] A. M. Jabbar, M. J. Hamood, and D. H. Mohammed, 'Ultra High Performance Concrete Preparation Technologies and Factors Affecting the Mechanical Properties: A Review', *IOP Conf. Ser. Mater. Sci. Eng.*, vol. 1058, no. 1, p. 012029, Feb. 2021, doi: 10.1088/1757-899X/1058/1/012029.

[51] R. Deeb, A. Ghanbari, and B. L. Karihaloo, 'Development of self-compacting high and ultra high performance concretes with and without steel fibres', *Cem. Concr. Compos.*, vol. 34, no. 2, pp. 185–190, 2012, doi: 10.1016/j.cemconcomp.2011.11.001.

[52] B. Mobasher, A. Arora, M. Aguayo, F. Kianmofrad, Y. Yao, and N. Neithalath, 'Developing Ultra-High–Performance Concrete Mix Designs for Arizona Bridge Element Connections', Arizona. Department of Transportation. Research Center, 2019.

[53] R. Karim and B. Shafei, 'Flexural response characteristics of ultra-high performance concrete made with steel microfibers and macrofibers', *Struct. Concr.*, 2021.

[54] D.-Y. Yoo, S. Kim, G.-J. Park, J.-J. Park, and S.-W. Kim, 'Effects of fiber shape, aspect ratio, and volume fraction on flexural behavior of ultra-high-performance fiber-reinforced cement composites', *Compos. Struct.*, vol. 174, pp. 375–388, 2017, doi: 10.1016/j.compstruct.2017.04.069.

[55] A. Arora, Y. Yao, B. Mobasher, and N. Neithalath, 'Fundamental insights into the compressive and flexural response of binder- and aggregate-optimized ultra-high performance concrete (UHPC)', *Cem. Concr. Compos.*, vol. 98, pp. 1–13, 2019, doi: 10.1016/j.cemconcomp.2019.01.015.

[56] C. Gu, G. Ye, and W. Sun, 'Ultrahigh performance concrete-properties, applications and perspectives', *Sci. China Technol. Sci.*, vol. 58, no. 4, pp. 587–599, 2015.

[57] M. Schmidt and E. Fehling, 'Ultra-high-performance concrete: research, development and application in Europe', *ACI Spec Publ*, vol. 228, no. 1, pp. 51–78, 2005.

[58] E. Fehling, M. Schmidt, J. Walraven, T. Leutbecher, and S. Fröhlich, 'Ultra high performance concrete (UHPC)', 2008.

[59] M. Rebentrost, G. Wight, and E. Fehling, 'Experience and applications of ultra-high performance concrete in Asia', in *2nd international symposium on ultra high performance concrete*, 2008, vol. 10, pp. 19–30.

[60] M. Zhou, W. Lu, J. Song, and G. C. Lee, 'Application of Ultra-High Performance Concrete in bridge engineering', *Constr. Build. Mater.*, vol. 186, pp. 1256–1267, Oct. 2018, doi: 10.1016/j.conbuildmat.2018.08.036.

[61] T. S. Chow, P. Eng, V. H. Perry, G. Culham, and D. Zakariasen, 'First use of UHPFRC in thin precast concrete roof shell for Canadian LRT station', *PCI J.*, 2005.

[62] ‘Jean Bouin Stadium’, *ductal ®*, Jun. 02, 2021. https://www.ductal.com/en/jean-bouin-stadium (accessed Apr. 23, 2022).

[63] M. Schmidt, E. Fehling, and E. Fehling, ‘Ultra-High-Performance Concrete: Research, Development and Application in Europe’, 2005.

[64] K. Wille, A. Naaman, and G. Parra-Montesinos, ‘Ultra-High Performance Concrete with Compressive Strength Exceeding 150 MPa (22 ksi): A Simpler Way’, *ACI Mater. J.*, vol. 108, pp. 46–54, Jan. 2011.

[65] Y.-S. Tai and S. El-Tawil, ‘Effect of component materials and mixing protocol on the short-term performance of generic ultra-high-performance concrete’, *Constr. Build. Mater.*, vol. 238, p. 117703, Mar. 2020, doi: 10.1016/j.conbuildmat.2019.117703.

[66] A. Alsalman, C. N. Dang, J. R. Martí-Vargas, and W. Micah Hale, ‘Mixture-proportioning of economical UHPC mixtures’, *J. Build. Eng.*, vol. 27, p. 100970, Jan. 2020, doi: 10.1016/j.jobe.2019.100970.

[67] P. S. Ambily, K. Ravisankar, C. Umarani, J. K. Dattatreya, and N. R. Iyer, ‘Development of ultra-high-performance geopolymer concrete’, *Mag. Concr. Res.*, vol. 66, no. 2, pp. 82–89, 2014, doi: 10.1680/macr.13.00057.

[68] Y. Liu, Z. Zhang, C. Shi, D. Zhu, N. Li, and Y. Deng, ‘Development of ultra-high performance geopolymer concrete (UHPGC): Influence of steel fiber on mechanical properties’, *Cem. Concr. Compos.*, vol. 112, 2020, doi: 10.1016/j.cemconcomp.2020.103670.

[69] S. Xu *et al.*, ‘Development and preliminary mix design of ultra-high-performance concrete based on geopolymer’, *Constr. Build. Mater.*, vol. 308, 2021, doi: 10.1016/j.conbuildmat.2021.125110.

[70] M. Alkaysi and S. El-Tawil, ‘Effects of variations in the mix constituents of ultra high performance concrete (UHPC) on cost and performance’, *Mater. Struct. Constr.*, vol. 49, no. 10, pp. 4185–4200, 2016, doi: 10.1617/s11527-015-0780-6.

[71] M. Nodehi and F. Aguayo, ‘Ultra high performance and high strength geopolymer concrete’, *J. Build. Pathol. Rehabil.*, vol. 6, no. 1, 2021, doi: 10.1007/s41024-021-00130-5.

[72] Y. Shi, G. Long, X. Zeng, Y. Xie, and H. Wang, ‘Green ultra-high performance concrete with very low cement content’, *Constr. Build. Mater.*, vol. 303, 2021, doi: 10.1016/j.conbuildmat.2021.124482.

[73] N. M. Azmee and M. F. Nuruddin, ‘Impact performance of low cement Ultra-high-performance concrete’, *WIT Trans. Ecol. Environ.*, vol. 223, pp. 481–488, 2017, doi: 10.2495/SC170421.

[74] R. Xiao, Z.-C. Deng, and C. Shen, ‘Properties of ultra high performance concrete containing superfine cement and without silica fume’, *J. Adv. Concr. Technol.*, vol. 12, no. 2, pp. 73–81, 2014, doi: 10.3151/jact.12.73.

[75] S. Kosmatka, B. Kerkhoff, and W. Panarese, *Design and Control of Concrete Mixtures*. 2002.

[76] P. Zhan, J. Xu, J. Wang, and C. Jiang, ‘Multi-scale study on synergistic effect of cement replacement by metakaolin and typical supplementary cementitious materials on properties of ultra-high performance concrete’, *Constr. Build. Mater.*, vol. 307, 2021, doi: 10.1016/j.conbuildmat.2021.125082.

[77] V. Malagavelli and R. P N, ‘High performance concrete with GGBS and ROBO sand’, *Int. J. Eng. Sci. Technol.*, vol. 2, Oct. 2010.

[78] Z. B. Haber, I. De la Varga, B. A. Graybeal, B. Nakashoji, and R. El-Helou, ‘Properties and behavior of UHPC-class materials’, United States. Federal Highway Administration. Office of Infrastructure …, 2018.

[79] F. W. Locher, *Cement: principles of production and use*. Verlag Bau+ Technik, 2013.

[80] ‘Flygeaske’, *Wikipedia*. Feb. 04, 2021. Accessed: Nov. 28, 2021. [Online]. Available: https://no.wikipedia.org/w/index.php?title=Flygeaske&oldid=21170207

[81] D. Moore and David Moore, *The Roman [[Pantheon, Rome|Pantheon]]: The Triumph of Concrete*.

[82] P. K. Mehta, ‘HIGH PERFORMANCE, HIGH-VOLUME FLY ASH CONCRETE FOR SUSTAINABLE DEVELOPMENT’, *undefined*, 2004, Accessed: Nov. 28, 2021. [Online]. Available: https://www.semanticscholar.org/paper/HIGH-PERFORMANCE%2C-HIGH-VOLUME-FLY-ASH-CONCRETE-FOR-Mehta/c6dd6374084831847f7ef9c3a66539ed9ad54d8c

[83] J. D. Birchall, A. J. Howard, and K. Kendall, ‘Flexural strength and porosity of cements’, *Nature*, vol. 289, no. 5796, pp. 388–390, Jan. 1981, doi: 10.1038/289388a0.

[84] F. de Larrard and T. Sedran, ‘Optimization of ultra-high-performance concrete by the use of a packing model’, *Cem. Concr. Res.*, vol. 24, no. 6, pp. 997–1009, Jan. 1994, doi: 10.1016/0008-8846(94)90022-1.

[85] ‘ACI 239R-18 : Ultra-High-Performance Concrete: An Emerging Technology Report’. https://www.bsbedge.com/productdetails/ACI/ACI239R/aci239r (accessed Nov. 29, 2021).

[86] Z. Wu, K. H. Khayat, and C. Shi, ‘Changes in rheology and mechanical properties of ultra-high performance concrete with silica fume content’, *Cem. Concr. Res.*, vol. 123, 2019, doi: 10.1016/j.cemconres.2019.105786.

[87] M. A. Mosaberpanah, O. Eren, and A. R. Tarassoly, ‘The effect of nano-silica and waste glass powder on mechanical, rheological, and shrinkage properties of UHPC using response surface methodology’, *J. Mater. Res. Technol.*, vol. 8, no. 1, pp. 804–811, 2019, doi: 10.1016/j.jmrt.2018.06.011.

[88] Y. J. Kim and J. Wang, ‘Development of ultra-high-performance concrete with various silica admixtures’, *ACI Mater. J.*, vol. 116, no. 2, pp. 33–44, 2019, doi: 10.14359/51714450.

[89] Z. Wu, C. Shi, K. H. Khayat, and L. Xie, ‘Effect of SCM and nano-particles on static and dynamic mechanical properties of UHPC’, *Constr. Build. Mater.*, vol. 182, pp. 118–125, 2018, doi: 10.1016/j.conbuildmat.2018.06.126.

[90] Z. Rong, W. Sun, H. Xiao, and G. Jiang, ‘Effects of nano-SiO2 particles on the mechanical and microstructural properties of ultra-high performance cementitious composites’, *Cem. Concr. Compos.*, vol. 56, pp. 25–31, 2015, doi: 10.1016/j.cemconcomp.2014.11.001.

[91] R. Yu, P. Spiesz, and H. J. H. Brouwers, ‘Effect of nano-silica on the hydration and microstructure development of Ultra-High Performance Concrete (UHPC) with a low binder amount’, *Constr. Build. Mater.*, vol. 65, pp. 140–150, 2014, doi: 10.1016/j.conbuildmat.2014.04.063.

[92] K. Huang, J. Xie, R. Wang, Y. Feng, and R. Rao, ‘Effects of the combined usage of nanomaterials and steel fibres on the workability, compressive strength, and microstructure of ultra-high performance concrete’, *Nanotechnol. Rev.*, vol. 10, no. 1, pp. 304–317, 2021, doi: 10.1515/ntrev-2021-0029.

[93] Y. Su, C. Wu, J. Li, Z.-X. Li, and W. Li, ‘Development of novel ultra-high performance concrete: From material to structure’, *Constr. Build. Mater.*, vol. 135, pp. 517–528, 2017, doi: 10.1016/j.conbuildmat.2016.12.175.

[94] Z. Li and Q. Pei, ‘Nano-materials on the strength of ultra-high performance concrete’, *Ferroelectrics*, vol. 578, no. 1, pp. 194–207, 2021, doi: 10.1080/00150193.2021.1902780.

[95] B. Graybeal, *Design and Construction of Field-Cast UHPC Connections*. 2014. doi: 10.13140/2.1.2839.0087.

[96] B. A. Graybeal, ‘Development of Non-Proprietary Ultra-High Performance Concrete for Use in the Highway Bridge Sector: TechBrief’, United States. Federal Highway Administration, 2013.

[97] P. Mehta and P. Monteiro, *Concrete: Microstructure, Properties, and Materials*. McGraw-Hill Education, 2014. Accessed: Dec. 03, 2021. [Online]. Available: https://www.accessengineeringlibrary.com/content/book/9780071797870

[98] P. Zhang, H. Yiliang, Y. Li, J. Zhao, H. Dong, and T. Chen, ‘Influence Factors on the Properties of Ultrahigh-Performance Fiber-Reinforced Concrete Cured under the Condition of Room Temperature’, *Adv. Civ. Eng.*, vol. 2018, pp. 1–9, Jul. 2018, doi: 10.1155/2018/2754735.

[99] N. Hamiruddin, R. Razak, K. Muhamad, mohd zulham affandi mohd zahid, and C. N. S. Aziz, ‘The Effect of Different Sand Gradation with Ultra High Performance Concrete (UHPC)’, *Solid State Phenom.*, vol. 280, pp. 476–480, Aug. 2018, doi: 10.4028/www.scientific.net/SSP.280.476.

[100] B. Graybeal, ‘Ultra-high performance concrete’, 2011.

[101] P. P. Li, Q. L. Yu, and H. J. H. Brouwers, ‘Effect of PCE-type superplasticizer on early-age behaviour of ultra-high performance concrete (UHPC)’, *Constr. Build. Mater.*, vol. 153, pp. 740–750, Oct. 2017, doi: 10.1016/j.conbuildmat.2017.07.145.

[102] C. Shi, Z. Wu, J. Xiao, D. Wang, Z. Huang, and Z. Fang, ‘A review on ultra high performance concrete: Part I. Raw materials and mixture design’, *Constr. Build. Mater.*, vol. 101, pp. 741–751, 2015, doi: 10.1016/j.conbuildmat.2015.10.088.

[103] E. Fehling, M. Schmidt, and S. Stürwald, Eds., *Ultra high performance concrete (UHPC): proceedings of the Second International Symposium on Ultra High Performance Concrete, Kassel, Germany, March 05-07, 2008*. Kassel: Kassel University Press, 2008.

[104] P. Rossi, ‘ULTRA-HIGH-PERFORMANCE FIBER-REINFORCED CONCRETES’, *Concr. Int.*, vol. 23, no. 12, Dec. 2001, Accessed: Nov. 29, 2021. [Online]. Available: https://trid.trb.org/view.aspx?id=716413

[105] J. I. Daniel, V. S. Gopalaratnam, and M. A. Galinat, ‘Report on Fiber Reinforced Concrete’, p. 66.

[106] G. L. Balàzs *et al.*, *fib Bulletin 1. Structural Concrete Textbook on Behaviour, Design and Perfo ance Up date d knowle d ge of the CEB/FIP Model Code 1990 Volume 1*. fib.

The International Federation for Structural Concrete, 1999. doi: 10.35789/fib.BULL.0001.

[107] 'Guide for Specifying, Proportioning, Mixing, Placing, and Finishing Steel Fiber Reinforced Concrete', *ACI Mater. J.*, vol. 90, no. 1, 1993, doi: 10.14359/4046.

[108] H. G. Russell and B. Graybeal, 'Ultra-High Performance Concrete: A State-of-the-Art Report for the Bridge Community', *undefined*, 2013, Accessed: Nov. 30, 2021. [Online]. Available: https://www.semanticscholar.org/paper/Ultra-High-Performance-Concrete%3A-A-State-of-the-Art-Russell-Graybeal/5f5051e955361d1c1226e4469954deed01967cbc

[109] X. Zhang and H. Zhang, 'Experimental Research on Ultra-High Performance Concrete (UHPC)', *IOP Conf. Ser. Mater. Sci. Eng.*, vol. 562, no. 1, p. 012045, Jun. 2019, doi: 10.1088/1757-899X/562/1/012045.

[110] P. Zhang, Y. Huang, Y. Li, J. Zhao, H. Dong, and T. Chen, 'Influence Factors on the Properties of Ultrahigh-Performance Fiber-Reinforced Concrete Cured under the Condition of Room Temperature', *Adv. Civ. Eng.*, 2018, doi: 10.1155/2018/2754735.

[111] N. Carino and H. Lew, 'The Maturity Method: From Theory to Application1', May 2001, doi: 10.1061/40558(2001)17.

[112] J. Park, Y. Kim, J.-R. Cho, and S.-J. Jeon, 'Early-Age Strength of Ultra-High Performance Concrete in Various Curing Conditions', *Materials*, vol. 8, pp. 5537–5553, Aug. 2015, doi: 10.3390/ma8085261.

[113] K. Koh, J. Park, G. Ryu, and S.-T. Kang, 'Effect of the Compressive Strength of Ultra-High Strength Steel Fiber Reinforced Cementitious Composites on Curing Method', *undefined*, 2007, Accessed: Dec. 03, 2021. [Online]. Available: https://www.semanticscholar.org/paper/Effect-of-the-Compressive-Strength-of-Ultra-High-on-Koh-Park/f6dd44a62392d6912cfadee18222386c35064554

[114] S. L. Yang, S. G. Millard, M. Soutsos, S. Barnett, and T. Le, 'Influence of aggregate and curing regime on the mechanical properties of ultra-high performance fibre reinforced concrete (UHPFRC)', *Constr. Build. Mater.*, vol. 23, pp. 2291–2298, Jun. 2009, doi: 10.1016/j.conbuildmat.2008.11.012.

[115] H. Yazıcı, 'The effect of curing conditions on compressive strength of ultra high strength concrete with high volume mineral admixtures', *Build. Environ.*, vol. 42, no. 5, pp. 2083–2089, May 2007, doi: 10.1016/j.buildenv.2006.03.013.

[116] B. A. Graybeal and Inc. PSI, 'Material Property Characterization of Ultra-High Performance Concrete', FHWA-HRT-06-103, Aug. 2006. Accessed: Dec. 04, 2021. [Online]. Available: https://rosap.ntl.bts.gov/view/dot/38714

[117] B. Graybeal and M. Davis, 'Cylinder or Cube: Strength Testing of 80 to 200 MPa (11.6 to 29 ksi) Ultra-High-Performance Fiber-Reinforced Concrete', *Aci Mater. J.*, vol. 105, pp. 603–609, Nov. 2008.

[118] S. Kazemi and A. Lubell, 'Influence of Specimen Size and Fiber Content on Mechanical Properties of Ultra-High-Performance Fiber-Reinforced Concrete', *Aci Mater. J.*, vol. 109, pp. 675–684, Nov. 2012, doi: 10.14359/51684165.

[119] E. Fehling, M. Schmidt, and S. Stürwald, *Ultra High Performance Concrete: (UHPC) ; Proceedings of the Second International Symposium on Ultra High Performance Concrete, Kassel, Germany, March 05 - 07, 2008*. kassel university press GmbH, 2008.

[120] Dr. K. A. Riding *et al.*, 'Ultra-High-Performance Concrete (UHPC) Use in Florida Structural Applications', Engineering School of Sustainable Infrastructure and Environment, University of Florida, Gainesville, Florida, 2020. [Online]. Available: https://fdotwww.blob.core.windows.net/sitefinity/docs/default-source/structures/innovation/uhpc/bdv31-977-105_deliv12d606df2d5bc476e99649a6caf0df0b7.pdf?sfvrsn=62dc2a2b_2

[121] H. Kim, T. Koh, and S. Pyo, 'Enhancing flowability and sustainability of ultra high performance concrete incorporating high replacement levels of industrial slags', *Constr. Build. Mater.*, vol. 123, pp. 153–160, 2016.

[122] K. H. Khayat, W. Meng, K. Vallurupalli, and L. Teng, 'Rheological properties of ultra-high-performance concrete—An overview', *Cem. Concr. Res.*, vol. 124, p. 105828, 2019.

[123] A. Alsalman, C. N. Dang, and W. Micah Hale, 'Development of ultra-high performance concrete with locally available materials', *Constr. Build. Mater.*, vol. 133, pp. 135–145, Feb. 2017, doi: 10.1016/j.conbuildmat.2016.12.040.

[124] J. Liu *et al.*, 'Combined effect of coarse aggregate and fiber on tensile behavior of ultra-high performance concrete', *Constr. Build. Mater.*, vol. 121, pp. 310–318, 2016.

[125] W. Meng and K. H. Khayat, 'Effect of hybrid fibers on fresh properties, mechanical properties, and autogenous shrinkage of cost-effective UHPC', *J. Mater. Civ. Eng.*, vol. 30, no. 4, 2018, doi: 10.1061/(ASCE)MT.1943-5533.0002212.

[126] Z. Wu, C. Shi, W. He, and L. Wu, 'Effects of steel fiber content and shape on mechanical properties of ultra high performance concrete', *Constr. Build. Mater.*, vol. 103, pp. 8–14, 2016, doi: 10.1016/j.conbuildmat.2015.11.028.

[127] D.-Y. Yoo, S.-T. Kang, and Y.-S. Yoon, 'Enhancing the flexural performance of ultra-high-performance concrete using long steel fibers', *Compos. Struct.*, vol. 147, pp. 220–230, 2016.

[128] L. Zhang, J. Liu, J. Liu, Q. Zhang, and F. Han, 'Effect of steel fiber on flexural toughness and fracture mechanics behavior of ultrahigh-performance concrete with coarse aggregate', *J. Mater. Civ. Eng.*, vol. 30, no. 12, 2018, doi: 10.1061/(ASCE)MT.1943-5533.0002519.

[129] K. Wille, A. E. Naaman, and G. J. Parra-Montesinos, 'Ultra-High Performance Concrete with Compressive Strength Exceeding 150 MPa (22 ksi): A Simpler Way.', *ACI Mater. J.*, vol. 108, no. 1, 2011.

[130] G. Shakhmenko, A. Korjakins, P. Kara, J. Justs, and I. Juhnevica, 'UHPC containing nanoparticles synthesized by sol-gel method', 2012, pp. 79–85.

[131] S. Abbas, A. M. Soliman, and M. L. Nehdi, 'Exploring mechanical and durability properties of ultra-high performance concrete incorporating various steel fiber lengths and dosages', *Constr. Build. Mater.*, vol. 75, pp. 429–441, 2015, doi: 10.1016/j.conbuildmat.2014.11.017.

[132] H. Ş. Arel, 'Effects of curing type, silica fume fineness, and fiber length on the mechanical properties and impact resistance of UHPFRC', *Results Phys.*, vol. 6, pp. 664–674, Jan. 2016, doi: 10.1016/j.rinp.2016.09.016.

[133] R. Wang and X. Gao, 'Relationship between flowability, entrapped air content and strength of UHPC mixtures containing different dosage of steel fiber', *Appl. Sci.*, vol. 6, no. 8, p. 216, 2016.

[134] A. Le Hoang and E. Fehling, ‘Influence of steel fiber content and aspect ratio on the uniaxial tensile and compressive behavior of ultra high performance concrete’, *Constr. Build. Mater.*, vol. 153, pp. 790–806, 2017, doi: 10.1016/j.conbuildmat.2017.07.130.

[135] J.-J. Park, D.-Y. Yoo, G.-J. Park, and S.-W. Kim, ‘Feasibility of reducing the fiber content in ultra-high-performance fiber-reinforced concrete under flexure’, *Materials*, vol. 10, no. 2, 2017, doi: 10.3390/ma10020118.

[136] M. A. Ibrahim, M. Farhat, M. A. Issa, and J. A. Hasse, ‘Effect of material constituents on mechanical & fracture mechanics properties of ultra-high-performance concrete’, *ACI Struct. J.*, vol. 114, no. 3, pp. 453–465, 2017, doi: 10.14359/51689717.

[137] B.-I. Bae, H.-K. Choi, B.-S. Lee, and C.-H. Bang, ‘Compressive behavior and mechanical characteristics and their application to stress-strain relationship of steel fiber-reinforced reactive powder concrete’, *Adv. Mater. Sci. Eng.*, vol. 2016, 2016.

[138] A. M. T. Hassan, S. W. Jones, and G. H. Mahmud, ‘Experimental test methods to determine the uniaxial tensile and compressive behaviour of Ultra High Performance Fibre Reinforced Concrete(UHPFRC)’, *Constr. Build. Mater.*, vol. 37, pp. 874–882, 2012, doi: 10.1016/j.conbuildmat.2012.04.030.

[139] D.-Y. Yoo, S.-W. Kim, and J.-J. Park, ‘Comparative flexural behavior of ultra-high-performance concrete reinforced with hybrid straight steel fibers’, *Constr. Build. Mater.*, vol. 132, pp. 219–229, 2017, doi: 10.1016/j.conbuildmat.2016.11.104.

[140] S. Erdogdu, U. Kandil, and S. Nayir, ‘Effects of cement dosage and steel fiber ratio on the mechanical properties of reactive powder concrete’, *Adv. Concr. Constr.*, vol. 8, no. 2, pp. 139–144, 2019.

[141] R. Ma, L. Guo, S. Ye, W. Sun, and J. Liu, ‘Influence of Hybrid Fiber Reinforcement on Mechanical Properties and Autogenous Shrinkage of an Ecological UHPFRCC’, *J. Mater. Civ. Eng.*, vol. 31, no. 5, 2019, doi: 10.1061/(ASCE)MT.1943-5533.0002650.

[142] D.-Y. Yoo, M. J. Kim, S.-W. Kim, and J.-J. Park, ‘Development of cost effective ultra-high-performance fiber-reinforced concrete using single and hybrid steel fibers’, *Constr. Build. Mater.*, vol. 150, pp. 383–394, 2017, doi: 10.1016/j.conbuildmat.2017.06.018.

[143] D. J. Kim, S. H. Park, G. S. Ryu, and K. T. Koh, ‘Comparative flexural behavior of Hybrid Ultra High Performance Fiber Reinforced Concrete with different macro fibers’, *Constr. Build. Mater.*, vol. 25, no. 11, pp. 4144–4155, 2011, doi: 10.1016/j.conbuildmat.2011.04.051.

[144] I. Lande and R. T. Thorstensen, ‘Locally Produced UHPC: The Influence of Type and Content of Steel Fibres’, *Nord. Concr. Res.*, vol. 64, no. 1, pp. 31–52.

[145] M. Gesoglu, E. Güneyisi, G. F. Muhyaddin, and D. S. Asaad, ‘Strain hardening ultra-high performance fiber reinforced cementitious composites: Effect of fiber type and concentration’, *Compos. Part B Eng.*, vol. 103, pp. 74–83, Oct. 2016, doi: 10.1016/j.compositesb.2016.08.004.

[146] R. Yu, P. Spiesz, and H. J. H. Brouwers, ‘Mix design and properties assessment of Ultra-High Performance Fibre Reinforced Concrete (UHPFRC)’, *Cem. Concr. Res.*, vol. 56, pp. 29–39, Feb. 2014, doi: 10.1016/j.cemconres.2013.11.002.

[147] R. Yu, P. Spiesz, and H. J. H. Brouwers, ‘Development of an eco-friendly Ultra-High Performance Concrete (UHPC) with efficient cement and mineral admixtures uses’, *Cem. Concr. Compos.*, vol. 55, pp. 383–394, Jan. 2015, doi: 10.1016/j.cemconcomp.2014.09.024.

[148] G. Hüsken and H. J. H. Brouwers, ‘A new mix design concept for earth-moist concrete: A theoretical and experimental study’, *Cem. Concr. Res.*, vol. 38, no. 10, pp. 1246–1259, Oct. 2008, doi: 10.1016/j.cemconres.2008.04.002.

[149] R. Karim, M. Najimi, and B. Shafei, ‘Assessment of transport properties, volume stability, and frost resistance of non-proprietary ultra-high performance concrete’, *Constr. Build. Mater.*, vol. 227, p. 117031, Dec. 2019, doi: 10.1016/j.conbuildmat.2019.117031.

[150] N. A. Soliman and A. Tagnit-Hamou, ‘Using particle packing and statistical approach to optimize eco-efficient ultra-high-performance concrete’, *ACI Mater. J.*, vol. 114, no. 6, pp. 847–858, 2017, doi: 10.14359/51701001.

[151] F. de Larrard and T. Sedran, ‘Optimization of ultra-high-performance concrete by the use of a packing model’, *Cem. Concr. Res.*, vol. 24, no. 6, pp. 997–1009, Jan. 1994, doi: 10.1016/0008-8846(94)90022-1.

[152] F. de Larrard and T. Sedran, ‘Mixture-proportioning of high-performance concrete’, *Cem. Concr. Res.*, vol. 32, no. 11, pp. 1699–1704, Nov. 2002, doi: 10.1016/S0008-8846(02)00861-X.

[153] S. A. Fennis, J. C. Walraven, and J. A. Den Uijl, ‘The use of particle packing models to design ecological concrete’, *Heron 54 23*, 2009.

[154] W. B. Fuller and S. E. Thompson, ‘The Laws of Proportioning Concrete’, *Trans. Am. Soc. Civ. Eng.*, vol. 59, no. 2, pp. 67–143, Jan. 1907, doi: 10.1061/TACEAT.0001979.

[155] A. H. M. Andreasen, ‘Über die Beziehung zwischen Kornabstufung und Zwischenraum in Produkten aus losen Körnern (mit einigen Experimenten)’, *Kolloid-Z.*, vol. 50, no. 3, pp. 217–228, 1930.

[156] J. E. Funk and D. R. Dinger, *Predictive process control of crowded particulate suspensions: applied to ceramic manufacturing*. Springer Science & Business Media, 2013.

[157] H. Brouwers, ‘Particle-size distribution and packing fraction of geometric random packings’, *Phys. Rev. E*, vol. 74, no. 3, p. 031309, 2006.

[158] F. Medonca, J. Hu, and G. Morcous, ‘Fresh and Hardened Behavior of UHPC Prepared with Different Mix Design Parameters’, 2019, vol. 2, no. 1.

[159] S. El-Tawil, Y.-S. Tai, B. Meng, W. Hansen, and Z. Liu, ‘Commercial production of non-proprietary ultra high performance concrete’, Michigan. Dept. of Transportation. Research Administration, 2018.

[160] P. Schießl, O. Mazanec, and D. Lowke, ‘SCC and UHPC—Effect of mixing technology on fresh concrete properties’, in *Advances in construction materials 2007*, Springer, 2007, pp. 513–522.

[161] A. Chkheiwer and J. Kadim, ‘Factors effecting on the compressive and tensile strength of reactive powder concrete made with local materials’, 2019, vol. 584, no. 1, p. 012002.

[162] A. Tafraoui, G. Escadeillas, and T. Vidal, ‘Durability of the Ultra High Performances Concrete containing metakaolin’, *Constr. Build. Mater.*, vol. 112, pp. 980–987, Jun. 2016, doi: 10.1016/j.conbuildmat.2016.02.169.

[163] K. Wille and C. Boisvert-Cotulio, ‘Material efficiency in the design of ultra-high performance concrete’, *Constr. Build. Mater.*, vol. 86, pp. 33–43, Jul. 2015, doi: 10.1016/j.conbuildmat.2015.03.087.

[164] K. Wille, A. E. Naaman, S. El-Tawil, and G. J. Parra-Montesinos, ‘Ultra-high performance concrete and fiber reinforced concrete: achieving strength and ductility without heat curing’, *Mater. Struct.*, vol. 45, no. 3, pp. 309–324, Mar. 2012, doi: 10.1617/s11527-011-9767-0.

[165] M. Hassan and K. Wille, ‘Experimental impact analysis on ultra-high performance concrete (UHPC) for achieving stress equilibrium (SE) and constant strain rate (CSR) in Split Hopkinson pressure bar (SHPB) using pulse shaping technique’, *Constr. Build. Mater.*, vol. 144, pp. 747–757, Jul. 2017, doi: 10.1016/j.conbuildmat.2017.03.185.

[166] J. Bu, X. Chen, L. Hu, H. Yang, and S. Liu, ‘Experimental study on crack propagation of concrete under various loading rates with digital image correlation method’, *Int. J. Concr. Struct. Mater.*, vol. 14, no. 1, pp. 1–25, 2020.

[167] M. Merzkirch, *Mechanical characterization using digital image correlation: advanced fibrous composite laminates*. Springer Nature, 2021.

[168] M. Frančić Smrkić, J. Košćak, and D. Damjanović, ‘Application of 2D digital image correlation for displacement and crack width measurement on RC elements’, *Građevinar*, vol. 70, no. 09., pp. 771–781, 2018.

[169] B. Liu, F. Yue, B. Chen, X. Man, L. Chen, and S. Jaisee, ‘Study on bond performance, flexural and crack extension behavior of base concrete prisms strengthen with strain-hardening cementitious composites (SHCC) using DIC technology’, *Constr. Build. Mater.*, vol. 251, p. 119035, Apr. 2020, doi: 10.1016/j.conbuildmat.2020.119035.

[170] R. S. Panah and M. Kioumarsi, ‘Application of building information modelling (BIM) in the health monitoring and maintenance process: A systematic review’, *Sensors*, vol. 21, no. 3, p. 837, 2021.

[171] A. Kohoutková, J. L. Vítek, M. Frantová, and P. Bílý, ‘The 12th International PhD Symposium in Civil Engineering’, 2018.

[172] ‘Prøvingsmetode for betong med metalliske fibere - Måling av bøyestrekkfasthet (proporsjonalitetsgrense og restfastheter)’, *NS-EN 14651*, 2005.

[173] ‘Areal- og volumberegninger av bygninger’, *NS 3940*, 2012.

[174] ‘Test method for flow of hydraulic cement mortar’, *ASTM C1437*, 2007.

[175] ‘Standard Test Method for Slump Flow of Self-Consolidating Concrete’, *ASTM C1611C1611M*, 2005.

[176] ‘520.027 Kvalitetskontroll av fersk betong - Byggforskserien’. https://www.byggforsk.no/dokument/286/kvalitetskontroll_av_fersk_betong (accessed May 19, 2022).

[177] ‘Prøving av herdnet betong - Del 4: Trykkfasthet - Krav til prøvingsmaskiner’, *NS-EN 12390-4*, 2019.

[178] ‘Prøving av herdnet betong Del 5: Prøvelegemers bøyestrekkfasthet’, *NS-EN 12390-5*, 2019.

[179] Y.-W. Chan and S.-H. Chu, ‘Effect of silica fume on steel fiber bond characteristics in reactive powder concrete’, *Cem. Concr. Res.*, vol. 34, no. 7, pp. 1167–1172, 2004.

[180] Z. Wu, C. Shi, and K. H. Khayat, ‘Influence of silica fume content on microstructure development and bond to steel fiber in ultra-high strength cement-based materials (UHSC)’, *Cem. Concr. Compos.*, vol. 71, pp. 97–109, Aug. 2016, doi: 10.1016/j.cemconcomp.2016.05.005.

[181] C. Shi, D. Wang, L. Wu, and Z. Wu, ‘The hydration and microstructure of ultra high-strength concrete with cement–silica fume–slag binder’, *Cem. Concr. Compos.*, vol. 61, pp. 44–52, 2015.

Appendix

All appendix is provided as an attachment are delivered as a supporting file, and submitted separately. This includes excel calculations, mixture and recipe development, Particle Size Distribution model, and Compressive and Flexural test results.